Limits of Restored Vision: Using Psychophysics to Predict What Sight Restoration Technologies Can Provide

Ezgi Irmak Yücel

A dissertation

submitted in partial fulfillment of the

requirements for the degree of

Doctor of Philosophy

University of Washington

2023

Reading Committee:

Ione Fine, Chair

Ariel Rokem

Michael B. Manookin

Program Authorized to Offer Degree:

Department of Psychology

University of Washington

Abstract

Limits of Restored Vision: Using Psychophysics to Predict What Sight Restoration Technologies Can Provide

Ezgi Irmak Yücel

Chair of the Supervisory Committee:

Ione Fine

Department of Psychology

Sight restoration technologies targeting vision loss caused by retinal degeneration have shown significant progress in the past 30 years. Light perception can be achieved through electrical or optogenetic stimulation, replacement of the degenerated cells, or targeting associated genes if the genome is known. An important question that arises is how similar the restored vision is to neurotypical vision. Combining psychophysical methodology with computational modeling, we studied two sight restoration methods, retinal prostheses and optogenetic therapy, to examine what limits restored vision and identify key features to improve for future development. We argue that establishing a better understanding of the link between sight restoration technologies and the underlying neurophysiology prior to implementation is key for developing these technologies in an ethical and cost-effective manner.

TABLE OF CONTENTS

LIST OF FIGURES

LIST OF TABLES

ACKNOWLEDGEMENTS

I am deeply indebted to numerous individuals whose contributions were integral to the successful completion of this journey. Firstly, I am extremely grateful for my advisor, Ione and my co-advisor Ariel for their advice, unwavering support, and willingness to guide me in many pivots I took during my graduate training. With their rigor and wisdom, I was able to complete my training to be a better scientist. Special thanks to Geoff for his mentorship and collaboration in almost all of my projects.

I was lucky to be surrounded by remarkable mentors at VisCog. I'd like to thank Michael, my primary post-doctoral advisor, for shouldering the responsibility of my early-doctoral training and helping me with charting my research path. I am thankful for my incredible post-doctoral advisors, —Tamar, Woon Ju, Dina, and Kim— for being my champions. I'd like to thank Scott and John Palmer for their guidance, and to my labmates, particularly Jasmine and Kelly, for the comradery and joy they brought to my life.

I extend my thanks to my collaborators Gislin, Sandra, Arathy, and Roksana, as well as the UW eScience Institute and Washington Research Foundation for supporting my work. A heartfelt acknowledgment is reserved for my participants who generously contributed their time and energy for my research.

Moving across the world and starting a PhD felt relatively easy thanks to my friends I made here, back home, and friends scattered across the world. I am grateful for the aghö crew, Özge, Doğa, and Orhun, who have consistently stood by me despite the ~~miles~~ kilometers between us. I would like to thank my secondary family in Seattle, Will, Jasmine, Terrènce, Gala, Caroline, Bahar, and my Turkish crew. Finally, writing my thesis over the past year would have been significantly more challenging without the incredible support of my partner Max. Thank you so much for your love and presence during my toughest moments.

The resilience that propelled me through six years of pursuing a Ph.D. and building a life abroad is all thanks to my family and my upbringing. I owe my deepest gratitude to my parents, İsmail and Şadiye Yücel, for everything I have accomplished. Ece and I are so fortunate to be your daughters. I am grateful to my family – Yücels and Kırankayas– who encouraged me to pursue my interests despite the distance.

DEDICATION

To my grandparents Nail and Nevin Yücel, Mürsel Kırankaya, and Ayşe Kırankaya who always wanted me to study. *'Senin kızın okudu.'*

Chapter 1. INTRODUCTION

Retinal processing, the initial step in visual perception, plays a foundational role by filtering all incoming visual information. Inherited retinal diseases (IRDs) such as Retinitis Pigmentosa (RP) and Age-related Macular Degeneration (AMD) impact photoreceptors and cause wide-scale retinal remodeling leading to gradual visual degradation and blindness. The visual information lost during this initial stage, as a result of photoreceptor degeneration, remains irrecoverable in the subsequent stages of visual processing. Individuals affected by IRDs are generally recommended to undergo symptom management, such as regular injections, as complete cures for these conditions are not currently available.

Sight restoration technologies ranging from molecular approaches to brain-computer interfaces, aim to alleviate vision loss due to retinal degeneration. One molecular approach is to avoid or slow down the progression of retinal degeneration such as gene-editing. While this method has the potential to fully restore neurotypical vision, the genetic factors associated with IRDs currently restrict its effectiveness to specific identified genes. A notable success in gene therapy is LUXTURNA (developed by Spark Therapeutics, USA), designed to address Leber's Congenital Amaurosis, a subtype of RP, and it has obtained FDA approval (Russell et al., 2017). In IRDs, the most substantial degradation occurs at the photoreceptor layer; the subsequent retinal layers and the rest of the visual cascade remain relatively intact. An alternative approach to sight restoration leverages the remaining healthy cells by bypassing the degenerated photoreceptors to elicit light perception in the subsequent layers. Artificial stimulation of the remaining neuronal population can be achieved through electrical stimulation or by modifying the cells with optogenetic proteins or chemically engineered photoswitches to render them light-sensitive. Over the past three decades, significant advancements have been made in inducing light perception

through electrical and optogenetic stimulation. In 2013, Argus II (Second Sight, Inc, USA, now Cortigent, Inc, USA) a retinal electrical implant with sixty electrodes became the first electrical implant to receive FDA approval for commercial use (Luo & da Cruz, 2016). In 2021, a patient treated with ChrimsonR optogenetic protein was able to locate objects in their treated eye using light-inducing goggles (Sahel et al., 2021) and currently four early-stage clinical trials for optogenetic therapy are ongoing (Prosseda et al., 2022).

The goal of these technologies is to provide restored vision matching up to the function and performance of the neurotypical vision. However, bypassing the initial neuronal processing and artificial stimulation renders restored vision inherently different from neurotypical vision. The aforementioned technologies generate phosphenes with spatial and temporal distortions (Fine & Boynton, 2015). Since it is an emerging technology, a lot is unknown and the expectations of clinicians, funding agencies, and patients are set based on animal models and clinical trial outcomes.

Alternatively, understanding the characteristics of restored vision prior to large-scale implementation could be achieved through modeling and predicting the outcomes from the established information on the neurophysiology and the device functioning. This approach allows the establishment of theoretical limits for comparison with empirical evidence. In our 'virtual patient' framework, we aimed to achieve this by simulating the restored vision based on psychophysical testing and neurophysiology in two types of sight restoration technologies: retinal implant and optogenetic therapy.

In the first half of the thesis, chapters two and three, we examine the perceptual experiences of patients who already have retinal implants with the goal of validating the predictions of the virtual patient paradigm. The latter half focuses on predicting perceptual outcomes of optogenetic therapy. This chapter provides a broad overview of the neuroanatomy and function of healthy retina, retinal degenerative diseases causing blindness, types of sight restoration technologies, and psychophysical methods adapted to testing restored vision.

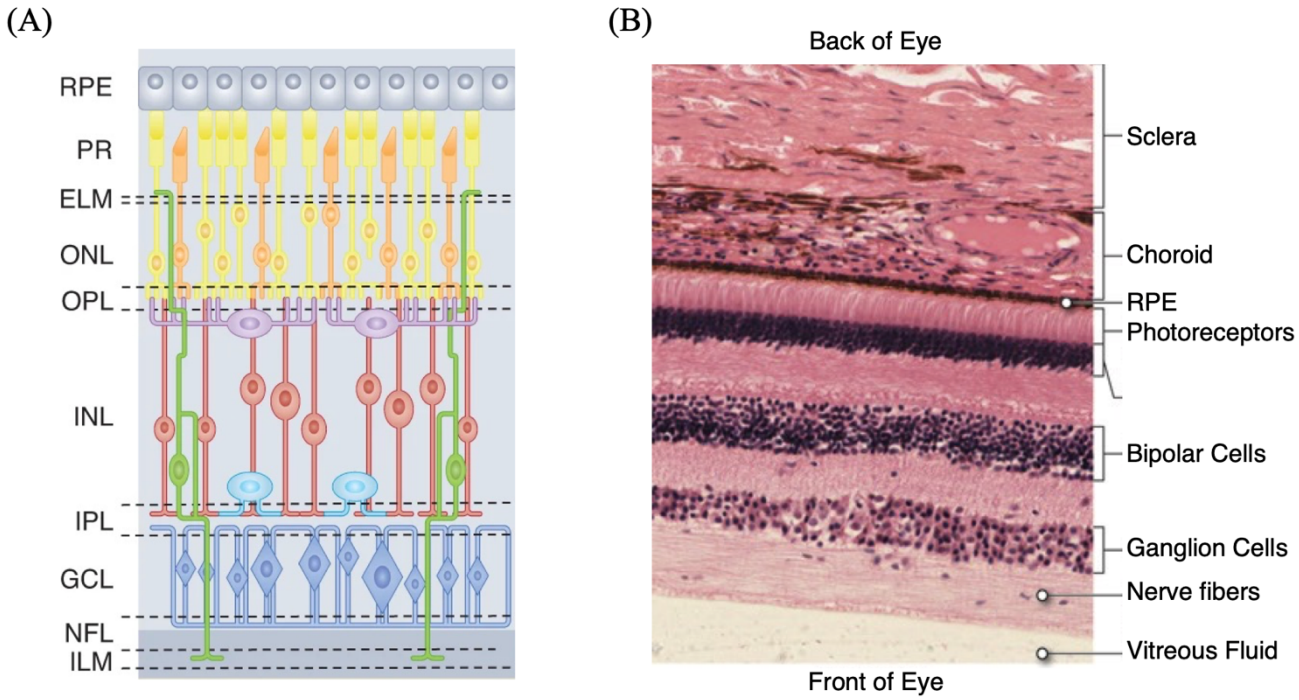

Figure 1 Laminar structure of the retina shown in (A) diagram adapted from Cehajic-Kapetanovic et al. (2022) with license number 5562830628141, (B) labeled stain tissue adapted from Cenveo with a CC-3 license.

1.1 The Neuroanatomy and Function of the Healthy Retina

The human retina is the innermost tissue of the eye with a laminar structure consisting of five major cell classes and their synapses: the cell bodies of photoreceptors, horizontal cells,

bipolar cells, amacrine cells, and retinal ganglion cells make up the three nuclear layers; separated by two plexiform layers, see Figure 1 (Rodieck, 1973). The furthest from the surface, Outer Nuclear Layer (ONL) consists of the first order neurons capturing photons, photoreceptor cell bodies and it is bound by Retinal Pigment Epithelium. Axons and dendrites of the photoreceptors, bipolar, and horizontal cells make up the Outer Plexiform Layer (OPL) and their cell bodies are in the Inner Nuclear Layer (INL). At the Inner Plexiform Layer (IPL), ganglion cells synapse with amacrine and bipolar cells and their cell bodies make up the Ganglion Cell Layer (GCL) (Dowling, 1987). The axons of ganglion cells enter Nerve Fiber Layer (NFL), forming bundles towards the Optic Nerve (ON) where retinal signals are relayed to Lateral Geniculate Nucleus (Pollock & Miller, 1986). The cell density across the retina is not uniform with perceptual consequences going from fovea towards the periphery (Wassle & Boycott, 1991).

Photoreceptors. Named after the shape of their outer segments: rods and cones are two general categories of photoreceptors in vertebrate retina (Baylor, 1987). They carry light-sensitive opsins or photopigments in their outer segments that absorb photons to initiate visual signaling, in a process called phototransduction. Depolarized at dark environments -also referred as 'dark current'-, rods and cones hyperpolarize in presence of light.

The photo-absorption rates, spectral sensitivities, and distributions of the photoreceptors vary. Rod density dips at fovea and peaks at 20° away from it. In their pioneering paper 'Energy, Quanta, and Vision' (1942), Hecht and colleagues estimated from psychophysical data that only a handful of photons are needed to elicit light response from a rod in dimly lit conditions. This is mainly due to high convergence of rod receptive fields in the periphery, making rod mediated vision highly sensitive but less precise (Curcio et al., 1990; Kawamura & Tachibanaki, 2022). Cones in the healthy human retina have three opsins receptive to short (S), medium (M), and long

(L) wavelengths. Color vision, due to relative excitation of S, M, and L cones are mediated by cones. Cone density peaks at fovea: foveal vision at ambient light has high acuity but it is less sensitive than rod-mediated vision (Curcio et al., 1990; Kawamura & Tachibanaki, 2022).

Weak signals are amplified at this stage of visual processing because all aforementioned photopigments initiate a G-protein cascade. Cones are about x30 times less sensitive due to faster recovery time of their opsins (Kawamura & Tachibanaki, 2022). Under bright daylight, human vision is cone-driven, and is sensitive to flicker at higher temporal frequencies. At mesopic conditions temporal sensitivity is dependent on both rod and cone photoreceptors (Umino et al., 2019). In designing sight restoration technologies, it is vital to consider amplification and adaptation features of phototransduction when bypassing the degenerated photoreceptor layers.

Bipolar Cells. Glutamate released from photoreceptor dendrites initially interacts with bipolar cells in the inner nuclear layer. There are over 10 physiologically distinct types of bipolar cells distributed throughout the retina, and they alter various aspects of the visual response, chromaticity and kinetics (Euler et al., 2014; Grimes et al., 2018) . Rods only connect with rod bipolar cells; whereas cones are linked to mainly two functionally distinct categories: ON vs OFF cone bipolar cells. The distinction here is whether the inhibition of glutamate release depolarizes (ON) or hyperpolarizes (OFF) the cell. The antagonism is due to feedforward or negative feedback connections with ***horizontal cells*** in the OPL (Dacey, 1999).

Rod bipolar cells relay the visual signal to ***AII Amacrine cells*** which share gap junctions with cone bipolar cells, exploiting the same subsequent retinal circuitry (Euler et al., 2014). Cone bipolar cells can differ in their tuning to wavelength (S-cone bipolar) or their receptive fields (midget bipolar). In rodents, there is an additional direct pathway between rods and OFF bipolar cells (Field & Rieke, 2002)

Ganglion cells. Retinal Ganglion Cells (RGCs) serve as the endpoint of retinal visual processing projecting their axons to Lateral Geniculate Nucleus (LGN) and Superior Colliculus. With more than 17 morphologically distinct types, ganglion cells multiplex input they receive from bipolar and amacrine cells (Field & Chichilnisky, 2007). The RGCs with the highest cellular density, Parasol and Midget cells were the earliest to be characterized due to the measurement methods available. Depending on where their dendrites are, Midget and Parasol RGCs receive excitatory/inhibitory input from bipolar cells that enables center-surround antagonism in their receptive fields (Dacey, 2004). Midget cells have receptive fields with small receptive fields and sustained responses project to parvocellular layers of Lateral Geniculate Nucleus, whereas parasol ganglion cells with larger receptive fields have faster kinetics and project to magnocellular layers of LGN (Kaplan, 2008). While the function and anatomy of all the distinct types of ganglion cells are not fully understood, it is clear that the visual stimulus is processed in multiple parallel pathways; for both visual and non-visual purposes (Field & Chichilnisky, 2007).

In the context of sight restoration, it's important to highlight the significant diversity in both function, morphology, and interaction among various retinal cell types. Bypassing the complex processing at the retina yields a challenge to attain neurotypical vision.

1.2 Retinal Degenerative Diseases (RDD)

1.2.1 *Inherited Retinal Degenerative Diseases Lead to Vision Loss*

Age-related Macular Degeneration (AMD) or Retinitis Pigmentosa (RP) belong to a family of inherited degenerative diseases identified by the dystrophy of photoreceptors and subsequent retinal re-modeling, causing partial or total vision loss. These diseases are classified according to

the type of inheritance—autosomal dominant, recessive, X-linked—, type of cells affected, identified defective genes, and which stage the disease is in (Dias et al., 2018). A list of RDDs with the current number of related genes and loci is presented in Supplementary Table 1.

AMD is the third leading cause of blindness worldwide where the first two —glaucoma and cataracts— are considered "preventable" with early detection and treatment (Bourne et al., 2013). Researchers project that by 2040, 288 million people will have age-related macular degeneration (Wong et al., 2014). The prevalence and demographics vary significantly across geographical region, access to treatment, and age. At the later stages of the disease, AMD can be classified as "wet" (or exudative) due to new blood cell formation; or "dry" (non-exudative) due to photoreceptor shortening and separation from RPE, both leading to subsequent retinal damage (Pfeiffer et al., 2020). While early AMD can be asymptomatic with minor distortions to vision, late AMD leads to central progressive vision loss. The progress of wet AMD can be prevented or slowed down by introducing suppressors to Vascular Endothelial Growth Factor (VEGF); however, there is currently no available cure for dry AMD (Mitchell et al., 2018).

Retinitis Pigmentosa is the generalized name given for a class of diseases affecting 1 in 4000 globally (Pfeiffer et al., 2020). Named after the observed pigmentation of the retina, RP is identified by photoreceptor loss starting from rods in the periphery, progressing towards cones in macula. In addition to pigmentation, no response from an electroretinogram (ERG), and size changes in retinal vessels are other indicators of photoreceptor death in RP (Petrs-Silva & Linden, 2013). RP patients initially lose night and peripheral vision due to degeneration of rods; describing their visual experience at daylight at this certain stage as 'tunnel vision', see Figure 2. The disease progresses to total vision loss due to complete photoreceptor atrophy and further retinal re-modeling.

There are currently 69 identified genes directly linked to types of RP (see Supplementary Table 1). with more than 100 associated genes shared with accompanying syndromes. The majority of gene mutations linked to RP is expressed in the eye, leading to retinal degeneration but a subset of gene mutations can lead to widespread abnormalities in the body such as renal dysfunction or poltdactyly (Dias et al., 2018). Bardet-Biedl and Usher Syndromes are two examples of about 30 accompanying diseases to RP.

The onset of IRDs vary according to the genes involved. However, unlike the cases of congenital blindness, individuals affected by IRDs experience neurotypical vision for certain portion of their lifetime. This brings about the opportunity to either rehabilitate or mimic normal vision through sight restoration methods.

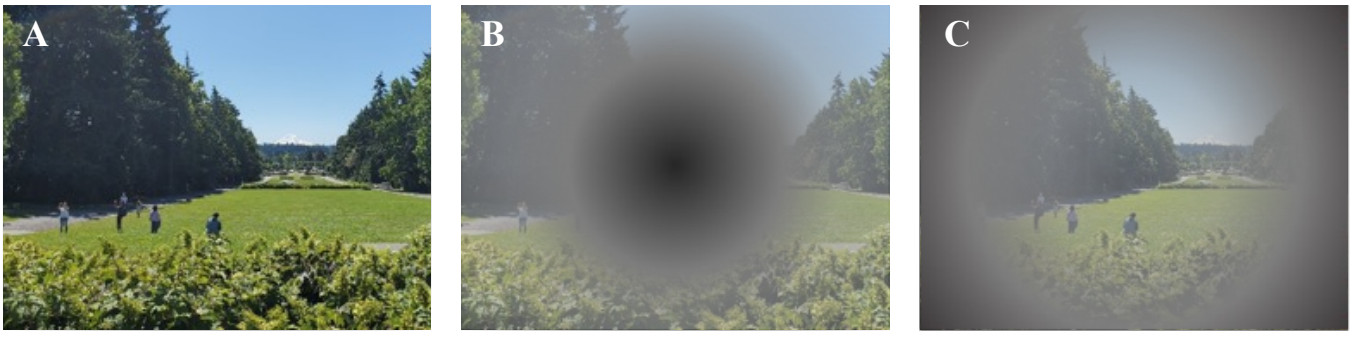

Figure 2 Demonstration of the progress AMD and RP. (A) Original Photo. (B) In AMD, patients initially lose central vision, (C) tunnel vision in RP patients. Adapted from Fine and Boynton (2015).

1.2.2 *Mechanisms of Retinal Degeneration and Re-modeling*

IRDs have a complex etiology but the cause of vision loss is common across all: degeneration of the photoreceptor layers and subsequent rewiring of the retinal circuitry. For instance, in dry AMD, the photoreceptor degeneration is triggered by the separation of photoreceptors from the Retinal Pigment Epithelium where vascularization in wet AMD is the reason for the loss of RPE function (Pfeiffer et al., 2020).

For the majority of IRDs, the main stages (or phases) that follow photoreceptor degeneration are as follows, see Figure 3:

Stage 1. Shortening of photoreceptor outer segments, some deficits are seen.

Stage 2. In addition to photoreceptor atrophy, mostly rods, photoreceptor outer segments continue to shorten, glial response and remodeling starts.

Stage 3. Large-scale photoreceptor loss -cones- and glial response, remodeling of inner layers, random firing of ganglion cells starts.

Stage 4. Almost all photoreceptors are lost, large-scale remodeling within inner nerve layer, gliosis (Cehajic-Kapetanovic et al., 2022).

Here, depending on the stage of IRDs, the type of sight restoration method available changes.

1.3 Sight Restoration Methods

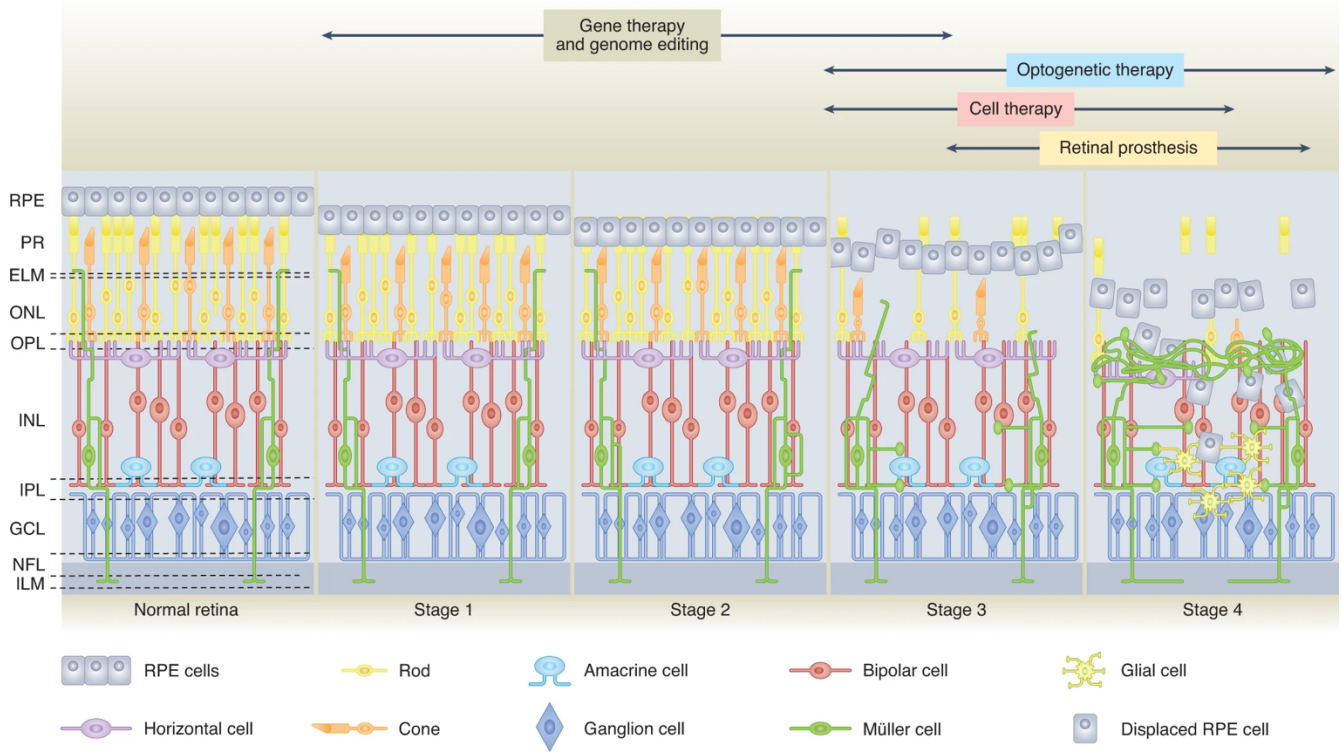

Figure 3 Diagram adapted from Cehajic-Kapetanovic et al. (2022) with license number 5562830628141 summarizing the anatomy, the stages of degeneration in retinal layers, and sight

restoration methods that are suitable for a given stage. The retina goes through major rewiring and remodeling as IRDs progress: if a method such as gene therapy can tackle degeneration at earlier stages, there is a chance of preserving inner layers and further circuitry in the visual cascade.

IRDs primarily affect the retinal cells and the rest of the visual cascade is considered relatively intact. Researchers, for the past 60 years, have explored restoring sight through utilizing remaining visual circuitry. Mainly, four categories of sight restoration methods emerged: molecular therapies, cell transplantation, cognitive methods such as sensory substitution, and electrical implants.

1.3.1 *Molecular Therapies*

As discussed in section 1.2.1, inherited gene mutations, in conjunction with environmental risk factors, lead to retinal degeneration. Identifying and targeting defects due to gene mutations has the potential of fully restoring vision, making molecular approaches one of the most promising methods. These approaches include gene-replacement therapy, genome editing, and optogenetic therapy.

Gene-replacement therapy, delivering the unmutated copy of defective genes via vectors, has been introduced as a proof-of-concept twenty two years ago (Acland et al., 2001). Targeting the single mutated gene 'RPE65' that causes Leber's Congenital Amaurosis (LCA), Acland and colleagues demonstrated restoration of visual function in a canine model. Clinical trials that followed showed similar efficacy in treating LCA due to RPE65 mutation; leading to FDA and EMA approval of LUXTURNA— drug that targets RPE65 via AAV delivery— in 2017 and 2018 respectively (Russell et al., 2017).

Adeno-associated viral (AAV) vector is the most commonly used viral transporter in the retina due to its safety and efficacy with RPE and photoreceptors but it can only carry up to 4.7 kb of information (Russell et al., 2017). This is a limiting factor: genetic information can be larger

than the vector's cargo capacity. In most cases, multiple genes are linked to a certain RDD (see Supplementary Table 1). While the cargo capacity can be increased by genetically modifying AAV (e.g. double AAV), or using another vector, targeting multiple genes at the same time remains a bottleneck in gene-replacement therapy.

Genome editing techniques, such as CRISPR-Cas9, have the potential to edit or inhibit the mutated gene of the patients with RDDs. Clinical trials of EDIT-101, a gene-editing product for CEP290 gene that causes LCA type 10, started in 2019 with adult and pediatric participants (Clinical Trial *NCT03872479*). Primarily interested in the number of adverse events and levels of toxicity, researchers also study visual function outcomes. Similar to gene-replacement therapy, if genome editing is established that it is a safe and effective method, it will require vectors with large cargo capacity and will need to have low immunogenic effects (Cehajic-Kapetanovic et al., 2022). Since the aim is to restore the function of degenerated cells, the aforementioned molecular techniques can only be applied in the earlier stages of RDDs. An alternative molecular approach that is viable in the later stages with major target cell loss and retinal remodeling is to genetically engineer non-light sensitive cells to respond to light.

Optogenetic therapy, where the ion channels of remaining light-insensitive cells are equipped with light sensitive proteins, is mutation independent and viable at the later stages of retinal degeneration, see Busskamp et al., (2012) for a review and a more detailed description in Chapter 6.

1.3.2 *Cell Transplantation*

Tissue engineering to either promote health of or replace the affected cells in RDDs is another approach in sight restoration. Mainly two categories of tissue engineering are relevant to RDDs: use of stem cells or scaffolds. Stem cells from the umbilical tissue, bone marrows or

induced pluripotent stem cells (IPSCs) are placed into the ocular/intraocular region to passively deliver growth factors and increase the probability of cell survival (Bahar, 2019; Cehajic-Kapetanovic et al., 2022). Alternatively, degenerated cells can be replaced by healthy transplants. Scaffolds, similar to extracellular matrices such as glial cells, provide structural and functional support to the cells. Scaffolds can be engineered or sourced from cadavers. In the context of RDDs, stem cells on scaffolds can have a better chance of long-term viability; however, biocompatibility of the materials used is a current issue that needs to be addressed.

The potential disadvantage of using stem cells from the patient is that the stem cells might carry the same genetic mutation; researchers need to modify the cells before transplantation. Currently, the clinical trials focus on immunocompatibility and long-term cell survival (Cehajic-Kapetanovic et al., 2022).

1.3.3 *Electrical Visual Implants*

In analogy to the mechanisms used by cochlear implants to stimulate signal propagation mechanisms in the cochlea, visual implants aim to mimic neurotypical vision by stimulating cells to represent the visual world in phosphenes. By altering the extracellular charge density, electrical stimulation of visual neurons enhances the probability of generating an action potential in a specific area, resulting in the perception of visual phosphenes. Visual implants, in general, consist of a stimulating electrode array, a powering, and a processing unit that can be located at various locations of the visual system.

1.3.3.1 History of Electrical Visual Implants

Electrical stimulation to generate visual phosphenes is an idea as old as the modern concept of electricity; as Benjamin Franklin discussed its potential use for deafness and blindness (W.

Watson, 1752). The foundational body of work for electrical visual implants came from studies by Otfrid Foerster (1929) and Krause & Schum (1931) electrically stimulating cortices of epilepsy patients under local anesthesia (Brindley & Lewin, 1968). They reported that if the occipital lobe is stimulated with a small electrode, patients perceived spots of light. Their students, Wilder Penfield and Rasmussen (1950) followed up with similar reports from the stimulation of the striate cortex.

Inouye and Holmes, situated at opposite corners of the globe, investigated lesions suffered by soldiers during World War I to reveal the retinotopic organization of the visual system, i.e. topographically close neuronal populations are sensitive to neighboring regions in the visual field (Fishman, 1997). Later in the 20th century, Hubel and Wiesel (1962) and Van Essen and colleagues (1984) recorded electrophysiological signals from the cat visual cortex to better map the retinotopic organization of the visual system. With these two key findings, one can potentially mimic normal visual experience by replacing visual stimulus with electrical stimulation, as the phophenes generated by electrically stimulating neighboring cells could reliably represent the visual scenes.

Brindley and Lewin (1968) were the first to use an electrical implant to generate phosphenes as a sight restoration technology. A patient with glaucoma and retinal detachment received an 81-electrode cortical implant and reported seeing phosphenes that changed brightness when the pulse duration and frequency supplied by the implant was altered (Yue et al., 2018). Ten years later Dobelle and colleagues (1979) incorporated a camera as input where the implanted patient reported seeing distinct phosphenes, paving the way for the next generation of electrical visual implants. Several other groups in that period experimented with alternative locations in the visual system such as LGN or the optic nerve.

1.3.3.2 Retinal Implants

Retinal implants have considerable advantages over other loci in the visual system for RDDs: (1) bypassing only the degenerated retinal circuitry, implants can exploit the healthy portion of the visual cascade with minimal alteration, (2) surgically, the retina is easier and safer to access and the techniques for implanting an electrode array are similar to pre-existing methods such as retinal re-attachment surgery.

Decades after the initial experiments in the 60s and 70s, the first major breakthrough was the acute implementation of a multielectrode array on the surface of the retina where the patients were able track the location of the electrode stimulated (Humayun et al., 1999). This meant that electrical stimulation of retinal cells translated into the retinotopic organization of the visual system. With that, it is assumed that if the electrodes become small enough to stimulate small groups of neurons, location based electrical stimulation can replicate the visual world.

Retinal implants generally are categorized based on where they are situated on the retina: epiretinal implants sit on the surface of the retina interfacing with ganglion cells and vitreous cavity, subretinal implants are positioned on the outer nuclear layer consisting of degenerated photoreceptors, and suprachoroidal implants are in between the choroid and sclera.

1.3.3.2.1 Epiretinal Implants

Epiretinal implants interface directly with retinal ganglion cells bypassing the OPL and INL. The main advantage of these implants is the ease of surgery as the techniques are derived from retinal re-attachment surgery. As described earlier in the history subsection, the proof-of-concept for a retinal implants were done by Humayun and colleagues (1999) on an acute epiretinal array. Another advantage is the heat dissipation due to vitreous fluid but this advantage is

accompanied by the effect of torque lifting up the electrode array from retinal surface. Another challenge related to epiretinal implants is the stimulation of ganglion cell axons that lies below the electrode array leading to streaky percepts than ideal point-like percepts (Beyeler et al., 2019).

To date, two epiretinal implants have been approved by regulatory agencies, Argus II by Second Sight, Inc (now Cortigent, Inc) received CE mark in 2011 and FDA in 2013; and IRIS (Pixium Inc, Paris) got CE mark in 2016.

The development of **Argus II** followed the clinical trials of Argus I (started in 2002), first generation 16 electrode epiretinal implant by Second Sight Inc (Humayun et al., 2003; Yanai et al., 2007). Its design modified from cochlear implants, Argus I had electrodes of alternating 260 μm or 520 μm diameters, with 800 μm electrode separation (Luo & da Cruz, 2016). Argus I clinical trials results were promising, safety of electrical stimulation and implantation was established, Argus I users were able to detect phosphenes generated by the implant and could complete visual function tasks (Humayun & Olmos De Koo, 2018),.

The second-generation device, Argus II has 60 electrodes with 200 μm diameter and 575 μm separation. Argus I and Argus II share internal and external components: externally, user wears glasses with a camera mounted in between the eyes to capture the scene, a video processing unit to translate scenes into signals and an external coil to transmit the signal to the retina. Extraocular electronics that consist of an internal coil that receives the signal, and an ASIC circuit produces the appropriate pulses are placed either on temporal bone in Argus I and sutured to the sclera in Argus II. Lastly, the intraocular microelectrode array tacked on one end electrically stimulates retinal ganglion cells (Yue et al., 2020). In Argus II, the extraocular electronics act as the necessary

return for the current flow which potentially can increase current spread leading to a decrease in resolution (Yoon et al., 2020).

With more than 350 users worldwide, Argus II is one of the better studied electrical implants. In chapters Chapter 2 and Chapter 3, I describe my work on identifying factors influencing the spatial resolution of Argus II. After the clinical trials, Argus II was commercially available with multiple centers across the world implanting it (see Yoon et al. (2020) for a review; Schaffrath et al. (2019) for the post-approval study). Unfortunately, in 2019, Second Sight, Inc announced that in order to accelerate the feasibility study of the cortical implant Orion, they suspended production of new Argus II systems (Second Sight, Inc, 2019). In 2020, due to financial setbacks the company announced mass layoffs including vision rehabilitation specialists, and in 2022 the company merged with Cortigent Inc, a subsidiary of Vivani Medical, Inc (Second Sight, Inc, 2022).

Intelligent Retinal Implant System (**IRIS**^{TM}) (Pixium Vision SA, Paris, France), with 150 electrodes, employed sensors instead of a camera to capture visual information and an optical link instead of RF coil for higher data transmission. Similar to Argus II, extraocular electronics were sutured to the sclera and intraocular electrode array consisted of micro-photodiodes with no need for external battery (Hornig et al., 2017). The clinical trials started in 2016 (NCT02670980) with 10 participants, with four participants experiencing six adverse events. At six months, the users performed better in visual function tasks such as square localization when the device was ON vs OFF, their visual field increased from 0 to a median 50º (Muqit et al., 2019). In 2017, the company announced that the life-span of IRIS was shorter than expected, in 2018 they announced their decision to halt the production, postpone further developments, and focus on their other implants (Rachitskaya et al., 2020).

In addition to Argus II and IRIS, experimental device **EPIRET3** by Epi-Ret (University of Aachen, Germany) employed an epiretinal positioning, with 25 electrodes of 100 μm (Humayun & Olmos De Koo, 2018). Unlike the previously mentioned, EPIRET3 had no external components transmitting data or energy and was coated in biocompatible material rather than hermetic case. The proof-of-concept study where 6 patients were implanted and explanted after a month showed success in safety and light perception (Klauke et al., 2011). However, after the end of this clinical trial, the group shifted its focus to 'Very Large Electrode Arrays' (VLARS) (Waschkowski et al., 2014).

1.3.3.2.2 Subretinal Implants

Subretinal implants are placed between the photoreceptor layer and Retinal Pigment Epithelium. The implantation surgery is more challenging than epiretinal implants due to retinal detachment and cutting choroid but subretinal implants are more stable since they are sandwiched between the layers (Humayun & Olmos De Koo, 2018). Electrodes stimulate bipolar layer, taking advantage of its inherent processing. However, in later stages of retinal degeneration, retinal remodeling makes it more challenging to predict visual outcomes.

Alpha-AMS (Retina Implant AG, Germany) was the only commercially available subretinal implant with CE approval. Its predecessor, Alpha IMS that was implanted in 29 patients had shown promising functional results but had issues with long term durability (Stingl et al., 2015). The internal parts consisted of a CMOS chip with 1600 photodiodes which was powered through a foil and a silicone power cable that connects to a ceramic casing under the ear containing receiving coils (Stingl et al., 2017). Unlike epiretinal implants previously discussed, Alpha AMS did not require an external camera since it employed photodiodes and incorporated natural eye and head movements into the stimulation. Despite promising clinical results, Retina Implant AG

announced its closure in 2019 due to regulatory and economic challenges (Rachitskaya et al., 2020; *Retina Implant*, 2019).

The design of **Boston Retinal Implant** Project's subretinal implant was inspired by Argus II, sharing similar components and a 100-electrode microelectrode array of 400 μm diameter implanted between the RPE and the retina (Cheng et al., 2017). This device is still in pre-clinical stage.

In addition to their epiretinal implant effort, Pixium Vision develops **PRIMA**, a photovoltaic implant that consists of an intraocular Near-Infrared powered chip with 143 hexagonal pixels and a video camera attached to an augmented-reality glass (Palanker et al., 2005; Lorach et al., 2015). This design is advantageous for capturing head and eye movements but can require additional illumination to activate photovoltaic pixels. The feasibility clinical trials are currently ongoing (NCT03333954).

1.3.3.2.3 Suprachoroidal Implants

One advantage of placing an electrode array between the sclera and choroid is the lower probability of retinal damage due to implantation and introduction of a foreign object into the eye. Two groups: Fujikado group in Japan (2011) developing Semichronic Suprachoroid Transscleral (STS) and Bionic Vision Australia (BVA) (Ayton et al., 2014; Shivdasani et al., 2014) have been developing suprachoroidal implants.

First generation of **STS** had 49 500 μm platinum electrodes of which 9 were active and 4 could elicit percepts. In its initial trials, the stimulation thresholds were higher compared to epiretinal implants but the participants were able localize objects better when the device was ON vs OFF (Fujikado et al., 2011b; Humayun & Olmos De Koo, 2018). The device was explanted

after a month and in 2017 it was reported that the further clinical trials with the updated STS were underway (Fujikado, 2017).

Between the year 2012-2014, **BVA** implanted the investigational suprachoroidal device consisting of 33 platinum electrodes in three patients with severe RP where they investigated various types of electrode-return positioning. Patients reported reliable percepts when stimulated with currents below the safety limits (Ayton et al., 2014). A second generation implant of 44 electrodes with better positioning and thresholds is currently being investigated for long-term safety of chronic implantation (Petoe et al., 2021).

1.3.3.3 Cortical Implants

The history of cortical stimulation to elicit percepts predates retinal stimulation (see Section 1.3.3.1). Most of the early work on cortical stimulation involved acute testing with no chronic implantation except for Dobelle and colleagues' study (1979) but the interest in developing a chronic cortical visual implant has been steadily growing in the past decade. While the surgery, long-term management and rehabilitation of cortical implants are much more complicated than implants targeting earlier areas in visual processing, a cortical visual implant can be a solution to a much larger population affected by diseases that affect not just retina but also the optic nerve and LGN.

Cortical implants targeting vision loss are implanted in the occipital lobe, directly stimulating visual areas. Ideally, the implant should lie on the calcarine sulcus over the retinotopic visual areas. However, due to the concavity of the sulci, positioning of a rigid electrode array is challenging. Dobelle and colleagues implanted an epicortical array consisting of 140-512 macroelectrodes that was situated between the skull and the cortical surface which produced

phosphenes but at high current amplitudes (Dobelle, 2000; Towle et al., 2020). The first patient to get the epicortical implant had it for 36 years (Dobelle, 2000). The group reported that the implantees could read Braille however the documentation was not sufficient (Bosking et al., 2017). Epicortical implants are less invasive however require high current amplitudes stimulating larger neuronal populations with the risk of causing seizures.

To achieve lower stimulating currents, intracortical implants employ protruding electrodes that contact with the cortex. Again, due to surgical difficulties, implantation over the calcarine fissure where the visual areas are is not recommended, missing out on stimulating neuronal populations that are responsible for early visual processing (Troyk, 2017).

As discussed earlier, Second Sight, Inc (now Cortigent, Inc) devoted its resources to developing cortical visual implants. **Orion** Cortical Visual Prosthesis has received its 'Breakthrough Device' title from FDA in 2018 which is granted for technologies with no approved alternatives and its availability would benefit the patients (Sandrian et al., 2023). Adapted from the Argus II technology, Orion consists of 60 electrodes 4.2mm/3.0mm separation (Beauchamp et al., 2020). 6 patients were implanted as part of the initial clinical trial (NCT03344848), results from one patient with RP were published where they were able to perceive letters through dynamic stimulation of the cortex at a rate of 30 forms (letters like 'C', 'U') per minute (Beauchamp et al., 2020). Similar to Argus II, the position of the percept depends on eye movements (Caspi et al., 2021). The clinical trials are still ongoing.

The Intracortical Visual Prosthesis (**ICVP**) developed by Illinois University of Technology group consists of Wireless Floating Microelectrode Array (WFMA) that consists of 16 electrodes placed on cortical surface (Niketeghad & Pouratian, 2019). After proof-of-concept and safety

studies with 6 rats, clinical trials are currently ongoing (NCT04634383) with preliminary results indicating phosphene generation with low current amplitudes and orientation discrimination (Barry et al., 2023).

In addition to the aforementioned two, Gennaris by Monash Vision Group, Australia using wireless electrode tiles and CORTIVIS (Miguel Hernández University of Elche) using a Utah array are currently being investigated for long-term safety and efficacy (Rosenfeld et al., 2020; Fernández et al., 2021).

1.3.3.4 Summary

The field of electrical implants is both relatively young in the context of commercial products, and old in terms of early investigational studies. Due to its ties to manufacturing, materials, and surgical technology available, trends can shift quite rapidly. The early 2000s saw an emphasis on retinal implant research whereas nowadays, the focus has switched to cortical stimulation. At the frontiers of innovation where for-profit companies share research responsibility with academia, this switch can be expected. However, advocacy for patients who were part of the past research should not be overlooked. Animal studies, acute implantation, and simulation can inform researchers and engineers prior to moving forward with clinical trials.

1.3.4 *Sensory Substitution/Augmentation and Other Cognitive Methods*

Sensory substitution devices (SSDs) aim to replace neurotypical visual perception or augment bionic vision through other modalities such as touch or sound. Widely used traditional visual aids such a cane or the Braille alphabet are in a way, prime examples of SSDs. Their success in helping patients navigate their environments and participate in their social life is undeniable;

and with each technological advancement like the introduction of smart phones and wearables, a new wave of SSDs has emerged to improve the quality of life of blind patients.

An early demonstration of a wearable SSDs was a tactile device placed on the back of the neck by Bach-Y-Rita et al. (1969) where the visual scenes were translated into vibrotactile stimulation. For visual-tactile SSDs choice of location is important due to the change in receptive field sizes on our body. In recent years, tongue, hands, and waist have been the candidate areas for tactile SSDs (Farnum & Pelled, 2020).

Vision-to-audio wearable SSDs where the visual features are represented in auditory stimuli such as pitch, timbre, or loudness of the sound are also getting traction as it has been demonstrated that the users are able to discriminate between tones at a much higher resolution than tactile two-point discrimination.

The main principle of representing the visual world with the aid of another modality is dependent on perceptual learning and neural plasticity; after enough practice, patients can use the output of SSDs to locate visual objects or detect motion. One advantage of SSDs over some sight restoration technologies discussed is that they can be utilized by both early and late-blind individuals. They are considered cost effective compared to the other sight restoration technologies since they generally do not require surgery. However, since they augment a different modality in use, they can be confusing and hard to get used to.

1.4 Visual Function Measures

As described in the earlier sections, restored vision is a different sensory experience than neurotypical vision therefore traditional measures of visual function need to be adapted to the artificial vision by sight restoration technologies. The “Harmonization of Outcomes and Vision

Endpoints in Vision Restoration (HOVER)" taskforce, formed in 2014, aimed to determine these unique needs and standardize practice across research groups. The importance of the standardization of outcome reporting lies in the ability to compare across technologies. Funding agencies, patient advocacy groups, and policy makers require objective measures to evaluate the efficacy of a sight restoration method.

The paper delineating the conclusions of the consortium (Ayton, Rizzo, et al., 2020), points out that there are multiple facets of visual outcomes for artificial vision: change in visual processing, change in quality-of-life of patients, device effectiveness are the main categories named. Not many research groups can conduct a study that covers all the prescribed outcomes; authors of the paper suggest using it as a guideline.

Psychophysical methods provide a unique direction in measuring visual outcomes: we can quantify the perceptual experience through systematic sampling of the stimulus. While the visual processing is non-linear and multi-dimensional, targeting individual features of an input-output relationship enables us to have a better theoretical understanding of a system. Consistent with the guidelines of the HOVER consortium, we divided psychophysical methods relevant to the sight restoration technologies focusing on two main categories: device effectiveness — how well the technology works focusing on how well the technology works— and visual processing —how the visual system works using the technology.

1.4.1 *Device Effectiveness*

The ability to collect reliable behavioral data to describe perceptual experience depends on how well the investigated technology works across users. In clinical trials, this need translates into conducting detection and discrimination threshold measurements, phosphene appearance matching, and phosphene localization tasks with sight recovery patients. These tests serve a dual

purpose: first, they help researchers understand the limits of restored vision, and second, they allow the providers to fine-tune and reassess the performance of the technology.

Phosphene threshold measurements are appropriate for electrical prostheses where the stimulation can be systematically varied to find the intensity required to deliver a reliable percept (usually at 60 or 80 percent correct). If the device allows for individual electrode stimulation, perceptual thresholds are estimated for each electrode and these threshold values are used in determining stimulus intensity required for daily use (Ayton et al., 2020). Prior to other psychophysical tasks that involve varying stimulus intensity, researchers needed to establish that the phosphene thresholds could be obtained consistently, with an acceptable rate of false alarms during the task.

Discrimination tasks in the context of sight restoration can look different based on the technology: for electrical implants establishing the patient's ability to discriminate between phosphenes generated from different electrodes can be done through a two-point discrimination task, whereas in devices with ensemble activation classical psychophysical discrimination tasks such as orientation or direction of motion can be adapted.

Qualitative evaluations of phosphene appearance by patients are essential at the initial assessment of the devices. This should be followed up by methodical testing of phosphene brightness, size, and shape.

1.4.2 *Visual Performance*

The primary aim of artificial vision metrics is to assess enhancements in visual acuity, which represents the smallest spatial detail an individual can consistently perceive. This provides clinicians, funding agencies, and designers a direct comparison to neurotypical vision and lack of vision without the therapy. Traditional methods of measuring visual acuity with optotype charts

such as Snellen or logMAR has been proven challenging with individuals with low vision and sight recovery patients because the lowest threshold of these tests is still higher than what is currently achieved by the sight restoration technologies and the testing requires multiple sessions due to individual variability (Ayton et al., 2020). Optotype charts modified for ultra-low vision such as frACT (Bach, 1996), Berkeley Rudimentary Vision Test (BRVT) (Bailey et al., 2012), or tests specifically targeting a sight restoration technology like BaLM (Bach et al., 2010) are some alternatives suited for individuals with vision lower than logMAR 1.60.

The optotype charts can be generalized to natural viewing conditions in neurotypical individuals but within the sight restoration context, it is important to consider changing percepts when the stimulus is dynamic. This can be due to many reasons: if it is a retinal implant with video capture, the sight recovery patient might have nystagmus that leads to regeneration of the signal; there might be neural adaptation due to continued stimulation; or the kinetics of cell signaling might be alien in a technology like optogenetic therapy. Unlike optotype charts, grating visual acuity and contrast sensitivity tasks can measure temporal sensitivity in addition to spatial contrast sensitivity. Sampling the perception of gratings with a range of spatial and temporal frequencies can inform researchers about the optimal viewing conditions using sight restoration technologies. An example of this approach is the work by Bittner, Jeter, and Dagnelie (2011) where they benchmarked grating visual acuity and contrast sensitivity tasks in patients with severe vision loss due to retinal degeneration. In Chapter 4, we use a contrast sensitivity task to predict visual performance of patients undergoing optogenetic therapy from animal cellular data.

Chapter 2. SPATIAL VISION IN ARGUS II – PSYCHOPHYSICS

Note: Portions of this chapter were published in Yücel et al., (2022).

2.1 INTRODUCTION

In 2013, Argus II developed by Second Sight Medical Products Inc, became the first electrical retinal implant to be approved for commercial market use by FDA following the CE mark granted by EU in 2011. Before then, visual implants were strictly experimental, and patients had access to these devices through clinical trials. The perceptual experience of clinically implanted Argus II patients has been variable (Erickson-Davis & Korzybska, 2021). In many patients a significant proportion of electrodes cannot elicit percepts within safe current density limits (Ahuja et al., 2013), and only limited pattern vision is generated by the device (Arevalo et al., 2021; da Cruz et al., 2016; Stronks & Dagnelie, 2014).

A variety of factors are likely responsible for the limited pattern vision found in Argus II devices (Caspi & Zivotofsky, 2015). These include the decoupling of retinotopic stimulation from eye-position (Caspi et al., 2017), the fact that the percepts produced by the electrodes are not well formed 'pixels' (Beyeler et al., 2019; Luo et al., 2016; Nanduri et al., 2012), and an inability to resolve individual electrodes.

Two-point discrimination (the ability to determine whether one or two percepts are seen when a pair of electrodes are stimulated) is thought to be a particularly useful measure for characterizing the ability to resolve individual electrodes within an array (Ayton, Rizzo, et al., 2020). Unlike other spatial acuity tasks, such as grating acuity or square localization, two-point acuity is not susceptible to blurring by eye-movements. Thus, two-point discrimination is useful for characterizing losses in spatial resolution at a retinal level. An ability to resolve whether one

or two electrodes have been stimulated is *necessary* but not *sufficient* for good visual performance with a prosthetic device; one previous study does suggests a correlation between two-point discrimination and grating spatial acuity in Argus II patients (Lauritzen et al., 2011).

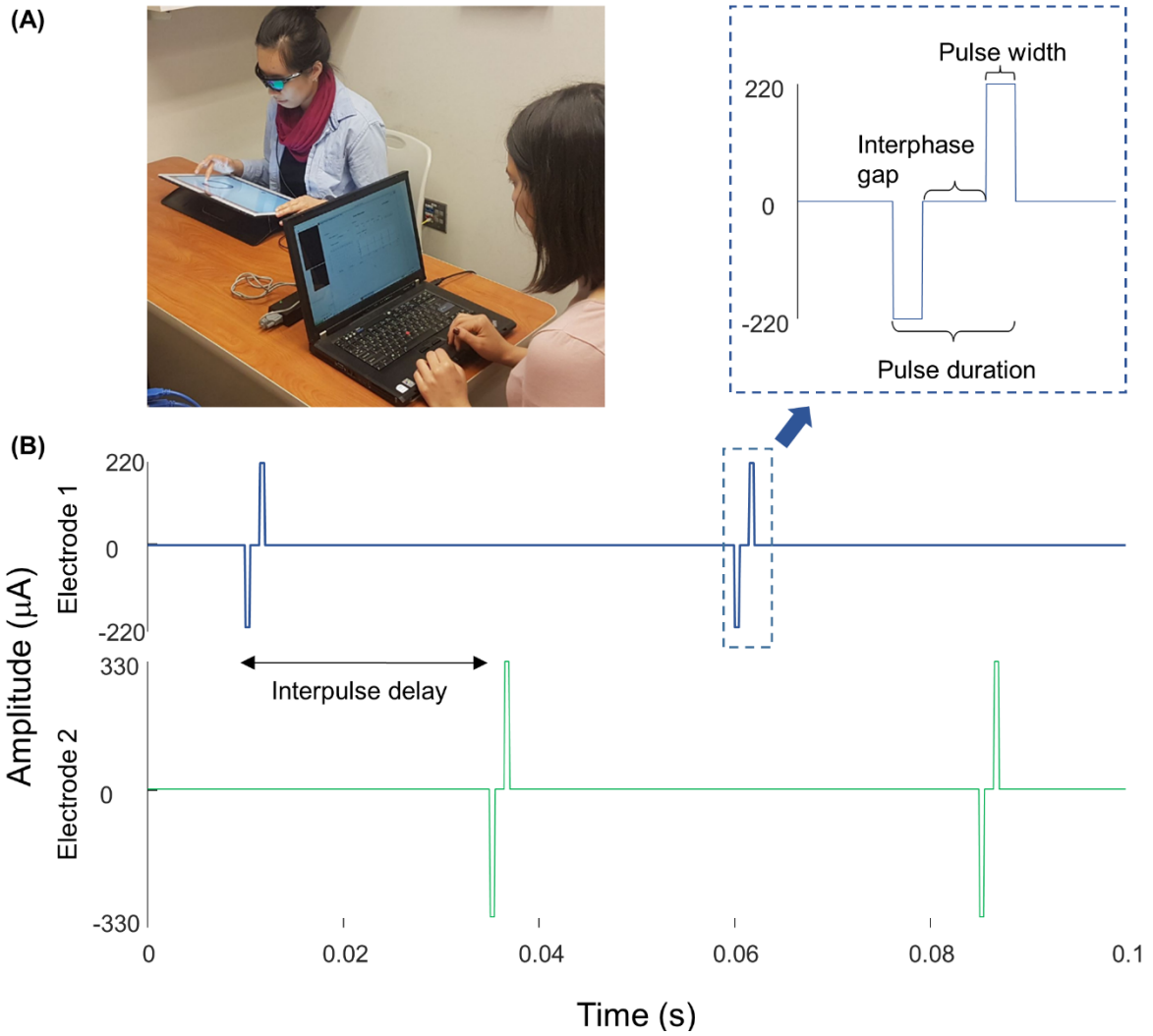

Figure 4 (A) Experimental setup. (B) Example pulse trains for an individual trial (not to scale) of the two-point discrimination paradigm. In all experiments we used square-wave, biphasic, cathodic-first pulse trains with a fixed pulse train duration.

Here we measured both current amplitude thresholds and two-point discrimination performance in three participants diagnosed with severe retinitis pigmentosa and chronically implanted with the Argus II epiretinal prosthesis (Table 1). Electrical stimulation was delivered directly to single or pre-selected pairs of electrodes (Figure 4). We measured single electrode thresholds using a yes-no procedure and measured two-point discrimination thresholds by simulating a pair of electrodes and asking participants both to report the number of phosphenes and draw the phosphene shape(s) on a tablet touch screen.

Having measured current amplitude and two-point discrimination thresholds we used a combination of regression analyses and simulations to examine the role of physical distance between electrodes, amplitude, axonal stimulation, height of the electrode above the retinal surface (lift), and retinal damage, with the goal of examining how these various factors affect both sensitivity and two-point discrimination.

2.2 Single Electrode Stimulation

2.2.1 *Experiment 1: Phosphene Thresholds*

Table 1 Patient demographics. All data reported in this paper were collected at Johns Hopkins University Wilmer Eye Institute.

Participant ID	**Second Sight participant ID**	**Implant**	**Eye**	**Age at Testing**	**Date of Implantation**	**Date of Testing**
S1	12-005	Argus II	Right Eye	83	2009	2019
S2	12-104	Argus II	Right Eye	61	2015	2019
S3	13-101	Argus II	Right Eye	74	2014	2019

Our initial participant pool consisted of nine participants with Argus II retinal prostheses (Second Sight, Inc.): six participants implanted and tested at the Retina Service at the University

of Minnesota, and three tested at the Lions Vision Research and Rehabilitation Center at Johns Hopkins University; one of these patients was implanted at Wills Eye Hospital in Philadelphia, the other two at the Johns Hopkins Wilmer Eye Institute.

Unfortunately, five of the six University of Minnesota participants almost never reported seeing two percepts when stimulated with a pair of electrodes, and one participant who did report seeing two percepts on a reasonable proportion of trials (7/49 in session 1; 35/90 in session 2) also reported seeing two percepts on 6/7 (no stimulation) catch trials. Consequently, we excluded the Minnesota participant data from further analysis.

Of the patients tested at Johns Hopkins, S1 was implanted as part of the Argus II Feasibility Study (clinicaltrials.gov trial NCT00407602), whereas S2 and S3 were implanted after Argus II became commercially available in 2013, see Table 1. The data described in this paper (Johns Hopkins participants) were collected in two sessions, with each session taking roughly three hours, including frequent breaks.

Data were collected at the Retina Service at the University of Minnesota and the Lions Vision Research and Rehabilitation Center at Johns Hopkins University and were provided to UW researchers in a de-identified format. The study was approved by IRBs of the University of Washington and Johns Hopkins University.

2.2.2 *Stimuli*

The Argus II retinal prosthesis consists of an epiretinal electrode array implanted in the macular region of the retina, an ASIC chip, RF transmitter and receiver coil, as well as glasses containing a mini camera (not used in our experiment) and a video processing unit (VPU), see Ahuja *et al.* (2011), for more detail. The signal from the VPU is received by the internal receiver coil, and the ASIC chip generates the electrical pulses that are then sent to the electrode array, a

grid of 6 × 10 platinum disk electrodes in a rectangular grid arrangement with 225 μm diameter and 575 μm center-to-center separation.

We stimulated electrodes directly by connecting the VPU of each participant's device to a psychophysical testing computer provided by Second Sight, Inc., see Figure 4A. Electrode stimulation was controlled by in-house software programmed in MATLAB by Second Sight Medical Products, Inc. (Mathworks, MATLAB Version: 7.1, R14SP3), that sent current waveforms directly to the electrodes (by-passing the camera). Stimuli consisted of biphasic, cathodic-first, charge-balanced, square-wave pulse trains with frequency, interphase gap, interpulse delay (the offset between pulses on different electrodes electrodes) and pulse train duration parameters as shown in Figure 4B and Table 2.

Table 2 Stimulation protocol and parameters for all experiments.

	Patient ID	**Experiment**	**Frequency (Hz)**	**Interphase gap (ms)**	**Interpulse delay (ms)**	**Duration (ms)**
1st Session	S1	Perceptual Threshold	20	0	N/A	250
	S2	Perceptual Threshold	6	1	N/A	250
	S3	Perceptual Threshold	6	1	N/A	250
	S1	Two-point Discrimination	20	0	25	250
	S2	Two-point Discrimination	20	0	25	250
	S2	Two-point Discrimination	6	0	83	500
	S3	Two-point Discrimination	6	1	83	500
	S3	Two-point Discrimination	6	1	83	500
2nd Session	S1	Perceptual Threshold	20	0	N/A	250
	S2	Perceptual Threshold	6	1	N/A	500
	S3	Perceptual Threshold	6	1	N/A	500
	S1	Two-point Discrimination	6	1	83	500
	S2	Two-point Discrimination	6	1	83	500
	S3	Two-point Discrimination	6	1	83	500

2.2.3 *Identifying Electrodes with Lower Perceptual Thresholds*

A proprietary fast threshold estimation procedure, SwiftPA (Second Sight Medical Products Inc, 2013) was used to determine which electrodes had electrical thresholds below the safety limit. Stimulation consisted of 0.46 ms, cathodic-first pulse trains of 1 second duration. Starting from the top left electrode, a yes-no procedure was used to determine whether stimulation produced a detectable phosphene. If participants failed to detect a phosphene the amplitude of the electrical stimulation was increased. If participants reported a phosphene the amplitude was held constant. After 3 consecutive correct detections, testing moved to the next electrode. We limited further testing to a subset of the electrodes which produced 3 consecutive correct detections at a current amplitude below the safety limit (10 electrodes in S1, 7 electrodes in S2, and 10 electrodes in S3). These electrodes were selected to have low thresholds, and to be spread as widely apart as possible on the array.

2.2.4 *Current Amplitude Detection Threshold Measurements*

We then used proprietary software (Argus II-Hybrid Threshold) provided by Second Medical Products Inc. to carry out an adaptive, single interval yes-no procedure to measure detection thresholds (50% detection performance) within electrodes pre-selected by the SwiftPA procedure, methodological details are explained more fully in Ahuja *et al.*, (2013).

To avoid adaptation effects (Horsager et al., 2009; Pérez Fornos et al., 2012) we interleaved threshold measurements across electrodes within each run. Up to six electrodes were tested within a single run. Each trial started with an audio prompt. Then one of the six selected electrodes (selected pseudorandomly) was stimulated at either 20 or 6 Hz, with a pulse train duration of either 250 or 500 ms (depending on what the participants used in their daily life, see Table 2), charge

density limit of 1 mC/cm^2, square-wave pulse width of 0.46 ms, and interphase gap of 0 or 1 ms. The amplitude of the stimulation was adapted through a staircase procedure. The participant was asked to report whether or not they had seen a phosphene on that trial using a game controller (yes/no) and feedback was given on each trial. Each run consisted of a maximum of 60 trials per electrode (5 blocks of 12 trials), for a maximum of 360 trials, and 4 catch trials per block (Second Sight Medical Products Inc, 2013). Each run was followed by a brief rest, which ended based on participant feedback.

Perceptual thresholds for detection at a given electrode were calculated by pooling data across all trials. The probability of reporting a percept as a function of stimulus intensity was fit with a psychometric function using maximum likelihood estimation, and the current amplitude detection threshold was defined as the stimulus amplitude at which the participant reported a percept 50% of the time (Ahuja et al., 2013; Watson & Robson, 1981; Wichmann & Hill, 2001).

2.2.5 *Two-point Discrimination Measurements*

For each participant, we selected electrodes with the lowest detection thresholds and paired them in all possible combinations. Stimulation was carried out at an amplitude twice the detection threshold, or at a maximum of 660 μA (the charge density limit of 1 mC/cm^2/phase for a 0.46 ms pulse). On each trial, we asked "how many shapes did you see" and asked them to draw the phosphene shape(s) on a tablet touch screen.

Parameters used for each participant are shown in Table 2. The pulse width was always 0.46 ms, with an interphase gap of 1 ms for S2 and 3, and no interphase gap for S1, based on the stimulation parameters each individual was accustomed to through daily use. Stimulation was interleaved, with either a 25 ms (20 Hz) or 83 ms (6 Hz) interpulse delay between the beginning

of each pulse on one electrode and the beginning of the corresponding pulse on the second electrode, Figure 4B.

In each experimental run, every possible pair of electrodes was tested 3 times. On each trial, participants verbally reported the number of shapes they were seeing, gave a qualitative description (e.g., “the one on the bottom is smaller,” “left one is twice as big as right one—they are side by side”) and traced the perceived phosphene shape(s) on a tablet (drawing data not reported here). Although the “correct” answer was always two percepts, participants were never given feedback as to how many electrodes had been stimulated. Importantly, the number of shapes drawn by the participant was almost always consistent with the number of shapes they verbally reported, suggesting that they were not reporting whether they saw one or two shapes on the basis of the overall brightness or size of the percept.

We included ~25% of catch trials, randomly interspersed, in which neither of the electrodes was stimulated. We deliberately used no stimulation as compared to single electrode stimulation during catch trials, because we were concerned that differences in brightness or size might allow participants to differentiate between single and paired stimulation in the absence of genuine pattern vision.

The order of the trials was pseudorandomized. We asked participants to avoid head and eye movements to maximize stability of the perceived phosphene locations, but to maximize participant comfort we did not use a chin rest.

2.2.6 *Results*

2.2.6.1 Current Amplitude Thresholds

Table 3 Current amplitude detection thresholds (50% detection performance) and reports of daily usage.

	Median threshold (µA)	**Interquartile range (µA)**	**Minimum threshold (µA)**	**Maximum threshold (µA)**	**Daily use**
S1	274	218-331	153	484	3-4 days a week, 3-5 hours a day, for an average of 20 hours a week
S2	476	355-621	217	645	Approximately once a month
S3	210	177-280	89	323	Used the device almost every day outdoors, for a limited amount of time, averaging about 2 hours a day.

Table 3 shows 50% current amplitude detection threshold values and self-reported daily usage for all three participants, and Figure 5 shows a histogram of current amplitude threshold values for all participants.

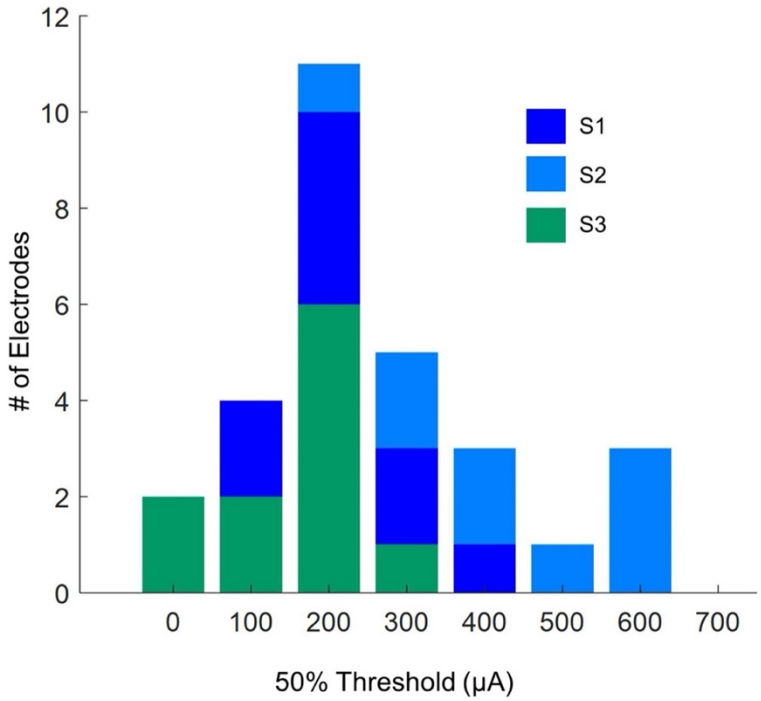

Figure 5 Histogram of current amplitude detection thresholds (50% detection performance).

Although we did not formally measure thresholds on all electrodes due to time constraints, we found that a significant proportion of individual electrodes did not elicit phosphenes using the SwiftPA procedure.

On the whole, the electrode sensitivity of our subject group seems comparable to that reported in other studies. In a previous study by Ahuja et al. (2013), detection thresholds could not be estimated within the range of amplitudes permitted by charge density safety limits in a significant proportion of electrodes (0-83% depending on participant). In a study by Naidu and colleagues (2020), thresholds could only be measured in 60% of electrodes. Xu and colleagues (2021) similarly could not measure individual thresholds in a significant proportion of electrodes.

2.2.7 *Two-Point Discrimination Thresholds*

In the paired electrode stimulation experiment, we asked the question "*How many shapes did you see?"* Participants could potentially report any value, and they were then asked to draw what they saw. Table 4 shows the reported number of percepts and the probabilities of each verbal response.

Given that we always used paired electrode stimulation, we were concerned that participants might shift their criterion for reporting two percepts over the course of the experiment. However, there was little evidence that the probability of participants reporting two (or more) percepts changed substantially either within or across sessions (although it should be noted that electrode pairs varied between sessions, Table 5, which may have masked some experience driven effects). For S3 there was a significant increase in the probability of reporting two percepts between the first and second ½ of trials in session 2. The reason for this is not clear but might possibly be due to an improved ability to recognized two percepts with experience. Since there was little effect of time on our two-point discrimination data, we did not use time as a factor in our

further analyses. The number of shapes participants drew consistently matched their verbal report, throughout every session.

The probability of reporting 1 or 2 (or more) percepts during catch trials (with no stimulation) also remained reliably low throughout the experiment (S1:0/15 trials, S2:2/12 trials, S3: 0/16 trials).

Table 4 Reported number of percepts and their frequency and probability in the two-point discrimination experiment.

Participant	Reported number of percepts	Frequency	Probability P("X"|2)
S1	"0"	0	0.00
	"1"	66	0.31
	"2"	114	0.69
	"3"	0	0.00
S2	"0"	2	0.04
	"1"	29	0.54
	"2"	20	0.37
	"3"	3	0.06
S3	"0"	0	0.00
	"1"	38	0.36
	"2"	67	0.64
	"3"	0	0.00

Table 5 Probability of reporting two percepts, within and across sessions.

Participant	Session	1st half of trials in session	2nd half of trials in session	Unique Electrodes Tested
S1	Session 1	0.73 [0.48,0.89]	0.93 [0.7, 0.99]	A4, A8, D1, E10, F2
	Session 2	0.68 [0.57, 0.77]	0.50 [0.4, 0.62]	A2, A4, A8, B3, B6, D1, D8, E10, E3, F2, F7
S2	Session 1	0.33 [0.12, 0.65]	0.56 [0.27, 0.81]	B6, B9, F7, F9
	Session 2	0.39 [0.2, 0.61]	0.44 [0.25, 0.66]	A10, B10, B5, B6, B9, F7, F9

2.2.8 *OCT Data*

Unfortunately, it was impossible to collect useable optical coherence tomography (OCT) images for the region of the retina including the array in S2 and S3. OCT data from S1, two years after implantation (2011), are shown in Figure 6. In this patient the array appears to be flush to the retinal surface, but there is some thickening (evidence of potential damage) of the retina underneath the array.

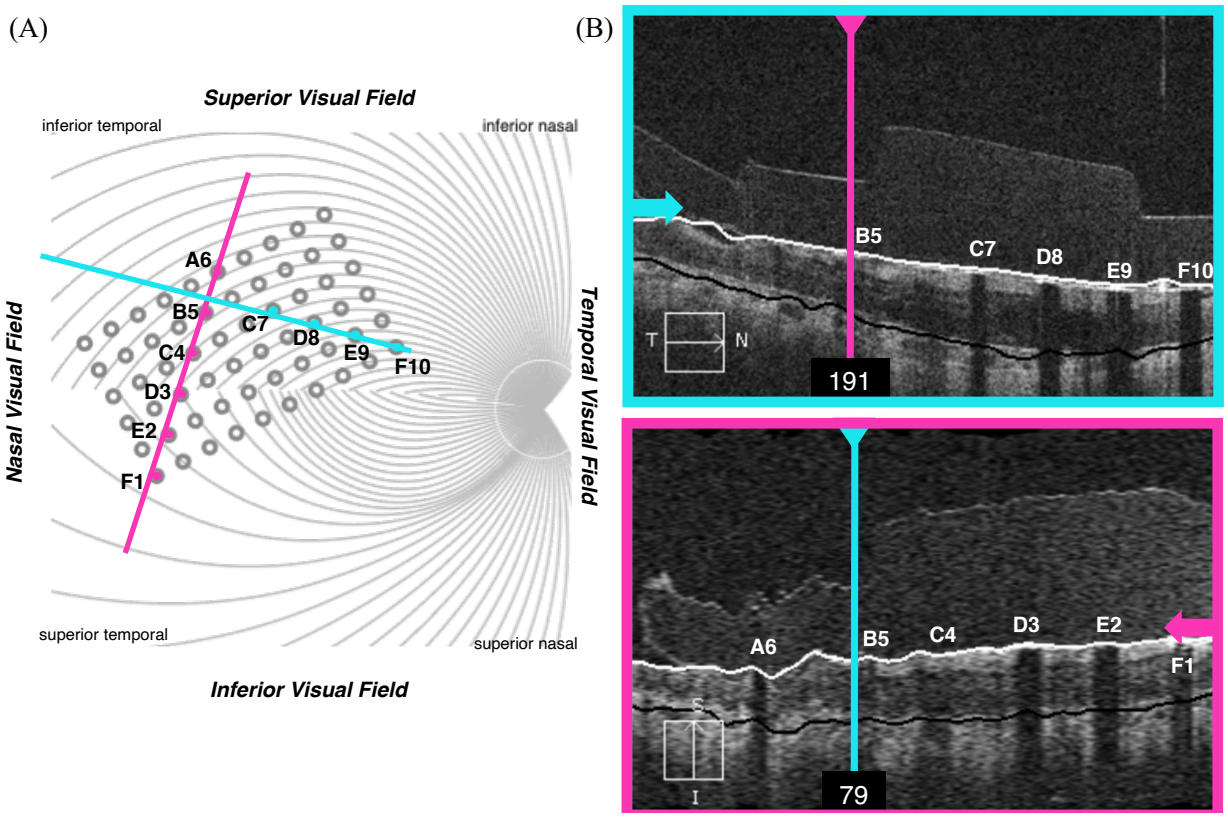

Figure 6 OCT data from participant S1. (A) Schematic showing the estimated location of OCT b-scans overlaid on the array (alignment was carried out using the registered OCT fundus image). The array schematic is flipped along the y-axis to reflect visual space coordinates, such that the top of the schematic represents the superior visual field and the inferior retina. (B) The metal electrodes block light from the scanning light source, casting shadows on the retinal image.

2.2.9 *Relationship with device use*

In a separate questionnaire, participants were asked how often they used their device. Participants varied widely in device use, see Table 3. S1, who had a median amplitude threshold of 274 μA and saw 2 percepts 69% of the time with paired stimulation, used the device most consistently, reporting using the device 3–4 days a week, 3–5 h a day, for an average of 20 h a week. S3, who had a median amplitude threshold of 210 μA and saw 2 percepts 64% of the time with paired stimulation, used the device almost every day when outdoors, but for a limited amount of time, averaging about 2 h a day. S2, who had a median amplitude threshold of 476 μA and saw 2 percepts only 37% of the time with paired stimulation, reported using the device once a month.

Chapter 3. SPATIAL VISION IN ARGUS II – MODELING

Note: Portions of this chapter were published in Yücel et al., (2022).

3.1 SIMULATION OF ARTIFICIAL VISION

Computational models play a crucial role in accurately describing the outcomes of artificial vision enabled by sight restoration technologies. The biggest implication is the usage of model outputs for stimulation protocols to further improve artificial vision. For example, for electrical implants, the working principle of considering every electrode as a 'pixel' like a scoreboard, or 'linear scoreboard model', fails in behavioral measurements where patients with implants report percepts other than circular, localized phosphenes (Beyeler et al., 2019). Prediction of artificial vision is important not only for the engineers or scientists but also for setting clear expectations for patients and regulators.

In the past two decades, the need for more realistic models with better predictive performances led to two main approaches: biophysical and perceptual models of artificial vision. Biophysical models such as Golden et al., (2018), Tong et al., (2020) or Vilkhu et al. (2021) focus primarily on simulating a network of biologically viable cells and compute their responses to visual stimuli. While this approach is most appropriate for sight restoration technologies that can target specific cell types such as molecular therapies, as suggested in the examples given earlier, they can predict cell signaling at high spatial and temporal resolutions.

Perceptual or phenomenological models tackle the problem from the opposite angle. Based on patient reports and behavioral measures the main idea is to 'reverse-engineer' the input-output relationship between the sight restoration technology and the user's percepts. Pulse2Percept

(Beyeler, Rokem, et al., 2017; Beyeler et al., 2019; Nanduri et al., 2008) developed by our group for the past decade is a good example, it was primarily driven by the desire to provide more realistic computational descriptions of patients' perceptions. To achieve this, we utilized a diverse set of psychophysical data obtained from behavioral responses to simple patterns of electrical stimulation in clinical and commercial Argus II population. These patterns included tasks such as brightness-matching across two electrodes or visual representations of perceptual outcomes resulting from stimulating one or two electrodes. The latest version of Pulse2Percept can now predict perceptual responses to stimulation generated by PRIMA and BVT24 in addition to Argus II.

The earlier version of Pulse2Percept (Nanduri et al., 2008) was based on a dataset that was collected from a small number of patients implanted during the early critical trials. We then collected data from two other clinical sites (University of Minnesota and Johns Hopkins University Wilmer Eye Institute) where we had the chance of working with patients who were implanted with Argus II after its commercialization. This way, we could (1) validate the past findings and (2) see if we can make any generalizations across the Argus II user population.

Pulse2Percept is a suite of Python based modules that can simulate a retina, various types of electrical implants, and computational models that estimate neural responses or visual percepts (Beyeler et al., 2017).

One issue related to epiretinal implants is the stimulation ganglion axonal bundles. Using Pulse2Percept, we could simulate a map of axonal bundles on the stimulation area to predict shapes of the percepts when a single electrode were stimulated (Beyeler et al., 2019). It was found that for Argus II, the position of the stimulated electrode predicted the shape of the percept. A natural question that followed was whether the change in shape and size of the percepts would affect the

functional spatial resolution provided by Argus II. To do so, we used the behavioral data discussed in Chapter 2 to predict functional electrode-electrode distance and modeled whether two-point discrimination in Argus II patients shifted due to axonal stimulation.

3.2 Estimating Electrode-Electrode Distance to and along Axonal Bundles

As an initial step we estimated distance to and along axonal bundles for each pair of electrodes. Both electrophysiological (Fried et al., 2009) and psychophysical data (Beyeler et al., 2019) suggest that axonal stimulation may contribute significantly to the poor resolution of retinal prostheses. Axonal stimulation is a particular concern for epiretinal prostheses, such as the Argus II which are placed on the nerve fiber layer, adjacent to the axon fiber bundles of retinal ganglion cells. Depending on stimulus conditions, participants implanted with the Argus II describe the phosphenes generated by epiretinal electrical stimulation of single electrodes as elongated, due to activation of passing axon fibers, resulting in perceptual distortions (individual electrodes producing 'streaks' instead of punctate spots) that vary in their length and orientation across the retinal surface in a way that can be predicted based on the known axon fiber trajectories (Beyeler et al., 2019; Nanduri et al., 2012).

It is not yet entirely clear how sensitivity to electrical stimulation falls off as a function of distance from the initial segment (Fried et al., 2009), with psychophysically estimated decay constants ranging widely from 500–1,420 μm (Beyeler et al., 2019). Nonetheless, if axonal stimulation plays a significant role in reducing resolution, then distance, both to and along a shared axon bundle should predict how many distinct percepts are seen when two electrodes are stimulated.

3.2.1 *Methods*

To provide a measure of the distance to and along axon bundles we used an existing computational model developed by Beyeler et al. (2019). This model begins by using ophthalmic fundus photographs in which an eye care provider marked the optic nerve, fovea, and the center of the implant on the fundus, using photos taken pre- and post-surgery. These landmarks were then used to estimate the array center with respect to the fovea, the array rotation with respect to the horizontal raphe, and the retinal distance between the fovea and the optic nerve head for each participant, see Figure 7. In the human retina, the extended raphe is typically located 15° ± 2° inferiorly to a horizontal line at the latitude of the fovea through the center of the optic disc. We approximated this by fitting a parabola centered on the optic nerve and approximating the horizontal raphe as parallel to the axis of symmetry on the abscissa (Jansonius & Schiefer, 2020). The spatial layout of axonal pathways was calculated using *pulse2percept* software (Beyeler, Boynton, et al., 2017a), that simulates pathways using a model (Jansonius et al., 2009) that assumes that the trajectories of the optic nerve fibers can be described in a modified polar coordinate system (r,ϕ) with its origin located in the center of the optic disc. Each nerve fiber is modeled as a spiral defined by the angular position of the trajectory at its starting point at a circle around the center of the optic disc, with a second parameter describing the curvature of the spiral.

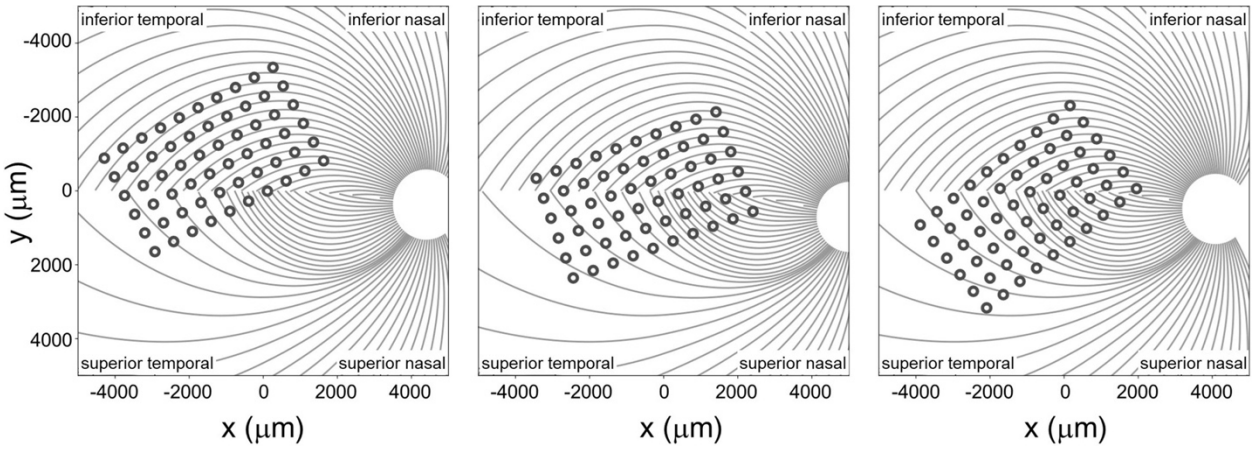

Figure 7. Estimated position of the electrode array on the retinal surface for all three participants (see Beyeler et al 2019 for estimation methods) overlaid on estimates of the axon fiber pathways for that participant. Note that all panels are in visual space coordinates, with the upper visual field at the top of the figure.

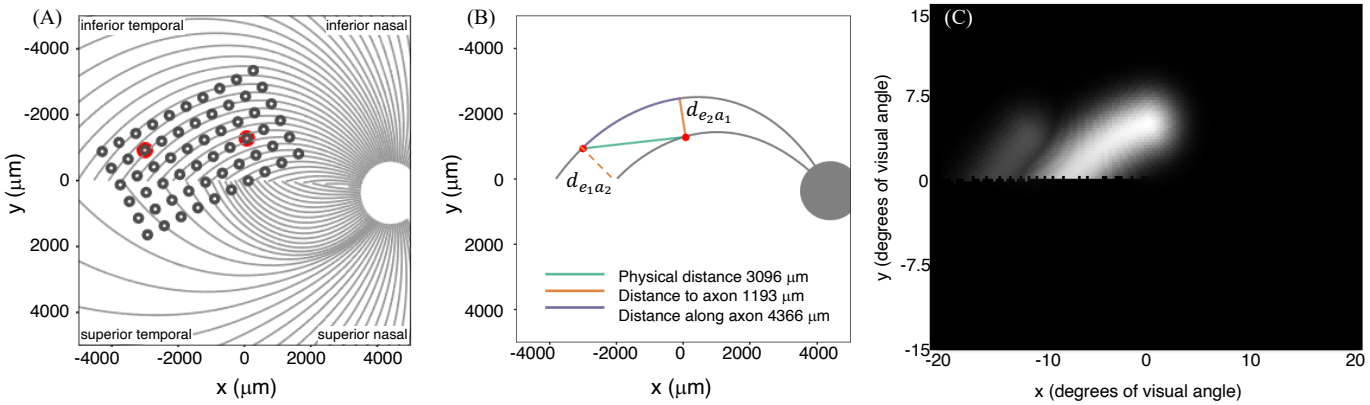

Figure 8. (A) Estimated position of the electrode array on the retinal surface for S1 (replotted from Figure 7A) (B) Examples of distance to and along axon fibers, $\boldsymbol{d_{e_1a_2}}$ and $\boldsymbol{d_{e_2a_1}}$ refer to the shortest distance from an electrode to the axonal bundle closest to fellow electrode (C) Predicted percept for the two electrodes shown in Panels A & B. Note that all panels are in visual space coordinates, with the upper visual field at the top of the figure.

Given that the size of the Argus II electrodes is large compared to the density of the underlying axon pathways, it was assumed that an electrode always sits on top of a ganglion axon fiber bundle. We simulated 400 axonal bundles, which provided sufficient resolution to ensure that there was an axonal bundle underneath every electrode.

We defined three inter-electrode distance values:

1. ***Physical distance*** was defined as the Euclidean center-to-center distance between two electrodes on the retinal surface.
2. ***Distance to axon*** ($d_{axon_{12}}$) was defined as the minimum distance between two electrodes (e_1, e_2) and the axons closest to them, Figure 8. This was calculated by:
    a. Selecting the axonal bundles a_1 and a_2 that fell beneath each of the two electrodes.
    b. Determining the closest Euclidean distance from the center of each electrode to the fellow axon bundle: $d_{e_1a_2} = \min[d(e_1, a_2)]$ and $d_{e_2a_1} = \min[d(e_2, a_1)]$
    c. Choosing the minimum distance of the pair, $d_{axon_{12}} = \min\left[d_{e_1a_2}, d_{e_2a_1}\right]$.

    (An alternative would have been to calculate the distance to the axon bundle midway between the two electrodes, but this would have essentially resulted in the same values, halved).
3 ***Distance along axon*** was defined as the distance between an electrode and the point on its axon that is closest to the axon of the other electrode.

3.2.2 *Results*

These three measures of distance on the retina were strongly correlated with each other. The Pearson correlation coefficient between physical distance and distance to axon was $r(337)= 0.58$, $p<0.0001$, between physical distance and distance along axon was $r(337)= 0.84$, $p<0.0001$, and between distance to axon and distance along axon was $r(337)= 0.28$, $p<0.0001$.

Intuitively, the reason for this is that (except when electrodes are on the opposite side of the Raphe) the shortest distance to the axon (orange line in Figure 8B) tended to fall along a line that was close to orthogonal to the distance along the axon (purple line), since axonal bundle curvature (purple

line) tended to be relatively small. As a result, these three distances form the edges of an approximate right triangle, with the hypotenuse as the Euclidean distance between two electrodes (green line) and distance to and along the axon (with a slight curvature) forming the other two sides. Because these three co-varying distance variables essentially contain 2 degrees of freedom, we only included physical distance and distance to axon as predictive factors in our modeling.

3.3 Regression Models

Next, we fit nested linear logistic models to determine which factors - physical distance between electrodes, mean amplitude of the currents of two electrodes, and distance to axon (as estimated in modeling stage I), best predicted our psychophysical data.

3.3.1 *Methods*

The probability of participants reporting 2 (or more) shapes when 2 electrodes were stimulated, P('2'|2), was modeled using logistic regression. We used a maximum likelihood chi-squared test to determine whether adding parameters improved model fits. Across all analyses that included current amplitude as a factor, subject identity had little additional predictive value and so it was not included as a factor.

Regression was done both using a two-factor model with inter-electrode distance and mean stimulation amplitude of the two electrodes as predictors, and with a three-factor model that included distance to axon across the pair of electrodes as a third predictor.

3.3.2 *Results – Two Factor Model*

We began with a two-factor model that included (1) inter-electrode distance and (2) the mean stimulation amplitude of the two electrodes as predictors.

A maximum likelihood chi-squared test shows that both factors statistically improved the fit to the data, Table 6.

Table 6. Logistic regression model parameters and statistical significance. The intercepts are not included in the table but are included in Equations 1 and 2.

		Estimate	**95% CI**		$\chi^2(1)$	**Pr(>χ^2)**
			lower	**upper**		
2-factor model	**Amplitude**	-0.003014	-0.005144	-0.000883	7.87	0.005022
	Physical Distance	0.000829	0.000575	0.001084	50.64	<.0001
3-factor model	**Amplitude**	-0.003	-0.005145	-0.000840	7.61	0.005802
	Physical Distance	0.000602	0.000309	0.000895	18.40	<.0001
	Distance to Axon	0.000503	-0.000876	-0.000129	7.20	0.007279

The best-fitting two-factor model predicts the probability of seeing two percepts as:

$$P(\text{"2"}|2) = \exp\left(-0.0599 - 0.00314(Mean\ Amplitude) + 0.000829(Distance)\right) \quad \text{Eq. 1}$$

Figure 9A shows the binned participant performance values and the surface predicting the probability of reporting 2 percepts based on the logistic regression model.

Figure 9B shows predicted 65%, 75% and 85% two-point discrimination iso-performance curves based on the surface of

Figure 9A.

As expected, the probability of seeing two percepts increased as a function of physical distance and decreased as a function of mean amplitude. We used this two-factor logistic regression model fit, whose surface is shown in

Figure 9A, to define the two-point discrimination threshold as the inter-electrode distance for which participants should report two percepts on 75% of trials at each participant's median current

amplitude detection threshold (S1 = 2394 µm/8.3°, S2 = 3127 µm/10.9°, S3 = 2161 µm/7.5°; reported in microns on the retina and degrees of visual angle, assuming a conversion of 288 µm = 1° (Drasdo & Fowler, 1974), shown with black bars in Figure 10A. For comparison, the approximate size of the Argus II prosthetic array was 3675 × 5975 µm/12.8x21°, with a distance between neighboring electrodes of 575 µm/2°. Thus, a spacing of about four electrodes is needed to report two percepts on 75% of trials.

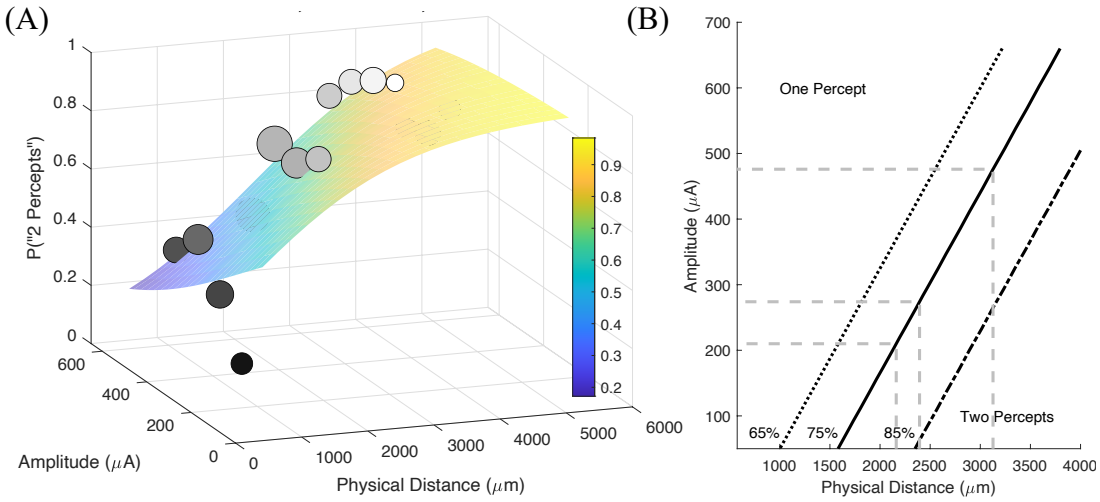

Figure 9. (A) Surface predicting the probability of reporting 2 percepts using logistic regression with mean detection threshold amplitude and physical distance as fixed factors. Individual data points are generated by binning the data (collapsed across participants) and calculating the probability of seeing two percepts in each bin. The grey-scale shade of the data point represents the probability of seeing two percepts, the size of the data point represents the number of observations in that bin. Surfaces were fit to the original trial-by-trial un-binned data. (B) 65%, 75% and 85% two-point discrimination iso-performance curves as a function of amplitude and physical distance. Gray dashed lines show predicted two-point discrimination thresholds for electrodes at the median current amplitude threshold values for S1-S3.

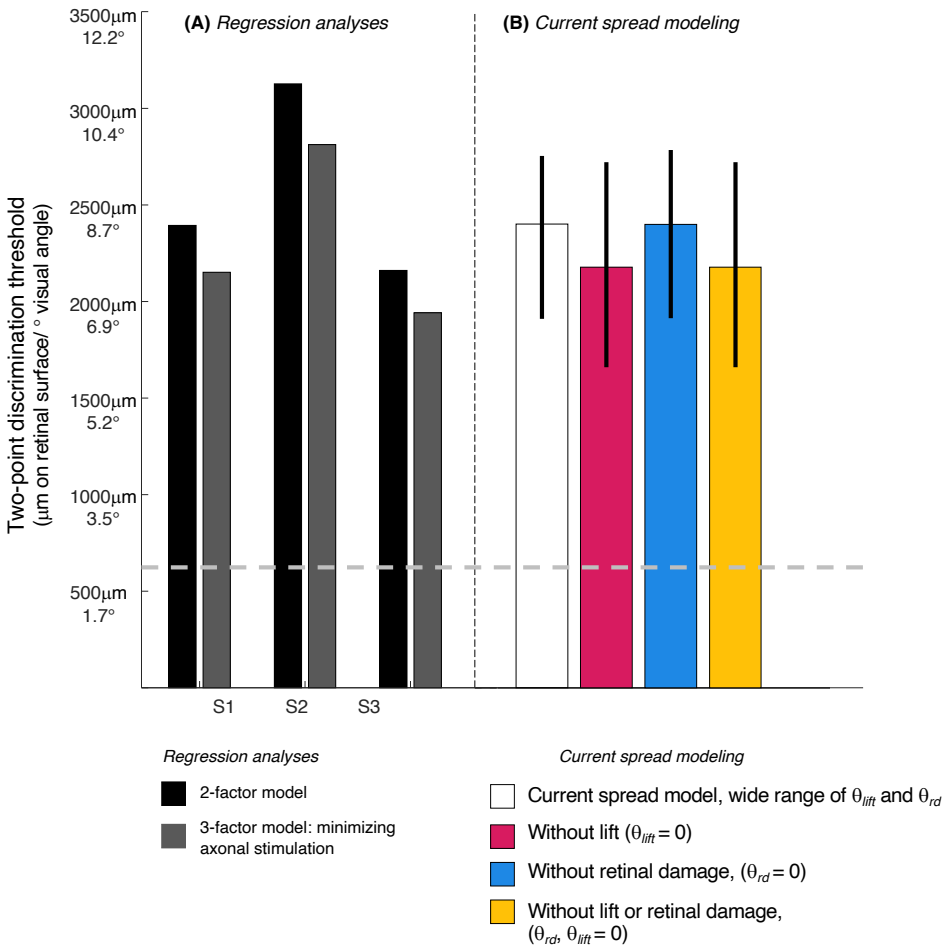

Figure 10 Predicted two-point discrimination thresholds. The gray dashed line shows the resolution limit (2°) that would be obtained if individuals saw two-points when neighboring electrodes were stimulated (Stronks & Dagnelie, 2014). (A) *Stage II. Regression analyses.* Black bars: The predicted 75% two-point discrimination thresholds with current amplitudes set to each participant's median current amplitude detection threshold; Gray bars: The predicted 75% two-point detection thresholds if axonal stimulation is minimized. (B) *Stage III. Current spread modeling.* Empty bar: Predicted 75% two-point discrimination thresholds across the full range of simulation parameterizations that could predict the iso-performance contour predicted by regression analyses; Blue bar: Predicted 75% two-point discrimination thresholds with no retinal damage ($\theta_{rd} = 0$); Pink bar: Predicted 75% two-point discrimination thresholds with the electrode flush to the retinal surface ($\theta_{list} = 0$); Yellow bar: Predicted 75% two-point discrimination thresholds with no retinal damage and the electrode flush to the retinal surface (θ_{rd}, $\theta_{list} = 0$). Error bars represent the 5-95% confidence range of simulation outcomes.

3.3.3 *Results – Three Factor Model*

Distance to axon also had significant predictive value, as shown in. Within this 3-factor model, the ability to predict whether one or two percepts were reported was best modeled as:

$$P(\text{"2"}|2) = \exp\big(-0.1839 - 0.0030(Mean\ Amplitude) + 0.000602\ (Distance) + 0.000502581(Distance\ to\ axon)\big) \quad \text{Eq. 2}$$

As noted above, physical distance and distance to axon were strongly correlated. Correlations between independent variables do not reduce the predictive power of a model but it becomes difficult to disentangle the separate effects of each explanatory variable on the explained variable (Kutner, 2005). Thus, the beta weights of regression Equation 2 should be interpreted with caution.

Therefore, to estimate the size of the effect of axonal stimulation on two-point discrimination thresholds we began with the 2-factor regression model described in Equation 1 and

Figure 9, fixed the best-fitting factor weights for these two factors, then added distance to axon as an additional factor. This allowed us to calculate the probability of reporting two percepts when the distance to axon was zero (i.e. the two electrodes fell on the same axon bundle, shown in the lower surface of Figure 11A) vs. when the distance to axon was equal to the physical distance (i.e. axonal stimulation was minimized, upper surface of Figure 11A).

Figure 11B shows 75% iso-performance contours for these upper and lower surfaces. As expected, the effects of axonal stimulation are smaller when the physical distance between the two electrodes is small. According to the model, if axonal stimulation were minimized, the physical distance between the electrodes that would result in a 75% two-point discrimination threshold for each participant's median current amplitude threshold would be S1 = 2151 μm/7.5°, S2 = 2812 μm/9.8°, S3 = 1942 μm/6.7°, respectively, shown by the dark gray bars in Figure 10.This

corresponds to a reduction in the two-point distance threshold of ~0.8° for S1 and S3, and ~1.1° for S2.

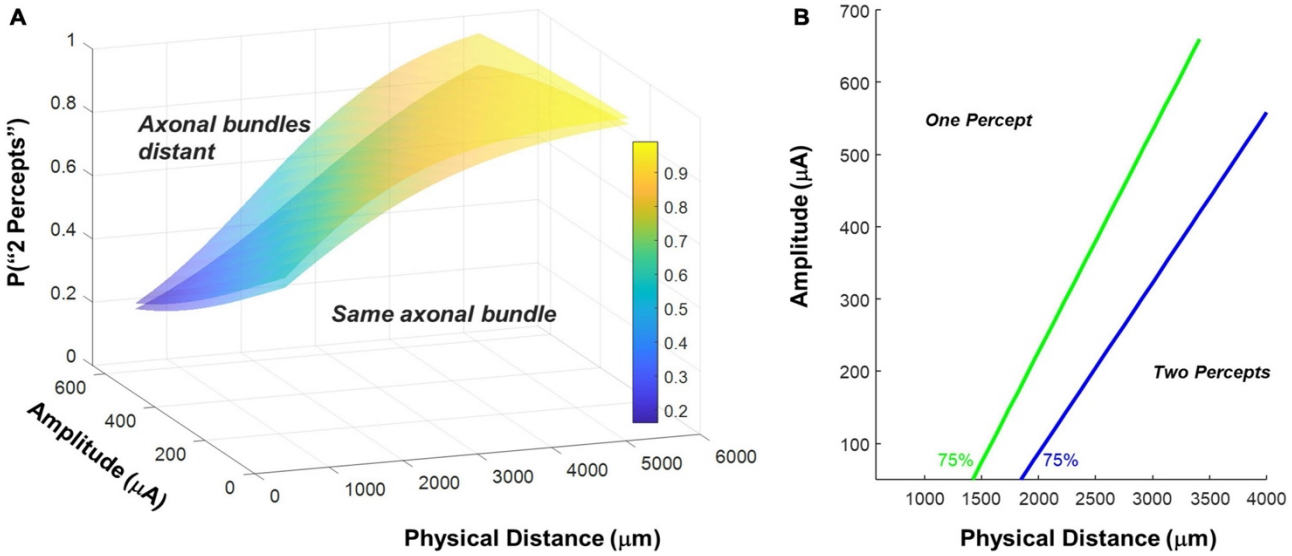

Figure 11. (A) Surfaces based on fitting the probability of reporting 2 percepts using logistic regression with amplitude and physical distance as fixed factors. Having fixed the weights for amplitude and physical distance, we included distance to axon as a factor. The lower surface represents predictions for distance to axon = 0 (the two electrodes fall on the same axonal bundle), the upper surface represents predictions for distance to axon = physical distance (minimizing axonal stimulation). (B) 75% two-point discrimination iso-performance curves as a function of amplitude and physical distance for distance to axon = 0 (the two electrodes fall on the same axonal bundle), and distance to axon = physical distance (minimizing axonal stimulation).

3.4 Current Spread Models

Having estimated the effect of axonal stimulation on two-point discrimination performance, we simulated a simplified 'scoreboard' model to identify how retinal damage and lift might influence both amplitude and two-point discrimination thresholds. According to the scoreboard model, the main determinant of whether one or two percepts are seen will be the

overlap of the current fields generated by the electrodes on the retinal surface. This overlap is affected by the physical distance between the electrodes along the retinal plane, 'lift' of the electrodes from the retinal surface, and the current amplitude on the electrodes.

As lift increases, so does the current amplitude required to elicit a percept. A larger current amplitude at a greater distance from the retina results in a broad current spread on the retinal surface. Extensive psychophysical work with early participants implanted with the Argus I and II devices has shown that, for individual electrodes, it is possible to predict the size, threshold and brightness of suprathreshold phosphenes as a function of frequency and amplitude, with reasonable accuracy, once the height of the electrode off the retinal surface is included as a factor (Ahuja et al., 2013; de Balthasar et al., 2008; Horsager et al., 2009; Nanduri et al., 2012).

Various types of retinal damage may also increase the current needed to generate a percept and thereby affect amplitude thresholds possibly two-point discrimination. Possible causes of retinal damage include severe disease-related degeneration, damage to the retina as a result of surgical implantation, or damage caused by the presence of the array. A variety of studies have found evidence suggestive of retinal damage in retinal prosthesis patients (Gregori et al., 2018; Lin et al., 2019; Patelli et al., 2020; Rizzo et al., 2019). The damage seems to have a variety of causes including inflammation, 'boggy' (*sic*) thickening, schisis and fibrosis, intraretinal fluid (IRF) cysts, as well as a "snowplow" effect of the electrode array pressing against the retina and causing adjacent thickening (Gregori et al., 2018; Patelli et al., 2020). While many of these conditions are common in late stage RP patients, they seem to be exacerbated in the implanted eye (Lin et al., 2019). In addition, over time many patients also develop membranes (both adherent to and separated from the retina) between the retina and the array. For example, Patelli and colleagues (2020) observed in one patient the formation of retinal fibrosis and schisis within two years of

implantation which resulted in higher thresholds in 34 out of 60 electrodes. After the removal of retinal fibrosis, 20 out of 60 electrodes were reactivated; suggesting this fibrosis was responsible for reducing electrode sensitivity.

3.4.1 *Methods*

We simulated current spread as a function of 3D distance from the edge of the electrode as follows:

$$I_{xyz} = \frac{I_0}{1+(k*r)^a} \qquad \text{Eq. 3}$$

Where I_0 is the stimulating current and r is the 3D distance from the edge of the electrode (Ahuja et al., 2008). Parameters k and a describe current spread. The range of k and a values were chosen to approximate previous psychophysical data describing threshold as a function of lift (Ahuja et al., 2013; de Balthasar et al., 2008), and be consistent with more elaborate neurophysiological models (Esler et al., 2018). The parameter a varied between 1-3, and k varied between 6-20, providing a parameterization of current spread that widely spanned the neurophysiologically plausible range. For both a and k, larger values represent higher amounts of tissue electrical resistance, so current amplitudes drop more quickly as a function of r.

Figure 12 shows two example simulations for a pair of electrodes, separated by d = 1400μm, a = 1.5, k = 15, lifted by 150μm and 750μm above the retinal surface. The higher an electrode is lifted off the retinal surface, the greater the electrode current required to produce an electric field gradient sufficient to elicit spikes in the axons passing through the retinal surface. The bottom panels represent a top view, showing current at the retinal plane. Both simulations of Figure 12 have a maximum current value of 100μA at the retinal surface, however the region of high current is much broader for the electrode pair that are lifted 750μm above the retinal surface.

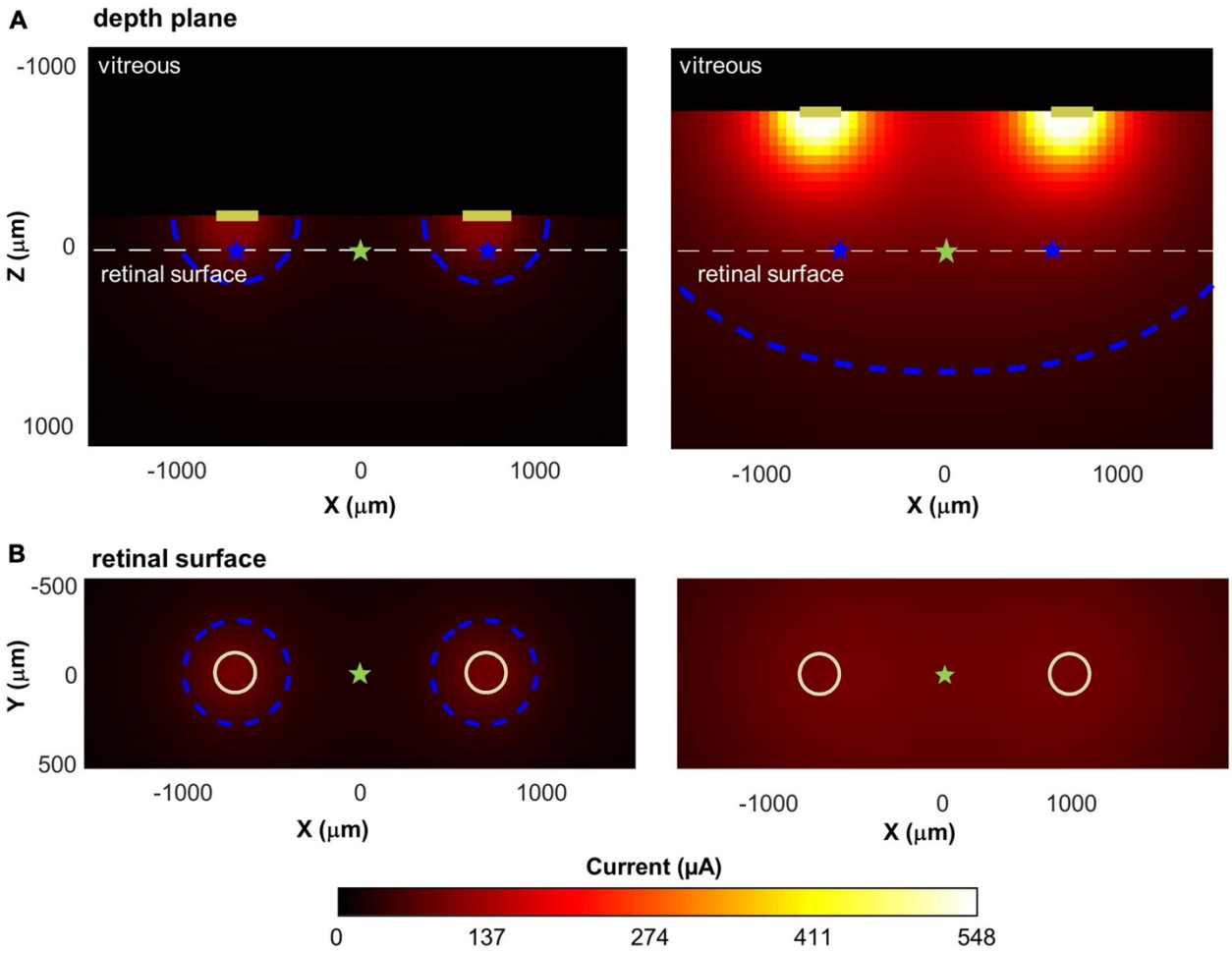

Figure 12. Illustration of current spread for two pairs of disc electrodes, separated by 1400μm, with different lifts from the retinal surface. Top: Cross-sectional view through the retina; Bottom: View of the retina from above. Current amplitude at the electrode was fixed to produce a maximum of 100μA of current on the retina. (A) Lifted 150 microns above the retinal surface. (B) Lifted 750 microns above the surface. The white dashed line in the upper panels shows the location of the retinal surface. Blue contour lines in each panel represent 50 μA; cyan star: the intermediate point between the electrodes; blue star: the point of maximum current on the retinal surface.

Thus, for electrodes that are lifted off the surface, the increased overlap between the current fields is likely to reduce the ability to differentiate two distinct phosphenes. We represented this overlap by calculating the decrease in current amplitude at the point intermediate between the

electrodes (I_{mid}, cyan stars) compared to the point of maximum current (I_{max}, blue stars), on the retinal surface. This 'dip' in current was calculated as:

$$dip = 100\left(\frac{I_{max}-I_{mid}}{I_{max}}\right) \quad \text{Eq. 4}$$

In Figure 12, when electrodes are lifted 150μm above the retinal surface (Panel A), I_{max} = 100μA, I_{mid} = 26μA, *dip* = 74%, whereas when electrodes are lifted 750μm above the retinal surface (Panel B), I_{max} = 100μA, I_{mid} = 93μA, *dip* = 7%.

We assumed that the measured threshold current for seeing a percept at an electrode (I_0) could be described as a multiplicative combination of three factors:

$$I_0 = \theta_{lift}.\theta_{rd} \cdot \theta_{baseline} \quad \text{Eq. 5}$$

$\theta_{baseline}$ is the current required to elicit enough spikes to reach psychophysical threshold for an electrode flush to the retinal surface in an RP patient whose retina is undamaged. We fixed $\theta_{baseline}$ = 50μA, based on the maximum sensitivity observed in previous psychophysical data (Ahuja et al., 2013; de Balthasar et al., 2008; Horsager et al., 2009).

θ_{lift} represents a multiplicative increase in electrode current required as a result of the electrode being lifted above the retinal surface. The value of θ_{lift} is monotonically increasing as a function of lift, with a nonlinear curve that depends on *a* and *k*, as described by Eq. 3.

θ_{rd} represents an additional multiplicative increase in the current amplitude required to reach threshold, which we propose is likely due to various types of retinal damage.

We simulated a wide range of *k*, *a,* θ_{rd}, and θ_{lift} (corresponding to lifts of 0-1000 μm) for single electrodes. For each combination of parameters, we used least squares function minimization to find the electrode current, I_0, required to reach threshold for that parameterization.

We then simulated pairs of electrodes across a wide range of physical distances (*d* = 250-8000 μm). Stimulation amplitude was fixed at twice threshold for that parameterization (or 660μm,

whichever was smallest). For each parameterization we calculated *dip*. A final parameter, *dip criterion,* is the dip value that results in a 75% two-point discrimination performance. We assumed that a 75% probability of seeing two percepts required a dip criterion>20%.

3.4.2 *Results*

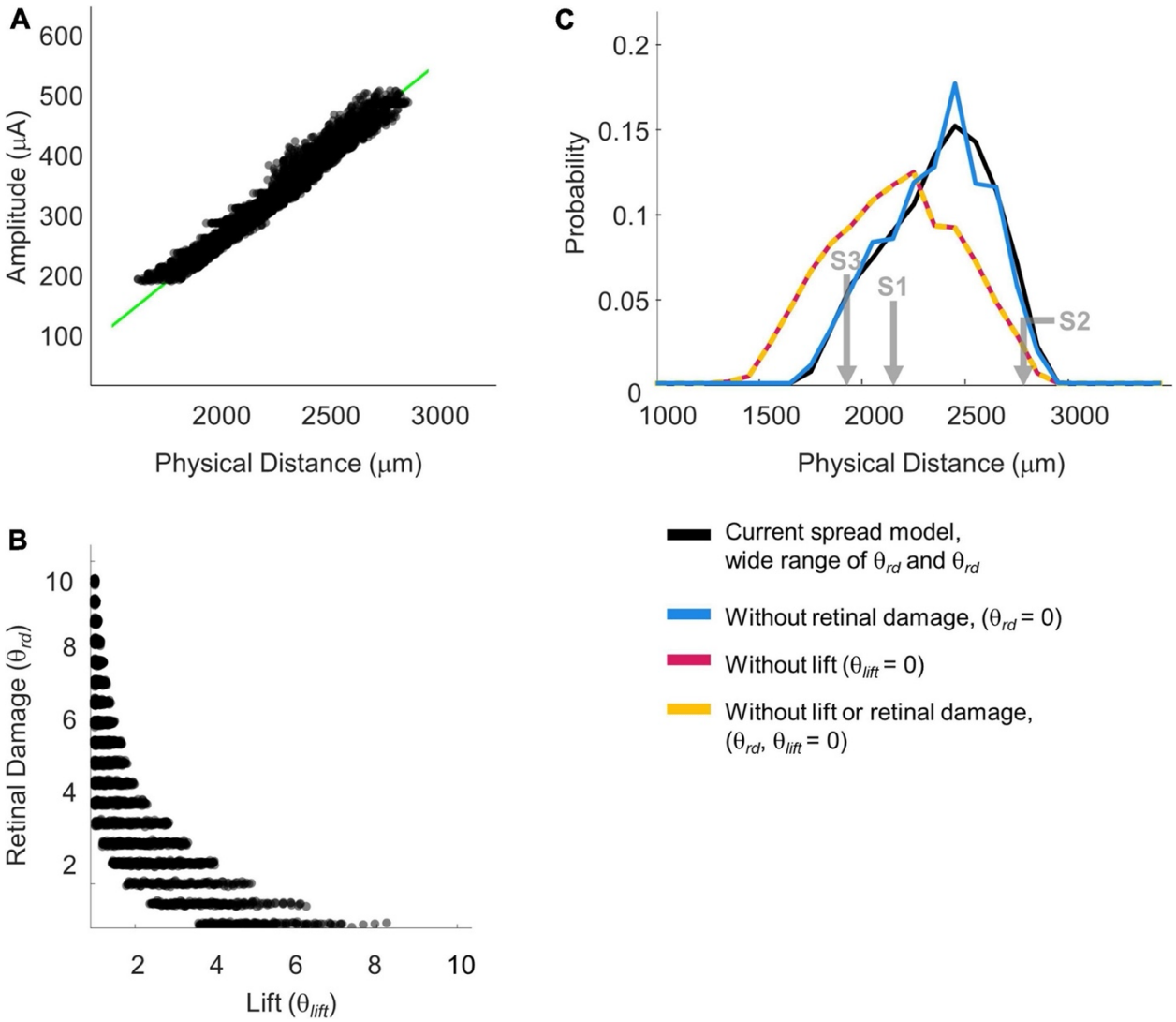

Figure 13. Simulation parameterizations that match participant performance. (A) The green line representing 75% iso-performance without axonal stimulation is replotted from Figure 11. Multiple overlapping black lines show simulated iso-dip contours sub-selected from parameterizations that matched the 75% two-point discrimination iso-performance curve. (B) Scatter plot of θ_{rd} vs. θ_{lift} for parameterizations which resulted in iso-dip contours (the black lines in Panel A) that closely resembled the predicted 75% iso-performance contour with minimal

axonal stimulation (the green line in Panel A). (C) Probability distributions of predicted two-point discrimination thresholds.

Across each simulated value of *a*, *k*, θ_{rd}, θ_{lift}, and *dip criterion* we calculated both the predicted detection threshold amplitude and the physical distance that produced *dip* = *dip criterion*. From these simulations we created iso-dip contours as a function of physical distance and I_0. We sub-selected those simulated iso-dip contours that were reasonably close (mean squared error < 20μA) to the predicted 75% iso-performance contour for minimal axonal stimulation and whose parameterizations resulted in single electrode thresholds between 177-660 μA. These successful parametrizations are shown in Figure 13A, with the green line representing the estimated 75% iso-performance curve for minimal axonal stimulation from the regression analyses described earlier, replotted from in Figure 13B.

Current amplitude thresholds in our patients were consistently higher (by a factor of 4-12x) than 50μA (see Table 3), suggesting that θ_{rd} and/or θ_{lift}, play an important role in determining threshold. This is confirmed by the scatter plots of θ_{rd} vs. θ_{lift} for successful simulations, in Figure 13B, where there is an absence of scatter points with both low θ_{rd} and θ_{lift}. Although the broad range of plausible outcomes generated by our simulations makes it difficult to definitively attribute the degree to which elevated thresholds and an inability to resolve individual electrodes can be attributed to retinal damage vs. lift; our simulations suggest that both damage and/or lift may play a role.

Next, using the parametrizations that successfully predicted two-point discrimination performance we examined how retinal damage (θ_{rd}) and lift from the retinal surface (θ_{lift}) affected spatial two-point discrimination thresholds. We calculated predicted two-point discrimination thresholds across all values of a, k, θ_{rd}, θ_{lift}, and *dip criterion*. The probability distributions of our predicted two-point discrimination thresholds of our current spread model, 2399 μm/8.3° (95%

confidence interval of 1908-2750 μm) spanned predicted thresholds for each participant when axonal stimulation was minimized, (S1 = 2151°, S2 = 2812, S3 = 1942μm).

Figure 13C also shows the predicted probability distribution of the two-point discrimination thresholds after having either set $\theta_{rd} = 0$ (blue curves), $\theta_{lift} = 0$ (pink curves), or both $\theta_{lift} = 0$ and $\theta_{rd} = 0$ (yellow curves). Median values across successful parametrizations are shown with error bars representing the interquartile range of simulation outcomes in Figure 10B.

According to our model, lift has an effect on two-point discrimination thresholds, when $\theta_{lift} = 0$, the median two-point discrimination limit fell from 2399 μm/8.3°to 2176 μm/7.6°, pink bar and curve in Figure 10B and in Figure 13C respectively. Thus, lift might have limited the ability to spatially resolve individual electrodes in our participants.

In contrast, the effect of retinal damage (θ_{rd}=0, blue bar and curves in Figure 10B and in Figure 13C) on two-point discrimination thresholds was very small. Our model includes the effect that retinal damage requires higher current amplitudes to reach threshold. In our model dip is calculated based on current amplitude on the retina. It is assumed, based on previous data (Greenwald et al., 2009; Nanduri et al., 2012), that brightness is linearly related to current. Since the effects of increasing current amplitude is simply to multiplicatively scale current on the retina, these increases in current amplitude have no effect on *dip*. Thus, our simulations suggest that the correlation between low thresholds and better two-point discrimination found in our participants is primarily driven by lift rather than retinal damage.

The yellow curve of $\theta_{lift} = 0$ and $\theta_{rd} = 0$, overlapping with the pink curve, can be thought of as a theoretical two-point resolution limit for the Argus II array if axonal stimulation, retinal damage and lift were not a factor: corresponding to an improvement of ~0.8°.

3.5 DISCUSSION

One of the main obstacles to the development of retinal prosthesis technology is that for many participants current amplitude thresholds tend to be relatively high across many or all electrodes, and only a minority of participants implanted with the Argus II clearly demonstrate pattern vision. Our aim was to understand what limits both sensitivity (perceptual thresholds) and the ability to spatially resolve two electrodes (two-point discrimination) in patients implanted with Argus II prostheses.

We measured perceptual detection thresholds, two-point discrimination thresholds, and collected self-reported daily use data. S1, who had a median amplitude threshold of 274 μA and two-point discrimination threshold of 2394 μm, used the device most consistently. S3, who had a median amplitude threshold of 210 μA and two-point discrimination threshold of 2161 μm, used the device averaging about two hours a day. S2, who had a median amplitude threshold of 476 μA and two-point discrimination threshold of 3136 μm, reported using the device once a month. While we cannot draw conclusions generalizable to larger population from a three-participant study, it is intriguing that patients S1 and S3, who had lower amplitude and two-point discrimination thresholds, used their devices far more often than S2, suggesting that two-point discrimination thresholds and or current amplitude thresholds are related to the functional utility of the device. Further research using two-point discrimination thresholds in larger cohort studies would be needed to establish the importance of this measure as a predictor of device usability in daily life functions.

Ultimately, according to our modeling, without axonal stimulation or lift our participants' spatial resolution performance would likely have improved by ~1.6-1.8°, or approximately 20%. Our simulated lower limit was approximately 2176 μm/7.6°, (interquartile range 1937-2718 μm),

equal to a spacing of almost 4 electrodes, corresponding to a logMAR acuity of roughly 2.7. This theoretical limit based on our simulations, is closely similar to that observed in the better performing Argus II participants (da Cruz et al., 2016; Humayun et al., 2012).

There are a variety of reasons why a pair of electrodes might merge into a single percept.

3.5.1 *Current field overlap & lift*

One reason for electrodes to merge into a single percept is overlap in electrode current fields, as demonstrated in Figure 12. This overlap is primarily driven by the physical distance between electrodes on the retinal surface and the lift of the array from the retinal surface. Threshold amplitude has previously been shown to be correlated with electrode-retina distance (Ahuja et al., 2013; de Balthasar et al., 2008; Shivdasani et al., 2014; Xu et al., 2021). However, our simulations suggest that current threshold is not a simple proxy for electrode-retina distance since retinal damage may also play a significant role in elevating thresholds.

3.5.2 *Receptive field overlap*

A second way percepts can overlap (also consistent with the 'scoreboard model') is when the phosphenes elicited by individual ganglion cells overlap. For the Argus II, receptive field sizes are small relative to the resolution of the array. The edge-to-edge separation of electrodes in the Argus II is approximately 1.3 degrees of visual angle. The Argus II is typically implanted over the fovea and subtends 20° of visual angle along its longer side. At 7 degrees eccentricity (2000μm from the fovea), most receptive field sizes are less than 1/3°, while at 15 degrees eccentricity (~4300μm from the fovea) most receptive field sizes are less than 1° (Dacey & Petersen, 1992). Thus, the loss of resolution caused by ganglion receptive field sizes was likely negligible, compared to the resolution of the array, and was not examined in our analysis. Theoretically, retinal

degeneration might lead to an increase in receptive field sizes: either due to some sort of perceptual adaption, or due to a sampling bias if ganglion cells with small receptive fields were differentially affected by disease. However, this effect would have to be unrealistically massive to have any effect on spatial resolution in our participants.

3.5.3 *Axonal Stimulation*

Percepts can also overlap because of axonal stimulation, when overlapping axon fiber bundles pass under, or close to, both electrodes in a pair. We found that a 'scoreboard + axon map' regression model, that included a factor based on axonal stimulation, outperformed the simple 'scoreboard' (limited to amplitude and Euclidean distance) model, suggesting that axonal stimulation did play a role in reducing the ability to resolve individual electrodes. However, as shown in Figure 10 and Figure 11, the effects of axonal stimulation on two-point discrimination performance were not particularly large: a regression analysis suggested that minimizing axonal stimulation would reduce the two-point discrimination threshold ~1 degree.

We did not model the effects of axonal stimulation on amplitude thresholds. However axonal stimulation is unlikely to affect current amplitude thresholds significantly - under most stimulation protocols axonal thresholds are very similar to thresholds near the ganglion soma (Jensen et al., 2005; Vilkhu et al., 2021).

3.5.4 *Retinal Damage*

As described in the Stage II modelling section, various types of retinal damage have been observed in Argus II patients (Gregori et al., 2018; Lin et al., 2019; Patelli et al., 2020; Rizzo et al., 2019) . It has been previously noted that some forms of damage such as edema or inflammation reduces the separation between the electrodes and the retina; leading the researchers to hypothesize

that this effect might serve to reduce perceptual thresholds (Gregori et al., 2018; Rizzo et al., 2019). However, this hypothesis has never been confirmed with behavioral sensitivity data.

Electrical resistance is likely to be influenced by electrode-retina distance and retinal damage in complex ways. Histopathological assessments of one post-mortem implanted eye suggests the formation of fibrosis and schisis consisting of compact collagen-rich membranes with macrophages (Patelli et al., 2020; Rizzo et al., 2019). On the one hand, the vitreous fluid has low resistance, and inflammation and IRF cysts are also likely to lower resistance; on the other, membranes and fibrosis are likely to increase resistance. We did not explicitly model these interactive effects, choosing instead to include a wide range of a and k values.

Our simulations suggest that retinal damage may well play a significant role in elevating thresholds. However, according to our simulations (if we are correct in our assumption that brightness scales roughly linearly with amplitude) the main impact of retinal damage is high thresholds, rather than a loss of the ability to resolve individual electrodes, since our dip calculation is unaffected by a linear scaling of retinal amplitude.

3.6 Strengths and Limitations of Our Two-Point Discrimination Paradigm

Although stimulating electrodes at double threshold amplitude was used to roughly match the percept brightness across electrodes, there likely remained significant differences in the brightness across electrodes (Greenwald et al., 2009; Nanduri et al., 2012). The percepts elicited by individual electrodes also likely differed dramatically in their shapes across the array (Beyeler et al., 2019; Luo et al., 2016).Percepts elicited by two-electrode stimulation were also consistently brighter than single-electrode stimulation Because many electrodes had stimulation levels near the

safety limit during the experiment, it was impossible to increase stimulation amplitude on single electrodes as a means of preventing patients from using brightness as a cue (Ayton, Barnes, et al., 2020). There was no way of minimizing differences in percept size between single and paired stimulation.

As a result, it is likely that stimulation from single vs. paired electrodes produced distinguishable percepts. Our goal was to prevent participants from using this information in making their 'one vs. two percept" judgments.

Participants were explicitly asked to report, *"How many percepts did you see?"*, and were told that brightness and the size of percepts would not provide a reliable cue. Participants reported one vs. two percepts with roughly equal frequency throughout the experiment. Importantly, their drawings (whether they drew one or two shapes) matched these verbal responses on a trial-by-trial basis. We also chose not to use single-electrode stimulation as catch trials and gave no feedback. However, results from this protocol should be interpreted very differently from those using a more traditional two-point discrimination methodology with single electrode catch trials and feedback (Ayton, Barnes, et al., 2020). With feedback our participants would likely have quickly learned to discriminate single and dual electrode stimulation simply based on the shape and/or brightness of percepts.

3.7 Comparison With Previous Studies – Spatial Vision

As shown in Table 7, grating acuity, direction of motion discrimination, and square localization are the most commonly used measures of the spatial resolution of the Argus II implant. While these tasks provide a good assessment of real-world spatial acuity, they are influenced by both eye and head-movements, and therefore cannot be used to measure losses in spatial resolution

at the retinal level, which is best assessed by two-point discrimination task. A previous study has found a correlation between two-point discrimination and grating spatial acuity in Argus II patients (Lauritzen et al., 2011), suggesting that resolution at the retinal level does influence visual performance on other tasks that are more closely related to 'real world' vision.

Table 7. Comparison of tasks used to measure spatial acuity

Task	**Within-array resolution required**	**Affected by Eye- & Head Movements**	**Literature**
Two-point resolution	Yes*	No	Lauritzen *et al.*, 2011
Grating acuity	Yes*, at frequencies above 2.9 logMAR in the Argus II (Stronks & Dagnelie, 2014)	Yes	Better than 2.9 logMAR Humayun et al., 2012: 21.88% Ho et al., 2015: 48.2-33.3% da Cruz et al., 2016: 38% Schaffrath et al., 2019: 10% Arevalo et al., 2021: 40%
Square localization / Direction of motion	Within array localization is not required for square localization or direction of motion (with feedback). For square localization (and possibly direction of motion) it is likely that many participants rely on scanning head-movements and use the percepts generated by the array as a merged single 'phosphene' (Peli, 2020).	Yes	Ahuja et al., 2011 Humayun et al., 2012 da Cruz et al., 2016 Arevalo et al., 2021 Ho et al., 2015 Naidu et al., 2020 Rizzo *et al.,* 2014 Schaffrath et al., 2019

* As described above, cues such as brightness and shape distortions are extremely difficult to entirely eliminate in Argus II participants.

Table 7 summarizes previous studies that assessed spatial vision with the Argus II across a range of tasks. Out of our nine original participants only three showed evidence of within array resolution and were selected for further testing. Although other studies have not examined two-point discrimination, the grating acuity task at spatial frequencies higher than 2.9 logMAR also

requires within-array resolution (though this task may be more difficult, due to blurring due to eye-movement/head motion).

In previous studies only 10-40% of Argus II patients performed better with the device on vs. off in a grating acuity task at frequencies higher than 2.9 logMAR, Table 7. In previous studies it has been difficult to find a clear link between either height from the retinal surface or retinal damage as measured using OCT and spatial performance (Rizzo et al., 2019). One reason for this may be that many tasks used for functional assessment (e.g. square localization) are not specifically designed to test within-array resolution while excluding the effects of eye-movements.

3.8 LIMITATIONS

One important limitation of our study is that we collected two-point discrimination data in just three participants, those tested at Johns Hopkins Eye Center. Moreover, as noted in the Methods, these three were selected as the best of 9 participants across two centers. Such a small participant group cannot support population level inferences; our data are best considered as three 'case studies' illustrating a range of outcomes. In addition, because our data were collected over a relatively small number of sessions, we do not have longitudinal data that might provide insight into the effects of the array shifting/lifting or continued retinal degeneration.

Our simulations also include significant uncertainty. First, our estimates of the distance to axon certainly includes variability due to errors in our estimation of axon bundle trajectories. Second, our estimates of current spread include a broad range of possible values, making our estimates of the relative importance of electrode lift and retinal damage quite broad. Finally, the *Rd* parameter that we interpret as retinal damage, simply reflects an increase in threshold unexplained by $\boldsymbol{\theta_{lift}}$, which potentially could be explained by other factors.

3.9 Future Directions

Placing an electrode array close to the surface without causing retinal damage is difficult (Gregori et al., 2018). It is therefore important to know whether successful outcomes depend on placing an array proximal to the retinal surface, avoiding retinal damage or (more likely) both. Unfortunately, we could not obtain high quality OCT images that would allow us to directly estimate the height of electrodes from the retinal surface, so our simulations can only indirectly infer the relative importance of retinal lift vs. retinal damage. However, our simulations do suggest, somewhat unsurprisingly, that avoiding both lift and significant retinal damage are likely to critical for a successful retinal implant. Future work relating two-point discrimination to imaging data that includes array-retina positioning, structural measures of retinal integrity, and more detailed computational modeling, based on data from a larger number of participants will likely be needed to fully understand the relative importance of these various factors in reducing the ability to resolve the percepts elicited by individual electrodes, and thereby develop implants which can successfully subserve pattern vision.

Chapter 4. TEMPORAL SENSITIVITY IN OPTOGENETIC STIMULATION – PSYCHOPHYSICS

4.1 ABSTRACT

One of the most promising techniques for ameliorating vision loss due to retinal degeneration is optogenetic restoration of light sensitivity in the eye (Busskamp et al., 2012; Gauvain et al., 2021). The remaining healthy cells can be endowed with light sensitivity using viral vectors that carry optogenetic proteins or photoswitches bypassing the degenerated photoreceptors. While researchers are identifying newer protein-vector-promoter combinations every passing day, the functional experience provided by optogenetically restored vision is still unknown. The results from animal models look promising and there are four human clinical trials ongoing. One key difference between the neurotypical and restored vision is the temporal kinetics in cell signaling: optogenetic response to light is slower and less amplified than healthy photoreceptor response. In this study, we aimed to benchmark optogenetic vision by using a traditional measure of visual acuity: the contrast sensitivity function (CSF). We simulated the optogenetic response by assuming an otherwise ideal but slower response to visual stimuli; and measured the CSF with regular monochromatic gratings and gratings filtered with the output of a temporal kinetics model based on the RGC firing rate data from rd1-mouse with '^{4x}BGAG$_{12,460}$:SNAP-mGluR2' photoswitch by Holt et al., (2022).

4.2 INTRODUCTION

The first proof-of concept of the optogenetic technique is rather recent: Boyden and colleagues in 2005 controlled neural spiking in rat hippocampus by introducing a microbial opsin, Channelrhodopsin-2 (ChR2). ChR2 is a light-gated cation channel found in green algae that opens within 50 μs after absorbing a photon (Nagel et al., 2003); adapting this feature led the researchers to achieve milliseconds temporal resolution in targeting specific cell populations, considered a paradigm shift by many. Since then, researchers have modified the technique changing the type of microbial and mammalian opsins or synthetic switches, target locations, and the type of optogenetic control.

Optogenetic stimulation of remaining healthy cells in the visual system is one of the promising ways of restoring vision in RDDs. Briefly explained in 0, the basic principle of optogenetic therapies of RDDs is to enable light sensitivity by introducing opsins that would bind to membrane of a target cell otherwise light insensitive.

Within the sight restoration field, the first major application of optogenetics was by Bi and colleagues (2006) who injected ChR2 to get light evoked ON responses from retinal ganglion cells in rd1 genetically modified mice. This study was followed by targets such as bipolar cells and photoreceptors and different opsins including halorhodopsin and G-protein coupled receptors.

The main advantage of optogenetic therapy over other sight restoration methods is that it is suitable for late stages of RDDs and that it is not necessary to know the underlying genetic mutations causing these diseases. More importantly, optogenetic techniques can enable us to target cells with high precision in spatial and temporal domains.

However, depending on the protein type and targeted cells, optogenetic methods face a sensitivity-speed trade-off. Mammalian native opsins expressed in visual systems are sensitive to

light but they have a slow response measured in seconds. Microbial opsins such as ChR2 and chemically-engineered receptors are faster but they require light intensities x1000-10000 larger than mammalian opsins, see an approximation at Figure 14.

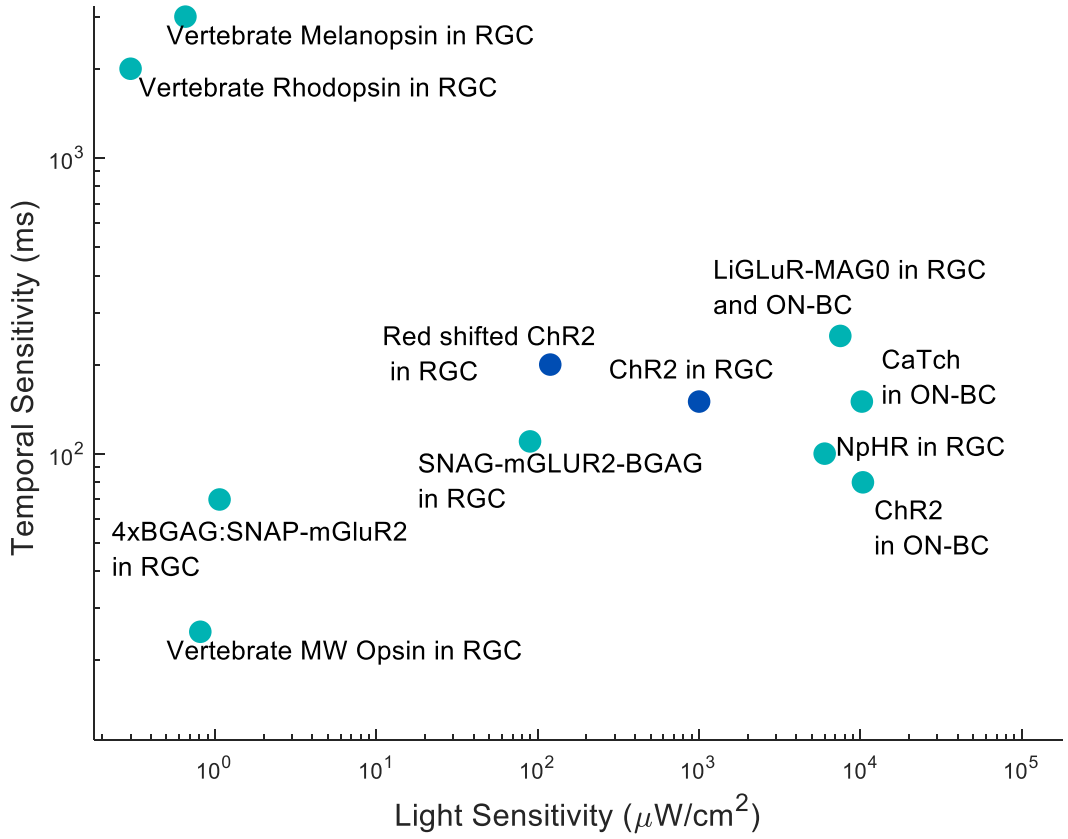

Figure 14 Sensitivity-Speed Trade-off in Optogenetic Proteins. (Estimated values for light and temporal sensitivity are adapted from Berry et al., (2019)). The dark blue scatters are two out of four compounds that are currently undergoing human clinical trials, rest are tested in animals.

The choice of protein, vector, and target cell population to get the fastest response to the dimmest light is an area of active research. In optogenetic vision, initial phototransduction that amplifies and modifies the photon at photoreceptors is bypassed; so, we expect an essential difference in sensitivity-speed trade-off from natural vision. In wild-type mice, photocurrent

response peaks after 73 ± 5 ms for S cones, 63 ± 5 ms for M cones, 205 ±10 ms for rods after dim flash stimulation (Nikonov et al., 2006).

Visual stimuli we encounter in our daily lives are not static, they move or change across time. In order to understand the temporal processing of the visual stimulus, we can, again, utilize methods from psychophysics. The relationship between the input and output can be formalized as a linear system where the function abides by certain criteria. This way, we narrow down the sample space from infinite possibilities to an input, its corresponding response, and a mapping function (Wandell, 1995; Watson, 1986).

With the limited information from animal models and early-stage clinical trials, it is vital to get an understanding of theoretical limits of vision provided by the optogenetic technology. In this chapter, we incorporated simulations of optogenetic vision to measurements of spatiotemporal contrast sensitivity. I first will summarize key concepts in linear systems theory and explain how it applies to temporal sensitivity. This summary and the subsequent model is mainly based on Watson's Working Model of Temporal Sensitivity (1986). Then I will describe contrast sensitivity as a measure of visual function in understanding the effect of optogenetic temporal delay.

4.2.1 *A Primer on Linear Systems Theory*

4.2.1.1 Homogeneity and Superposition

Homogeneity refers to the scalability of the output as much as the input. Meaning, if the input intensity increases by a factor of *c*, the output signal also increases by *c.*

A system satisfies the principle of *superposition* if the response to a combination of inputs is the same as the sum of the responses to the inputs separately (Wandell, 1995; Watson, 1986).

A linear system is homogenous, additive, and therefore abides by the principle of superposition.

4.2.1.2 Linear Time-Shift Invariance

A system is linear if the relationship between the input and the output does not change over time or space. With that, we can estimate the linespread or harmonic functions of the responses to a variety of input from a singular input.

4.2.2 *Temporal Sensitivity*

The human eye can detect rapid changes in the intensity of visual input up to a certain flicker rate. As the temporal frequency of contrast change increases, the percept merges into a continuous appearance. This effect has been used in various technologies such as LED screens.

4.2.3 *Spatiotemporal Contrast Sensitivity Function*

The relationship between the features of stimulus and sensitivity can be formalized in a contrast sensitivity function (CSF), where we take systematic measurements at various steps of spatial and/or temporal frequencies to determine the contrast needed for discrimination or detection. This is a powerful tool that is useful not only for basic vision science goals such as identifying the receptive fields of a neuronal population but also it can be used as a simple measure of visual acuity.

As described in the previous section, the early visual processing can be considered as a shift-invariant linear system. Building on this notion and the harmonic nature of stimuli, we can utilize CSFs to study pattern recognition in the visual system, (see Wandell, 1995, Chapter 7). In other words, CSFs can be considered as a basis function to translate any input to neural signal and consequently, perceptual output.

The temporal and spatial contrast sensitivity functions are not independent, the relationship between the contrast sensitivity at various levels of temporal frequency changes according to the

spatial frequency. Therefore, when measuring temporal sensitivity, we need to sample spatial frequency at its varying level if we want to build a kernel that describes any visual input.

Within the context of temporal sensitivity, factors that modulate temporal contrast sensitivity function are:

- **Spatial Frequency:** There is a non-linear relationship between spatial and temporal frequencies. At higher temporal frequencies, change in spatial frequency does not really affect the contrast sensitivity; whereas at lower temporal frequencies, high spatial frequency increases the contrast sensitivity due to 'sustained' temporal contrast sensitivity function (Watson, 1986).
- **Background Intensity:** The relationship between overall background intensity and temporal frequency is also non-linear. Contrast sensitivity increases faster in high temporal frequencies than low and overall TCSF curve shifts at higher background intensities,
- **Duration:** Similar to the edge effects in spatial frequency, if the stimulus onset and offset is abrupt, higher frequencies are introduced. This issue can be eliminated by using a Gaussian window or having a duration longer than 100 ms. Using a Gaussian window increases sensitivity by ¼ (Watson, 1979). The effect of increased sensitivity at higher durations could potentially be modeled by probability summation: as the number of opportunities to detect the stimulus increases with duration, overall probability of detection increases as well.
- **Eccentricity:** While spatial contrast sensitivity changes across the retina due to underlying physiology, temporal contrast sensitivity is rather constant if the size of the receptive fields are controlled for (Watson, 1986).`

- **Eye-movements:** Even at fixation, involuntary eye movements constantly updates the retinal image (Ratnam et al., 2017). In normal vision, these fixational eye movements are considered beneficial in dynamic sampling of the visual field by 'whitening' or equalizing the spatial energy across temporal domain (Kuang et al., 2012). Early work demonstrated that stabilizing the retinal image decreases the contrast sensitivity for static visual stimuli (Kelly, 1979a; Kulikowski, 1971). This effect holds if the duration of visual stimulus is long enough for dynamic stimuli.

4.3 METHODS

This study was approved by the University of Washington's Institutional Review Board Study 3868). All participants gave their informed consent in the beginning of the experiment. Participants not affiliated with the Fine Lab were paid an honorarium in accordance with the approved IRB.

4.3.1 *Participants*

Our participant pool consisted of 6 naïve (5 female assigned-at-birth) observers with a median age of 27 (22-52). All participants had normal or corrected to normal visual acuity (≥ 0.2 logMAR or 20/30).

4.3.2 *Stimuli*

We measured the spatiotemporal contrast sensitivity through a 2AFC orientation task on symmetric,45º or -45º slanted, counterphase Gabor patterns with a stimulus size covering 10º prior

to the Gaussian envelope. We animated the static gabor gratings by multiplying with a sine wave of varying frequency. The dynamic, flickering stimuli had a duration of 800 ms. We applied a linear ramp to the sine wave to control for edge effects. We varied spatial (min: .25, max: 36 cpd) and temporal frequencies (min: 3, max: 30 Hz) of the stimulus depending on the condition. The contrast of the target varied from 0.001 to full depending on the participant's response history. The minimum difference between two steps of contrast was 0.0169.

The stimulus was presented on a 32`` Display++ linearized monitor (Cambridge Research Systems Ltd) in Mono++ mode with native 10-bit depth, connected to a Dell Optiplex 7000 Tower with an AMD Radeon graphics card. The factory-maximum and measured refresh rate of the monitor aligned at ~120 Hz. The participant viewed the stimuli on a chin-rest 80 centimeters away from the monitor in a dark experimental room.

The experiment was programmed on MATLAB (Mathworks, MATLAB, version r2022a) and Psychtoolbox (Kleiner et al., 2007). The code can be found in the repository, https://www.github.com/ezgirmak/qtCSF.

4.3.2.1 Optogenetic Stimulation Modeling

Based on the work by Berry group (Berry et al., 2017, 2019; Holt et al., 2022), we modeled the temporal kinetics of the '$^{4x}BGAG_{12,460}$:SNAP-mGluR2' designed protein. This 'pseudo-linear' model predicts neural spiking in rd1 mice to a flash of light or a movie stimulus.

Both in Berry et al. (2019) and Holt et al., (2022), it has been observed that a flash stimulus increases or suppresses (based on the protein) baseline firing rate of rd1 mouse retina injected with optogenetic proteins for the duration of the stimulus with a duration-dependent post-stimulus overshoot. Replicating the figures 2C and 2D of Holt et al (2022), we formulated a series of first-

order differential equations to describe an impulse response function for a flash stimulus with the following parameters:

- τ_{on}: linear filter time constant when the stimulus is 'ON'
- τ_{off}: linear filter time constant whent the stimulus is 'OFF'
- τ_b: baseline firing rate recovery time constant
- *a*: scale factor of the stimulus influence on the linear filter
- *b*: scale factor of the stimulus influence on the baseline firing rate
- baseline: baseline firing rate
- S(t): Stimulus at a given timepoint

$$\frac{dy}{dt} = \frac{-a*S(t)-(baseline-y)}{\tau_{on}} \quad \text{Eq.6}$$

$$\frac{dy}{dt} = \frac{-a*S(t)-(b(t)-y)}{\tau_{off}} \quad \text{Eq. 7}$$

$$\frac{db}{dt} = \frac{b*a*S(t)-(baseline-b(t))}{\tau_b} \quad \text{Eq. 8}$$

Here, when the stimulus is 'ON', the firing rate decreases in proportion to the stimulus intensity with the rate of τ_{on} while the baseline firing rate shifts with a rate of τ_b ; when the stimulus is 'OFF' the firing rate approaches the baseline with a time constant of τ_{off}.

The main reason for our model to have two time constants for the linear filter and a time constant for the baseline firing rate is to simulate the different slopes pre and post-stimulus; also the post-stimulus overshoot that was observed in both Berry et al. (2019) and Holt et al. (2022). While we cannot speculate why exactly the baseline firing rate shifts depending on the stimulus duration, we incorporated this overshoot and shift into our model affecting the output.

As explained in the introduction of this chapter, we used the linear system theory to extrapolate from the impulse response function to image stimuli. We considered each pixel as

independent for the first portion of the experiment and calculated the change in intensity with the effect of temporal delay in changing the stimulus. Due to the computational limitations of storing individually processed frames (~200k) the simulations were done during the experimental session.

4.3.3 *Procedure*

Our study consisted of one 1-hour experimental session. In the beginning of first session, after obtaining the informed consent, participants were asked to view printed out versions of the stimuli to familiarize themselves with the stimuli and the task. The experimenter ran a demo consisting of full contrast, larger aperture gabors with feedback sounds. They gave verbal feedback on what a correct/incorrect response is and answered clarification questions by the participants.

The first experimental session consisted of two main conditions: *baseline* where we measured the spatiotemporal contrast sensitivity function with unaltered stimuli; *optogenetic* where the model output was presented in the spatiotemporal CSF measurement. Both conditions had two versions: in one the temporal frequency was fixed at predetermined values (1.875, 3.75, 7.5, 15.0, 30.0 Hz) and the spatial frequency was fit through a staircase method; in another spatial frequency was fixed at predetermined values (0.50, 1.4565, 4.2426, 12.3586, 36 cpd).

These 2x2 conditions were presented to the participants pseudo-randomly based on the latin square method – except for two participants where the order of two conditions were switched– . Each condition took approximately 15 minutes with 250 trials and participants could take breaks in between.

Each trial began with a fixation spot and an audio prompt. Participants received feedback on their choice of the orientation of the bar through two other tones played after trial. The contrast

and temporal/spatial frequency of the target for a given trial was determined by a Bayesian estimation method adapted from Lesmes and colleagues (2010).

4.3.3.1 Spatiotemporal Contrast Sensitivity Estimation

Measuring CSFs in a non-adaptive fashion is prohibitively time-consuming; multiple adaptive staircase procedures were developed to cut down on experimental duration, see Pelli & Bex, (2013), Watson & Ahumada, (2005). The method we used, Quick CSF (qCSF) is a Bayesian adaptive contrast sensitivity estimation procedure developed by Lesmes and colleagues (2010) where multiple parameters of CSF are estimated on a trial-by-trial basis. While the original paper validated good precision with only 25 trials, we opted for 50 trials per condition.

Lesmes and colleagues (2010) sped up the estimation procedure by updating a multivariate probability density function imposed on a pre-defined function for CSF based on previous trials and refining future trials. They fit a *truncated log-parabola* in the following form:

$$S'(f) = \log_{10}(\gamma_{max}) - \kappa\left(\frac{(\log_{10}(f) - \log_{10}(f_{\max})}{\frac{\beta'}{2}}\right)^2 \quad \text{Eq. 9}$$

Where $\gamma_{\max}$ is the peak sensitivity or *gain*, f_{max} is the peak frequency, β is the bandwidth, δ is the truncation at the lower frequencies, κ = log10(2) and β′ = log10(2β). While qCSF was previously used for estimating spatial contrast sensitivity, since temporal CSF function has a similar truncation in lower levels, we opted for using the same formula for measuring tCSF.

These four main parameters: $\gamma_{\max}$, f_{max}, β, and δ are estimated directly through a Bayesian method similar to QUEST (Watson & Pelli, 1983) where the 2D stimuli space is optimized based on the information from the previous trials, please see Lesmes et al. (2010) for a detailed description of the methods.

As explained earlier, we estimated CSFs for both varied temporal and spatial frequencies. We selected our priors for the Bayesian estimation method based on Lesmes et al. (2010) for spatial; Kelly, (1979) for temporal frequencies. These priors can be found in Table 8.

Table 8 Priors used for the qCSF Bayesian estimation method for two versions of the experiment

	Peak Gain ($\gamma_{\max}$)	Peak Frequency (f_{max})	Bandwidth (β)	Truncation (δ)
Spatial Frequency	75	1	2.5	.1
Temporal Frequency	75	5	2.5	.1

These priors were then readjusted in 50 trials per set frequency at 12 levels. Meaning, for each iteration of qCSF algorithm, we ended up estimating contrast sensitivity at 12 points between the predetermined limits (spatial frequency: 0.25-36 cpd, temporal frequency: 3-30 Hz).

We then estimated spatiotemporal contrast sensitivity surfaces by fitting our psychophysical data to an exponential function described in Kelly (1979b), where they described the non-separable relationship between spatial and temporal domains in terms of *velocity (v)* = $\frac{spatial\ frequency}{temporal\ frequency}$.

The expansion of the equation 4 in their paper is as follows:

$$G(\alpha, v) = kv\alpha^2 \exp(-2\alpha/\alpha_{\max}) \qquad \text{Eq. 10}$$

where $\alpha = 2 * \pi * f_s$, $k = a + b|log(v/3)|^3$ and $\alpha_{\max} = c/(v+2)$. Here we fit three constants a, b, c through function minimization.

4.4 RESULTS

4.4.1 *Optogenetic Modeling*

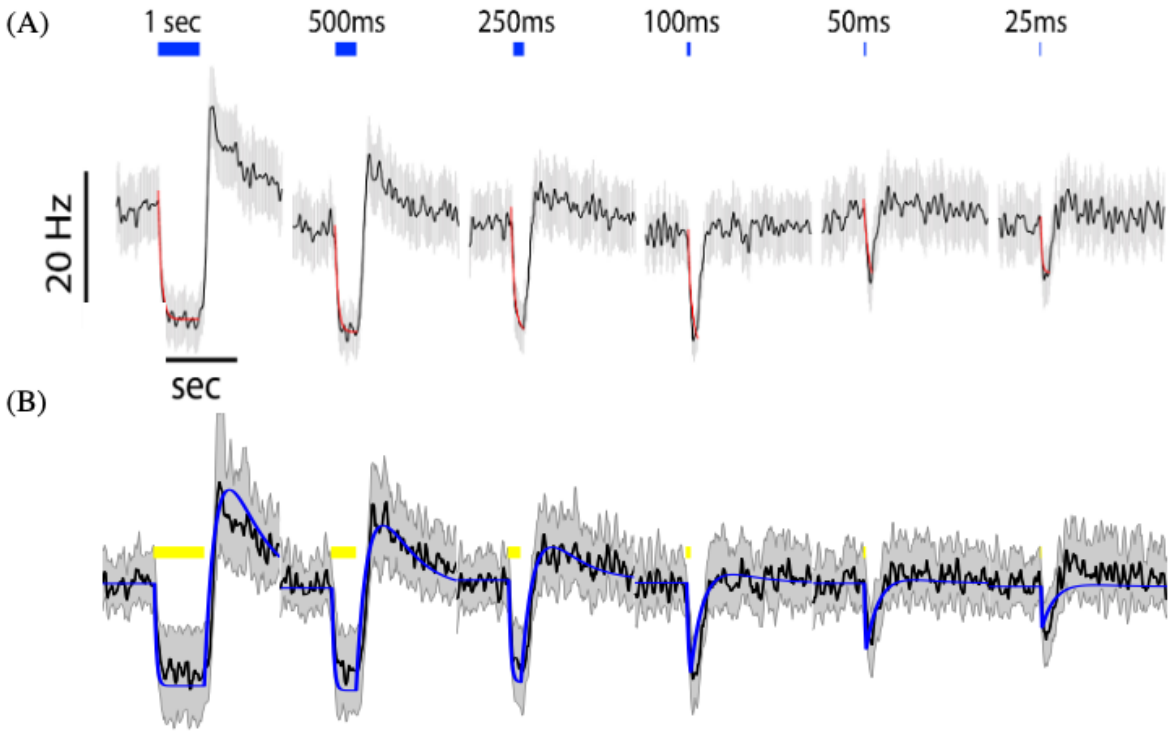

Figure 15 Modeling temporal kinetics of optogenetic protein. (A) Average firing rate data from 93 RGCs from Holt et al. (2022), Figure 2D. (B) Simulated normalized timeseries of the average firing rate The duration of stimulus affects the overall change in the firing rate when the stimulus is on; shifts the baseline firing rate as well.

We simulated the average firing rate of 93 retinal ganglion cells measured in-vitro by Holt et al (2022) using three first-order differential equations described in the Methods section. The stimulus-dependent decay and recovery contants τ_{on} and τ_{off} were estimated to be 0.05 and 0.3 respectively. The baseline shift seen in the work of Berry et al. (2019) and Holt et al., (2022) is mediated by the third differential equation (see Eq. 8) and captures the effect of stimulus duration for a flash stimulus. Even when no assumptions are made for adaptation or lateral inhibition effects and each pixel of a frame is considered as a flash stimulus; the differential response based on

duration and the shift in average baseline firing rate modifies the stimulus from the original intensities.

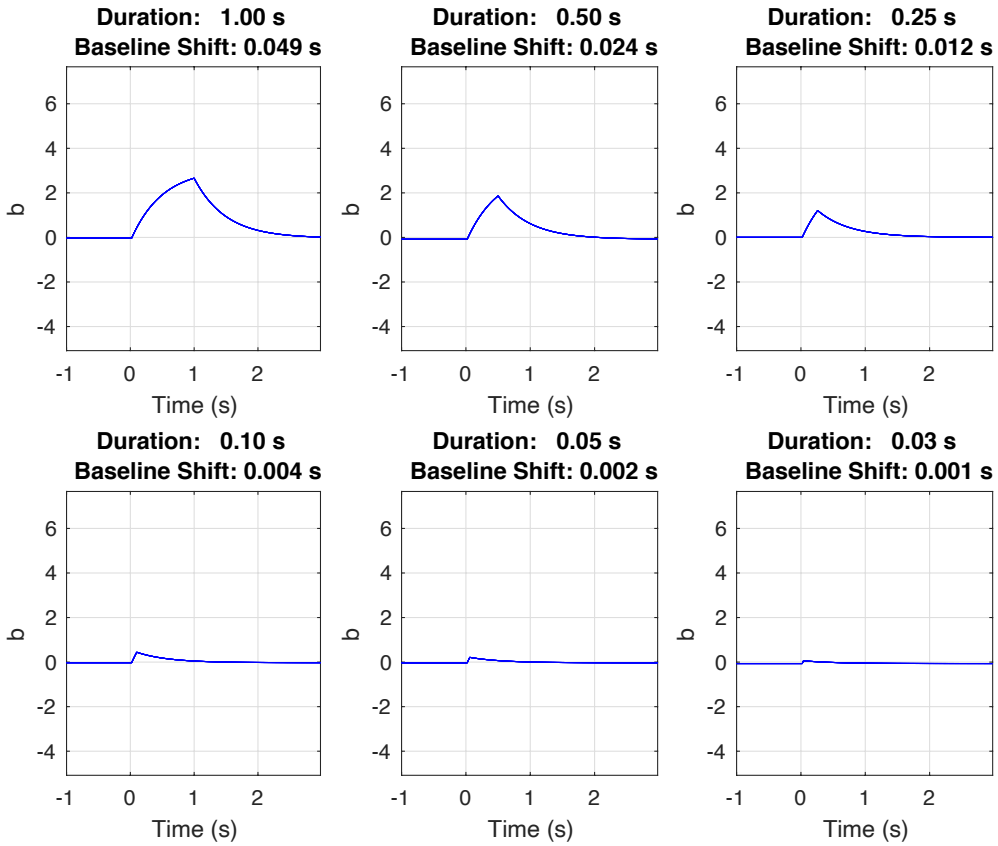

Figure 16 Shift in average baseline firing rate over time in the optogenetic simulations.

Since the contrast change is faster for a given timepoint, the optogenetic delay has more noticeable effects on dynamic than static stimuli. In Figure 18, three stills at timepoints (4.92, 5.25, 5.59s) were captured after each frame of a 10 second natural scene movie was filtered with the optogenetic model. The static objects in the scene, such as the pigeon or two men sitting in the middle decrease in overall contrast but moving stimuli such as people walking saw more drastic changes. In this experiment, we filtered classical, flickering gabor gratings and presented participants with both filtered and unfiltered stimulus. An example of a single pixel timecourse

can be seen in Figure 17. Due to the convolution of stimulus with optogenetic model output, the signal amplitude narrows, and phase shifts and this effect depends on temporal frequency.

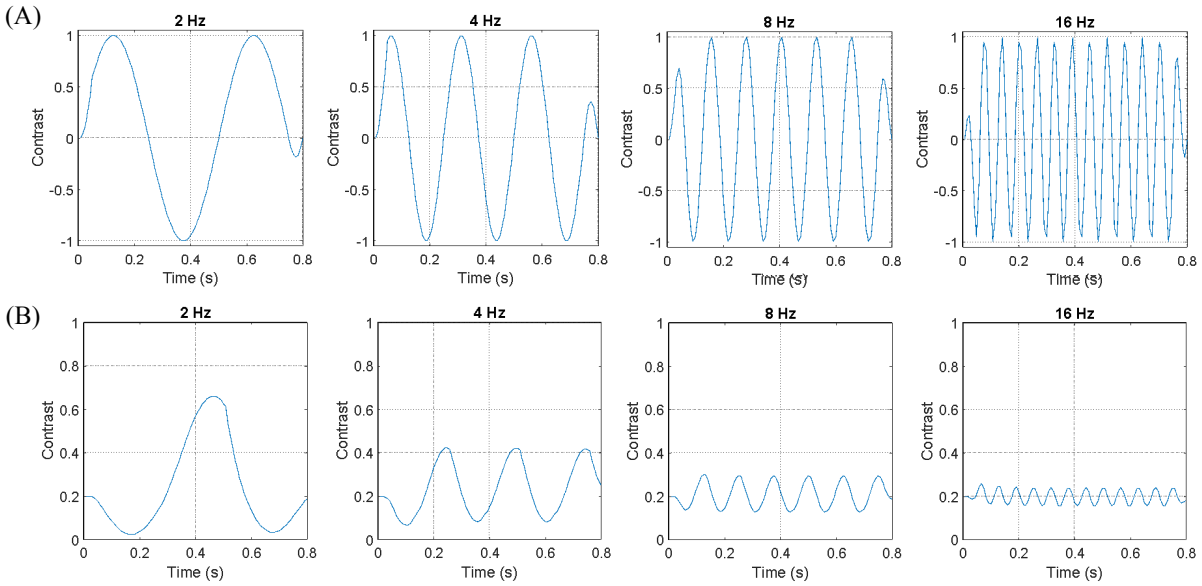

Figure 17 Stimulus timecourse with and without optogenetic filtering. (A) Contrast change over time for the original stimulus at various temporal frequencies. (B) Output of the optogenetic model for the same temporal frequencies as (A). Contrast amplitude narrows with increasing temporal frequency and phase shifts.

Figure 18 The effects of optogenetic delay is more apparent in moving stimulus. (A) A still (5.25s timepoint) from the original stimulus, a 10 second natural scene in Athens. Two men sitting

indicated by the left frame are static, right frame focuses on woman walking towards the camera. (B) The output of optogenetic modeling before and after the 5.25 timepoint for two frames from (A).

4.4.2 *Spatiotemporal Contrast Sensitivity Function is a Reliable Measure for Simulated Optogenetic Vision*

We estimated the spatiotemporal contrast sensitivity function for six participants completing two conditions: one viewing unaltered flickering gratings and one where the gratings were filtered by the output of our optogenetic protein model. Using the qCSF procedure described in the Methods, we were able to procure psychometric curves for both conditions. However, in the version of the experiment where the spatial frequencies were fixed and the qCSF staircase estimation was run on the range of temporal frequency values, at the highest fixed temporal frequency, 36 cpd, the estimations did not match the complimentary condition with same trials (possibly due to an artifact), we were forced to remove all trials in all conditions at 36 cpd (see Supplementary Figure 1).

4.4.3 *Optogenetic Visual Acuity is Ten-Fold Worse than Neurotypical Vision*

Results aggregated for each subject indicated a significant decrease in logcontrast sensitivity in optogenetic condition (M = 1.23, sd = 0.06) than in baseline condition (M = 2.21, sd = 0.13), $t(5) = 27.17$, $p < 0.0001$). Since contrast sensitivity values are in log10 space the average difference in sensitivity of 0.98 accounts for a ten-fold change. In addition, the four parameters estimated by qCSF procedure gives a more nuanced understanding of underlying function. Average peak gain parameter estimated by qCSF procedure was 1002 ± 79 for the baseline condition and 63 ± 6 for the optogenetic condition (for medians, see Figure 19A). Both across spatial and temporal frequency, baseline peak gain is significantly larger than optogenetic peak gain, except for the

highest frequency tested where the gain diminishes for both conditions. The means of average qCSF parameters except for the peak frequency can be found in

Table 9.

Table 9 Average estimated parameters from qCSF procedure for baseline and optogenetic conditions with 95% confidence intervals. AULCSF is the area under the CSF curve, Peak gain is the maximum contrast sensitivity reached, bandwidth is the full-width at half maximum, and truncation is the low frequency plateau. The peak frequency is not reported because we averaged over varying spatial and temporal frequencies.

	AULCSF	**Peak Gain (γ_{max})**	**Bandwidth (β)**	**Truncation (δ)**
Baseline	3.532 [3.111, 3.953]	1001.613 [842.904, 1160.322]	2.825 [2.587,3.065]	0.099 [0.094, 0.104]
Optogenetic	2.007 [1.679, 2.335]	63.349 [51.172, 75.525]	3.298 [3.019, 3.578]	0.147 [0.100, 0.195]

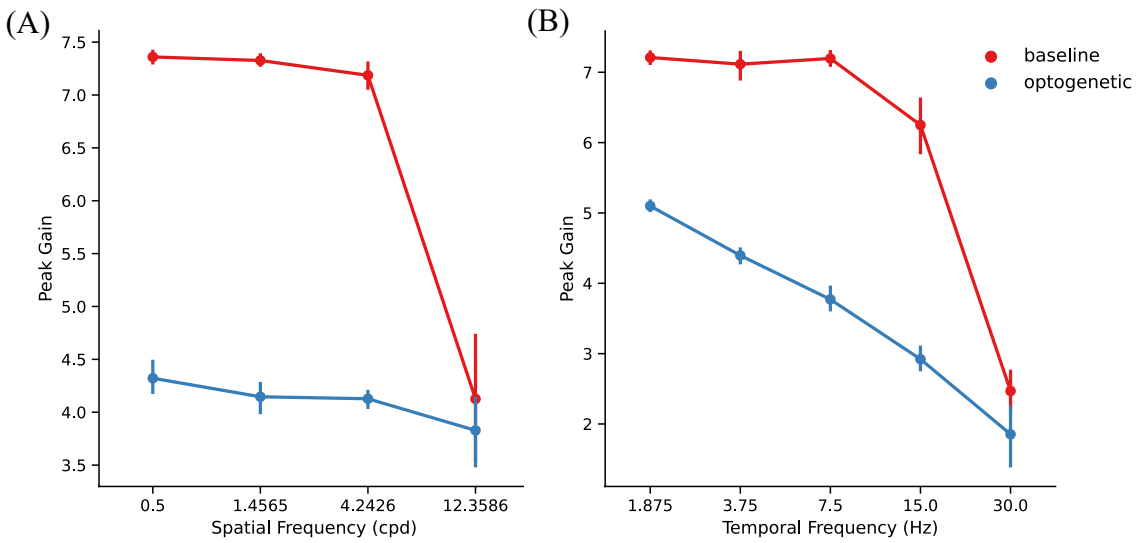

Figure 19 Change in log peak gain across (A) spatial and (B) temporal frequencies.

The surface fits based on Kelly model indicate the same relationship for individual subjects (Figure 20) with an average difference of 0.98 in the log space.

4.4.4 *Temporal Contrast Sensitivity is Mediated by Spatial Frequency*

The CSF surfaces obtained using the Kelly model show that contrast sensitivity decreases overall under the optogenetic condition. However, this decrease varies across different combinations of temporal and spatial frequencies. In Figure 21, we plotted aggregated sensitivity values across temporal frequencies for three values selected from the range of spatial frequencies (0.25 cpd, 2.39 cpd, 22.91 cpd). At higher spatial frequencies, the effect of temporal frequency change diminishes due to decrease in contrast sensitivity. At lower temporal frequencies, sensitivity peaks between 5-10 Hz depending on the spatial frequency, in line with previous literature. Likewise, in Figure 22, the relationship between spatial frequency and contrast sensitivity is mediated by temporal frequency plotted at three different values sampling the range (1.88 Hz, 7.5 Hz, 24.33 Hz). In both figure, contrast sensitivity diminishes at higher spatial frequencies.

In the runs where we estimated the temporal frequency via qCSF staircase method, median peak temporal frequency was 5.68 Hz across all five spatial frequencies tested; and when they were viewing the filtered stimulus, peak temporal frequency was 3.04 Hz (see Figure 23A). Upon further investigation where we investigate the mediatory effect of spatial frequency, we selected runs at lower spatial frequency (0.5 cpd) where the peak median temporal frequency was 7.08 Hz for baseline condition; 3.28 Hz for optogenetic condition. Meaning, at the peak spatial frequency, peak contrast sensitivity is achieved at lower temporal frequencies in optogenetic conditions.
In the runs where we estimated the spatial frequency via qCSF staircase method, median peak spatial frequency for baseline and optogenetic conditions were 1.52 and 1.82 cpd, respectively,

Figure 24A. Compared to the temporal frequency estimations, peak spatial frequency did not vary across two conditions which means spatial frequency, in general, acts as a low-pass filter.

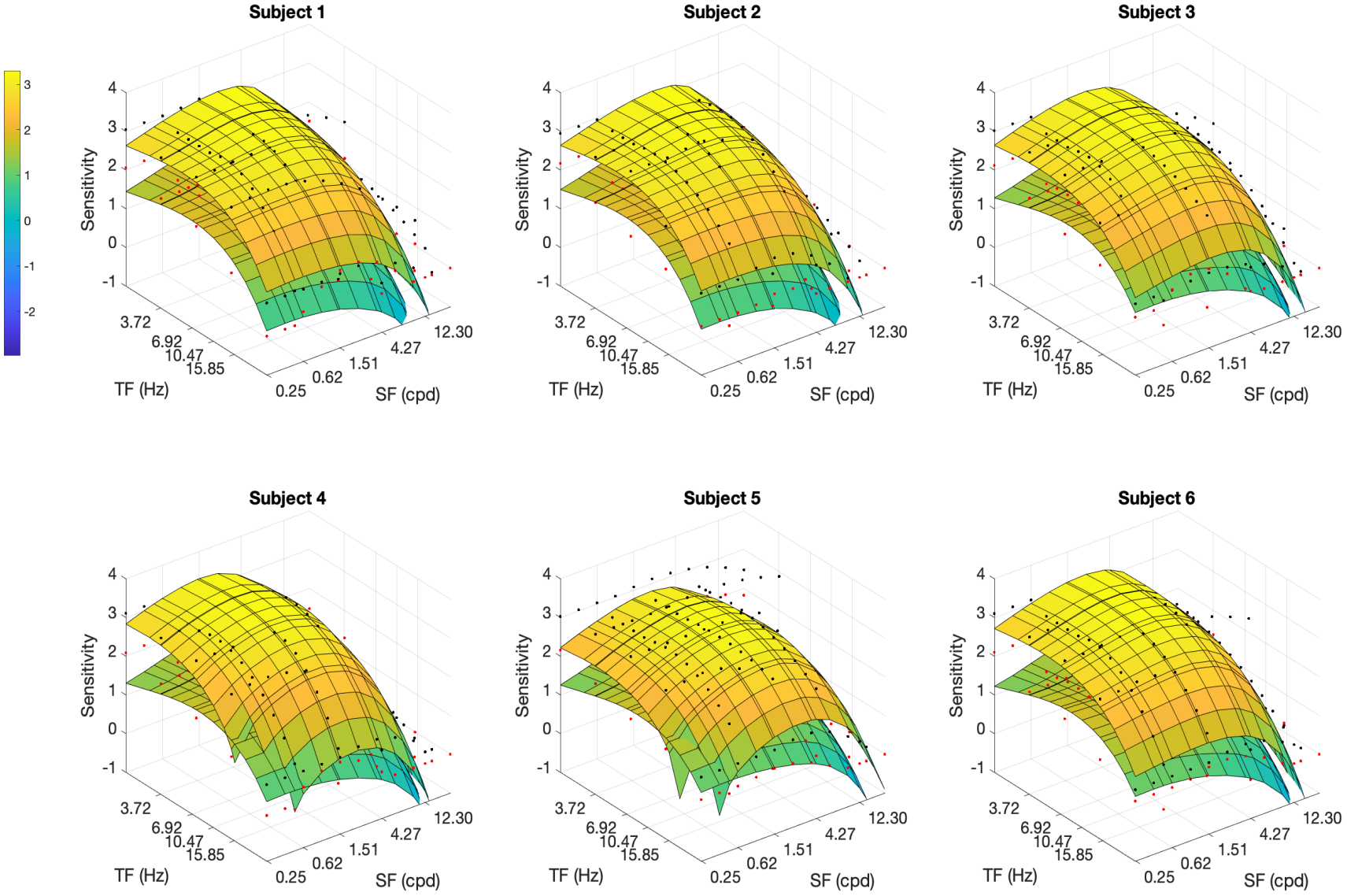

Figure 20 Surface fits for baseline (top) and optogenetic (bottom) conditions based on Kelly (1979) model. Here, we fit three parameters (a, b, c) to the estimated contrast sensitivity values (black: baseline, red: optogenetic) for a given combination of spatial and temporal frequency.

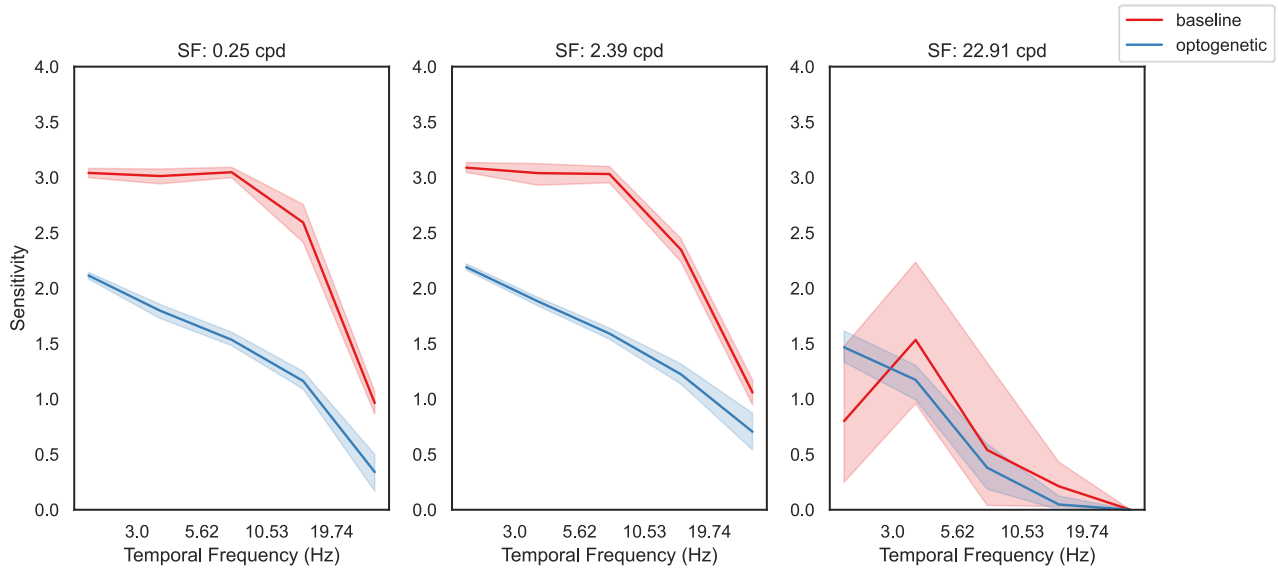

Figure 21 Relationship between contrast sensitivity and temporal frequency at three spatial frequency rates (0.25 cpd, 2.39 cpd, 22.91 cpd). The difference between optogenetic and baseline conditions decreases as the temporal frequency increases but the rate of change is not consistent across varying spatial frequencies. Error bars are the 95% confidence intervals.

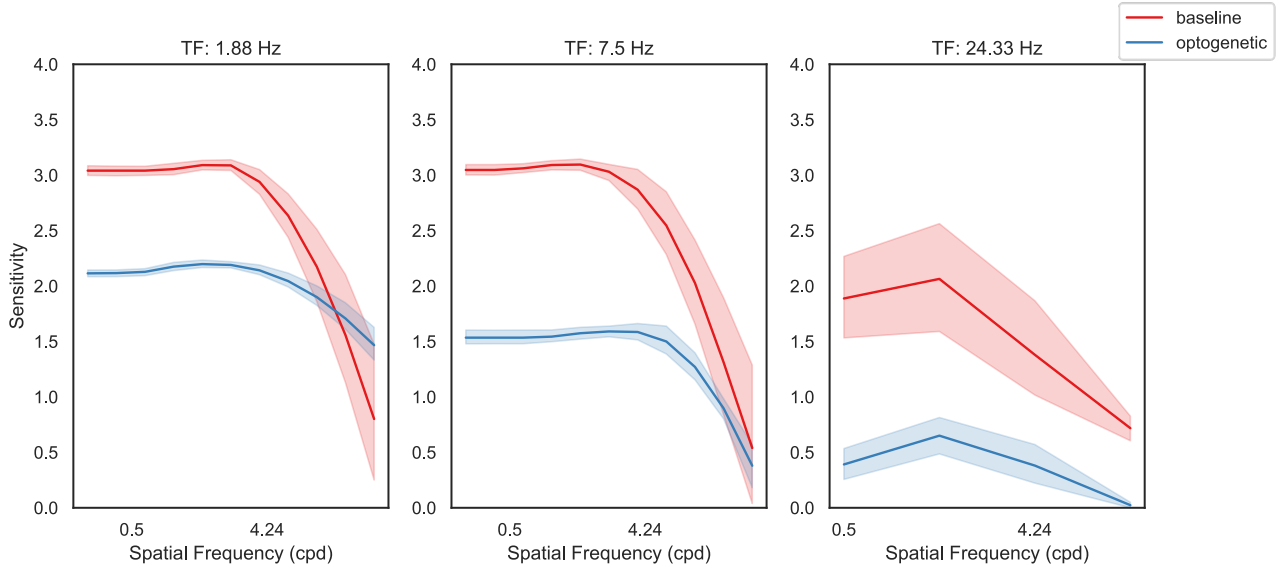

Figure 22 Relationship between contrast sensitivity and spatial frequency at three temporal frequency rates (1.88 Hz, 7.5 Hz, 24.33 Hz). The difference between optogenetic and baseline conditions decreases as the spatial frequency increases but the rate of change is not consistent across varying temporal frequencies. Error bars are the 95% confidence intervals.

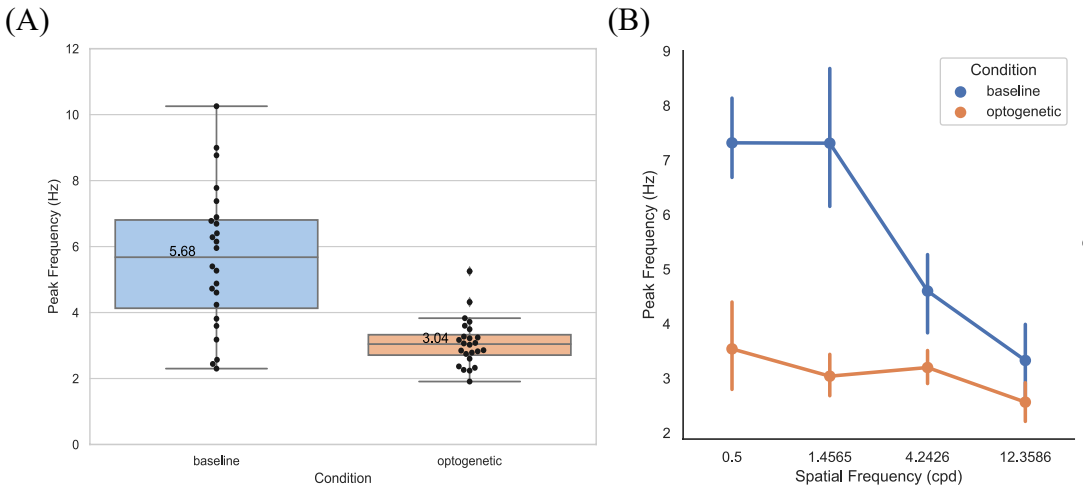

Figure 23 (A) Peak temporal frequency from the qCSF procedure across baseline and optogenetic conditions. Each scatter point represents a single qCSF run. (B) Same dataset, replotted as mean temporal frequency across spatial frequency, error bars indicate 95% CI.

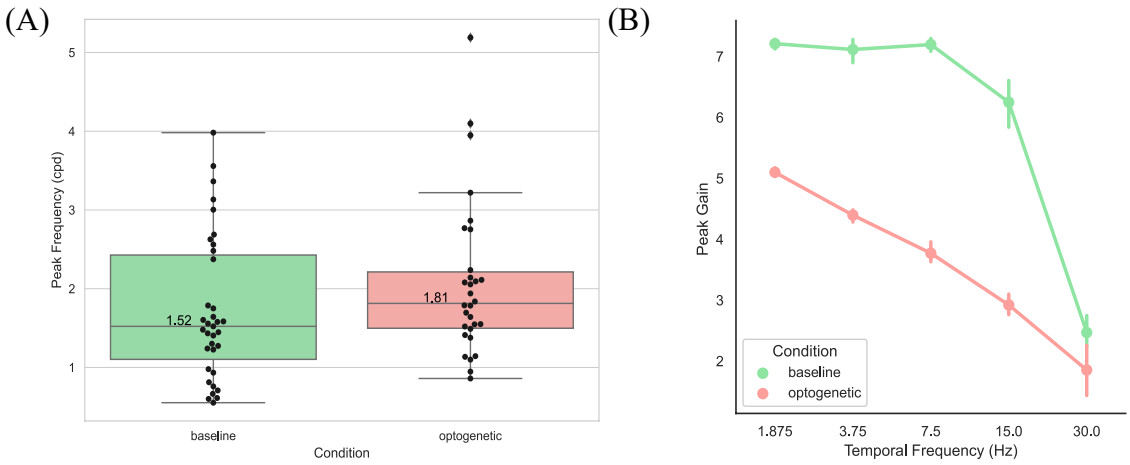

Figure 24 (A) Peak spatial frequency from the qCSF procedure across baseline and optogenetic conditions. Each scatter point represents a single qCSF run. (B) Same dataset, replotted as mean spatial frequency across temporal frequency

4.5 Discussion

Optogenetic therapy is promising in restoring light sensitivity in the degenerated retina. In the effort of finding the optimal protein-promoter-vector combo that yields an artificial vision

closest to sight, it is crucial to utilize the large body of work in the animal model field to estimate the clinical performance in the next stage in development. While behavioral tests are done to evaluate vision in animal models, the perceptual experience across species are vastly different and might not translate at the clinical testing stage. Hence, predicting human perceptual experience from data that is common across species (e.g. spike count when stimulated), can give researchers a better understanding of what to expect.

Visual acuity is one of the key clinical outcome measures when evaluating the efficacy of sight restoration technologies in humans and it is traditionally measured via established optotype charts such as Snellen Acuity or Pelli-Robson chart. How well the performance in optotype charts translates into functional vision is a crucial question in the artificial vision domain mainly because optogenetic stimulation bypasses initial phototransduction by neurons and has a varying temporal kinetics leading to delays in signaling.

In this study, our goal was to predict whether visual performance would decrease due to decrease in temporal sensitivity in optogenetic therapy. To do so, we created a modular framework we call 'virtual patients': sighted individuals viewing visual stimulus filtered by optogenetic model outputs. This way, we could focus on individual differences in optogenetic vision compared to neurotypical vision, assuming a best-case scenario for the technology.

4.5.1 *Optogenetic Delay Shifts Peak Sensitivity To Lower Temporal Frequencies*

We focused on the chemically engineered photoswitch '^{4x}BGAG$_{12,460}$:SNAP-mGluR2' investigated by Holt et al. (2022), one of the state-of-the-art optogenetic molecules currently being investigated in mice. We built a model of temporal sensitivity based on the change of average baseline firing rate during photoactivation. The non-linear response profile of retinal ganglion cells

was modeled through three differential equations accounting for initial suppression, recovery, and post-stimulus overshoot.

We then conducted a within-subjects contrast sensitivity task with two conditions: baseline, where we presented a dynamic gabor without any filter and optogenetic, where presented the same stimulus after filtering with the optogenetic model.

There was a ten-fold decrease in contrast sensitivity in the optogenetic conditions across six participants, an expected result based on the decrease of stimulus contrast after convolving it with the optogenetic model output (see Figure 17). The amplitude and phase of the filtered stimulus depends on temporal frequency, so we expected to see change in estimated contrast sensitivity at different temporal frequencies. Indeed, we found that peak sensitivity shifted towards lower temporal frequencies in the optogenetic condition; but this change was not observed in the spatial frequency domain (Figure 23 &

Figure 24). Meaning, the optogenetic model acted as a low-pass filter, in addition to decreasing contrast sensitivity.

4.5.2 *Limitations*

Our study design restricted us to conduct qCSF, the Bayesian adaptive estimation paradigm (Lesmes et al., 2010b) for either spatial or temporal frequency, rather than sampling a range of spatiotemporal frequency pairs. We had to remove the highest spatial frequency tested, 36 cpd, from all conditions due to an abnormal increase in contrast sensitivity in the baseline condition where temporal frequency varied according to the estimation staircase (Supplementary Figure 1).

Our optogenetic model focused only on the effect of temporal delay on spatiotemporal contrast sensitivity while there are many other factors that differentiates optogenetic restored vision from neurotypical vision. The unselective stimulation of ON-OFF cells is projected to

provide unnatural vision (Esquenazi et al., 2021), in addition to the spatial distortions due to retinal remodeling and degeneration inherent to the diseases. At greater light intensities, axonal stimulation might be a factor decreasing spatial resolution (Ferrari et al., 2020).

We based our model on firing rate data from rd1 mouse model. Mouse models are efficient and are similar at the cellular level, however, they differ due to lack of fovea and certain types of retinal ganglion cells, and uniform inner limiting membrane (Roska & Sahel, 2018). Since temporal kinetics depend on gated-channel responses, we were confident incorporating mouse data but for more complex behaviors, mouse data should be used in caution, keeping the divergences from mammalian retina in mind.

4.5.3 *Future Directions*

The virtual patient framework is designed to be modular and able to account for various types of sight restoration technologies. Current optogenetic model can account for two types of photoswitches from Berry et al. (2019) and Holt et al. (2022) but the underlying parameters can be adapted for other optogenetic methods as long as the temporal sensitivity data is available. A natural follow-up would be to present sighted participants gratings filtered through different protein models and comparing cross-protein contrast sensitivity, similar to the theoretical work by Bansal group (2021).

Our model did not account for eye or head movements when computing change in contrast in the optogenetic condition. Natural head and eye movements changes the position of the visual stimulus on the retina; delay in response should exacerbate the blurring effect observed. A potential advantage of virtual patient framework in this context is that the micro-saccades of participants were accounted for in a within-subjects design. However, they were instructed to fixate and all had normal or corrected-to-normal visual acuity. Nystagmus is a common occurrence in patients

suffering from retinal degeneration, so it is important to account for large-scale eye movements in simulating optogenetic response in humans.

Human contrast sensitivity changes with several other factors such as eccentricity of the stimulus, mean luminance, age of the viewer, and retinal degeneration. Our participant pool had a median age of 27 (22-52). Either including the effect of the aforementioned factors into the model or doing the same task with a more representative sample group would benefit future studies.

4.5.4 *Conclusion*

The results in this study demonstrate that spatial resolution of the optogenetic vision also depends on stimulus motion. A computational model focusing on the kinetics of rodent optogenetic response was used as a filter to flickering Gabor stimulus and was presented to sighted participants. Contrast sensitivity was measured to be lower by a factor of 10 after optogenetic filtering than when viewing unfiltered stimulus. Notably, the difference between the optogenetic and unfiltered stimulus was influenced by the change in temporal frequency more than spatial frequency. Peak contrast sensitivity was reached at lower temporal frequencies in the optogenetic condition than the baseline condition. Meaning, the range of visible dynamic stimulus is narrower when there is a temporal delay.

The major implication of these results is that at clinical testing stage, dynamic grating tasks should be used for measuring functional vision. A patient who has undergone optogenetic therapy with a similar temporal profile might perform better at static optotype charts, but their performance might drop when viewing dynamic stimulus such as a car passing by.

Chapter 5. DISCUSSION

5.1 SUMMARY

The effects of losing sight are profound and life changing. While the first three leading causes of blindness -uncorrected refractive error, glaucoma and cataract-, are treatable or preventable, individuals affected by inherited retinal degenerative diseases such as certain types of Age-related Macular Degeneration and Retinitis Pigmentosa, are currently only offered management of the symptoms with no current potential cure to the diseases causing it.

Sight restoration technologies target vision loss due to retinal degeneration. The success of these technologies in providing functional vision will improve the quality-of-life of the affected population and alleviate the psychological, financial, and societal burden. In the past thirty years, major progress has been achieved in inducing light perception using electrical implants, optogenetic proteins and photoswitches. In addition, gene therapies such as LUXTURNA (Spark Therapeutics, USA), targeting RPE65 related retinal degeneration, has been approved for clinical use to treat Leber's Congenital Amaurosis (Russell et al., 2017).

At the forefront of the sight restoration development, there is a need for a consensus on harmonizing the visual outcomes, measuring efficacy, comparing different methods, and incorporating the feedback from the affected patients (Ayton, Rizzo, et al., 2020; Sandrian et al., 2023). Some visual function measures are adapted from neurotypical or low vision where artificial vision provided by sight restoration technologies are qualitatively different; similar to vocoder-like output of cochlear implants. Methods specifically designed for restored vision such as device ON vs. OFF tests can vary significantly across research groups or technologies investigated. An alternative approach can be to prototype restored visual outcomes from past literature and compare predictions to patient outcomes.

This thesis attempted to fill the gap between the theoretical pre-clinical work and clinical outcome measures by combining psychophysical methods and computational modeling. Focusing on two methods: electrical and optogenetic stimulation, we characterized factors influencing spatial resolution of the restored vision. Main findings were:

1. The perceptual experiences of Argus II patients are highly variable. The outcome measures that depend on camera input with ensemble array stimulation might not capture the spatial resolution limits provided by these devices. An alternative measure that bypasses the camera, two-point discrimination, revealed that spatial resolution is lower than theoretical predictions.
2. Simulations factoring in current spread, distance between electrodes, distance of the array from the retina, axonal stimulation and retinal damage showed that minimizing these factors would improve the spatial resolution of Argus II.
3. Optogenetic stimulation has potential to closely mimic healthy photoreceptor signaling but our simulations showed that the temporal delay in cell response of state-of-the-art optogenetic technology will decrease the spatiotemporal contrast sensitivity and this effect is mediated by temporal frequency. When measuring functional vision, tasks involving dynamic stimuli should be incorporated to get a better picture.

5.2 Why Is Measuring Visual Performance Via Psychophysical Methods Important?

Systematic characterization of stimulus-response relationship can reveal information about the underlying mechanisms. Psychophysical methods adapted to sight restoration technologies are especially important at the emergence of the field to objectively describe device effectiveness

across methods, research sites, and individuals. Similar to the early psychophysical studies of neurotypical vision in the 20th century, the sight restoration field can benefit from establishing response properties of carefully controlled stimulus.

Unlike daily-use measures, psychophysical results can be implemented in modeling of restored vision. Preprocessing of the visual input is a common feature across most sight restoration technologies. Psychophysical results can be 'reverse-engineered' to change preprocessing methods to provide an improved perceptual experience to the patients. As a recent example, Granley and colleagues (2023) proposed a stimulus encoding model of electrical stimulation based on psychophysical measures that can adapt to individual percepts. This encoder combines behavioral response and modeling to provide optimal stimulation parameters.

5.3 Why Is Modeling Restored Vision Important?

Restored vision through any technology described in this thesis is a novel experience, similar to cochlear implant percepts or language acquisition. Words from a foreign language sound hard to decipher until the learner is exposed to it for a sustained period. Before comparing restored vision to neurotypical vision, the characteristics of the restored vision can be better defined through simulation and modeling.

In the context of sight restoration, modeling can take various orthogonal approaches: physiology-oriented models and perception-oriented models, similar to bottom-up vs top-down dichotomy in neural processing. Schools of researchers focus on building a detailed descriptive model of underlying physiology, biophysical and electrical constraints to simulate restored vision (for example, see Golden et al., 2019 for a physiological model of electrical stimulation; Tong et al., 2020 for a biophysical model of electrical stimulation; Antolik et al., 2021 for a physiological

model of cortical optogenetic stimulation). Alternatively, the perceptual experience of restored vision can be modeled through behavioral response data utilizing the available technology (for examples, see Beyeler, Boynton, et al., 2017b; Esquenazi et al., 2021 for models of epiretinal stimulation and perceptual learning).

Both approaches can elucidate the artificial vision provided by sight restoration technologies prior to the widespread applications informing researchers on what is the most probable outcome of a given intervention. An example can be the functional assessment of Argus II and Alpha-IMS by Stronks and Dagnelie (2014) where they predict the theoretical psychophysical outcomes.

Chapter 2 and Chapter 3 of this thesis describe a series of psychophysical tasks completed with nine Argus II users, approximately 2% of the worldwide population. We were fortunate to have collaborators that work with individuals with Argus II but the majority of clinical testing was done with a limited number of participants. Another benefit of simulating restored vision is the ability to sequentially test and pilot stimulation methods and parameters that influence phosphene generation with sighted participants. This way, the researchers can gain insights in a fast, efficient, and cost-effective manner without burdening our clinical population with extensive testing.

Setting up patient and clinician expectations prior to choosing a sight restoration technology is a challenge that can be overcome through simulated artificial vision. Since this is an emerging field, patients have limited access to testimonies of past users unlike an individual getting a LASIK operation. Simulations can be informative for patients, caregivers, and clinicians prior to the operation. In the same vein, funding and regulatory agencies can use simulations and model outcomes as a benchmark when approving or assessing performance of any technology discussed.

In Chapter 4, we assessed a type of optogenetic photoswitch at its pre-clinical testing stage by building a model based on the results from animal models. While there were many assumptions, we focused on the effect of only one parameter and saw the cumulative effect of the difference between neurotypical and optogenetic signaling through sighted participant's response across conditions. This will potentially inform optogenetic sight restoration researchers once the therapy proceeds to clinical setting.

5.4 Ethical Considerations

Regulatory agencies such as FDA can fast-track technologies targeting rare diseases such as RP as a 'Humanitarian Use Device' (HUD) which are exempt for efficacy requirements usually required for a pre-market approval (Sandrian et al., 2023). In addition, companies can seek 'Investigational Device Exemption' (IDE) or 'Breakthrough Device Designation' to accelerate their clinical investigations. While there is an undeniable benefit to expediting regulatory processes, long-term consequences of permanent implantation/injection to the patients are a major concern.

A notable case is Argus II by Second Sight. Inc (now Cortigent, Inc) (*Humanitarian Device Exemption (HDE)*), which was approved by FDA in 2013 and was implanted in more than 350 patients. The device was commercially available until 2019, when the company suspended its production and promised long-term support for its existing Argus II patients. However, according to a report by Rachitskaya and colleagues (2020), Argus II users have not been able to access support in the emergency events such as device dysfunction during daily use since the company laid off their rehabilitation experts. The users were promised firmware updates that would improve their perceptual experience and target technical difficulties, but the update was not delivered. The

research on these technologies continues, for example, Bajaj and colleagues (2019) implemented an investigational thermal camera for Argus II users to detect heat, which could potentially be a valuable source of information while navigating. In all tasks that involve mobility, object and person identification, thermal camera outperformed the standard camera. Ideally, these results could be implemented without an additional surgery for patients who already have the device. However, Argus II users might have to face difficult decision between keeping an obsolete technology implanted or go through another invasive surgery to explant it. The decision to get a chronic implant that involves an invasive surgery and long-term training and rehabilitation should be supported by extensive research, well-informed clinicians, and the involvement of patient advocacy groups.

There needs to be more guidance on under what circumstances a long-term implant or injection is available from health organizations and regulatory bodies. Above all, when regulating clinical trials, emphasis should be made on long-term support of for-profit companies to avoid instances such as Argus II deprecation.

In a recently published ethics study conducted with patients with Orion cortical implant, authors share patient anecdotes where they share their feedback on their device, its long-term compatibility, the discrepancy between their expectations and the outcome (Levy et al., 2023). One patient shares:

> *'You have the device implanted and if you leave it in the way the agreement is written, or the contract, whatever you want to call, I think after five years you're essentially on your own, so if there's some reason you need to get it taken care of you're on the hook for it. And so, with the financial trouble of Second Sight, I was wondering if I was going to be able to get it taken out. [P4]' (Levy et al., 2023).*

Notably, the majority of the Orion patients said that they were aware of the limited functionality of the devices and were more motivated by their contribution to science and the development of improved sight restoration technologies. However, the researchers discussed that the perceived risk of participating does not align fully with what is covered in the informed consent, mainly in terms of 'high expectations with regard to the long-term technological advancement of Orion and similar devices', the ability to participate in other interventions, and the financial risks of having a chronic visual implant (Levy et al., 2023).

The variable experience of our participants in the Argus II spatial resolution study is similar to what is described in the Levy study. One participant reported that they would only use the device once a month or during clinical testing due to headaches; that they do not get enough benefit from it to use it more frequently. Almost all of our participants used other assistive devices such as walking cane in conjunction with Argus II, similar to Orion users. Nevertheless, they also were motivated by their irreplaceable contribution to future development.

More systematic research and discussion in the area of neuroethics is needed to minimize the potential risks discussed in this section and protect the interests of patients using sight restoration technology. More research focused on prototyping and modeling as discussed previously can enable progress without direct testing at clinical trials.

5.5 Future Directions

With the advancements in material engineering, surgical tools, genetic engineering, and modeling, sight restoration is one of the most exciting areas of research to be in. The technologies discussed in this thesis are the early proof-of-concepts and with every scientific breakthrough they will improve.

To summarize the recent milestones:

5.5.1 *Electrical Prostheses*

- Palanker and colleagues (2022) demonstrated 12-24 month safety of PRIMA (Pixium Vision, SA, Paris, France) in patients with AMD who has peripheral vision. The participants were able to perceive light at the scotoma in the central vision through the implant and simultaneously use their peripheral vision. With the device on and is set to the user's preferred magnification, four out of five patients achieved the Landolt prosthetic acuity of 20/63-20-98 (Palanker et al., 2022).
- Orion cortical prosthesis clinical trials are ongoing with six patients.

5.5.2 *Biological Alternatives*

- Nanocarriers for ophthalmic drugs that can go through ocular barrier with less resistance promise improved biocompatibility (Li et al., 2023).
- Clinical trials for gene editing drugs such as ZVS203e are ongoing with 9 participants (NCT05805007)
- Optogenetic proteins like bReaChES that can generate light perception at indoor lighting with detection rate of up to 50 Hz are at pre-clinical stage (Bansal et al., 2021).
- Neurotransmitter stimulation, where engineered fluid chips stimulate remaining retinal circuitry are in early stages of development (Iezzi & Finlayson, 2011).

The question of which therapy will provide the vision closest to neurotypical vision currently has no clear answer. Each method has a unique advantage and challenges to overcome. A combination of methods, such as using electrical implants/optogenetic therapy as an alternative after neuroprevention and gene editing methods can potentially yield the optimal restored vision.

BIBLIOGRAPHY

Acland, G. M., Aguirre, G. D., Ray, J., Zhang, Q., Aleman, T. S., Cideciyan, A. V., Pearce-Kelling, S. E., Anand, V., Zeng, Y., Maguire, A. M., Jacobson, S. G., Hauswirth, W. W., & Bennett, J. (2001). Gene therapy restores vision in a canine model of childhood blindness. *Nature Genetics*, *28*(1), Article 1. https://doi.org/10.1038/ng0501-92

Ahuja, A. K., Behrend, M. R., Kuroda, M., Humayun, M. S., & Weiland, J. D. (2008). An *In Vitro* Model of a Retinal Prosthesis. *IEEE Transactions on Biomedical Engineering*, *55*(6), 1744–1753. https://doi.org/10.1109/TBME.2008.919126

Ahuja, A. K., Dorn, J. D., Caspi, A., McMahon, M. J., Dagnelie, G., daCruz, L., Stanga, P., Humayun, M. S., Greenberg, R. J., & Group, A. I. S. (2011). Blind subjects implanted with the Argus II retinal prosthesis are able to improve performance in a spatial-motor task. *British Journal of Ophthalmology*, *95*(4), 539–543. https://doi.org/10.1136/bjo.2010.179622

Ahuja, A. K., Yeoh, J., Dorn, J. D., Caspi, A., Wuyyuru, V., McMahon, M. J., Humayun, M. S., Greenberg, R. J., & daCruz, L. (2013). Factors Affecting Perceptual Threshold in Argus II Retinal Prosthesis Subjects. *Translational Vision Science & Technology*, *2*(4). https://doi.org/10.1167/tvst.2.4.1

Antolik, J., Sabatier, Q., Galle, C., Frégnac, Y., & Benosman, R. (2021). Assessment of optogenetically-driven strategies for prosthetic restoration of cortical vision in large-scale neural simulation of V1. *Scientific Reports*, *11*(1), Article 1. https://doi.org/10.1038/s41598-021-88960-8

Arevalo, J. F., Al Rashaed, S., Alhamad, T. A., Al Kahtani, E., Al-Dhibi, H. A., for the KKESH Collaborative Retina Study Group, Mura, M., Al Kahtani, E., Nowilaty, S., Al Rashaed, S., Al-Dhibi, H. A., Al-Zahrani, Y. A., Kozak, I., Al-Sulaiman, S., Al-Abdullah, A., Al-Bar, A., Al Dhafiri, Y., Al Qahtani, A., Al Rubaie, K., … Fernando Arevalo, J. (2021). Argus II retinal prosthesis for retinitis pigmentosa in the Middle East: The 2015 Pan-American Association of Ophthalmology Gradle Lecture. *International Journal of Retina and Vitreous*, *7*(1), 65. https://doi.org/10.1186/s40942-021-00324-6

Ayton, L. N., Barnes, N., Dagnelie, G., Fujikado, T., Goetz, G., Hornig, R., Jones, B. W., Muqit, M. M. K., Rathbun, D. L., Stingl, K., Weiland, J. D., & Petoe, M. A. (2020). An update on retinal prostheses. *Clinical Neurophysiology*, *131*(6), 1383–1398. https://doi.org/10.1016/j.clinph.2019.11.029

Ayton, L. N., Blamey, P. J., Guymer, R. H., Luu, C. D., Nayagam, D. A. X., Sinclair, N. C., Shivdasani, M. N., Yeoh, J., McCombe, M. F., Briggs, R. J., Opie, N. L., Villalobos, J., Dimitrov, P. N., Varsamidis, M., Petoe, M. A., McCarthy, C. D., Walker, J. G., Barnes, N., Burkitt, A. N., … for the Bionic Vision Australia Research Consortium. (2014). First-in-Human Trial of a Novel Suprachoroidal Retinal Prosthesis. *PLoS ONE*, *9*(12), e115239. https://doi.org/10.1371/journal.pone.0115239

Ayton, L. N., Rizzo, J. F., Bailey, I. L., Colenbrander, A., Dagnelie, G., Geruschat, D. R., Hessburg, P. C., McCarthy, C. D., Petoe, M. A., Rubin, G. S., Troyk, P. R., & for the HOVER International Taskforce. (2020). Harmonization of Outcomes and Vision Endpoints in Vision Restoration Trials: Recommendations from the International HOVER Taskforce. *Translational Vision Science & Technology*, *9*(8), 25. https://doi.org/10.1167/tvst.9.8.25

Bach, M. (1996). The Freiburg Visual Acuity Test—Automatic Measurement of Visual Acuity. *Optometry and Vision Science*, *73*(1), 49.

Bach, M., Wilke, M., Wilhelm, B., Zrenner, E., & Wilke, R. (2010). Basic quantitative assessment of visual performance in patients with very low vision. *Investigative Ophthalmology & Visual Science*, *51*(2), 1255–1260. https://doi.org/10.1167/iovs.09-3512

Bach-Y-Rita, P., Collins, C. C., Saunders, F. A., White, B., & Scadden, L. (1969). Vision Substitution by Tactile Image Projection. *Nature*, *221*(5184), Article 5184. https://doi.org/10.1038/221963a0

Bahar, N. (2019). *Sight Restoration via Ocular Tissue Engineering*. https://doi.org/10.13140/RG.2.2.32195.25126/1

Bailey, I. L., Jackson, A. J., Minto, H., Greer, R. B., & Chu, M. A. (2012). The Berkeley Rudimentary Vision Test. *Optometry and Vision Science*, *89*(9), 1257. https://doi.org/10.1097/OPX.0b013e318264e85a

Bajaj, R., Sadeghi, R., Barry, M. P., Gibson, P., Caspi, A., Roy, A., & Dagnelie, G. (2019). Seeing Heat: Efficacy of a Thermal Camera in the Argus II Retinal Prosthesis System. *Investigative Ophthalmology & Visual Science*, *60*(9), 4017.

Bansal, H., Gupta, N., & Roy, S. (2021). Theoretical analysis of optogenetic spiking with ChRmine, bReaChES and CsChrimson-expressing neurons for retinal prostheses. *Journal of Neural Engineering*, *18*(4), 0460b8. https://doi.org/10.1088/1741-2552/ac1175

Barry, M. P., Sadeghi, R., Towle, V. L., Stipp, K., Puhov, H., Diaz, W., Grant, P., Collison, F. T., Lane, F. J., Szlyk, J. P., Dagnelie, G., & Troyk, P. R. (2023). Preliminary visual function for the first human with the Intracortical Visual Prosthesis (ICVP). *Investigative Ophthalmology & Visual Science*, *64*(8), 2842.

Beauchamp, M. S., Oswalt, D., Sun, P., Foster, B. L., Magnotti, J. F., Niketeghad, S., Pouratian, N., Bosking, W. H., & Yoshor, D. (2020). Dynamic Stimulation of Visual Cortex Produces Form Vision in Sighted and Blind Humans. *Cell*, *181*(4), 774-783.e5. https://doi.org/10.1016/j.cell.2020.04.033

Berry, M. H., Holt, A., Levitz, J., Broichhagen, J., Gaub, B. M., Visel, M., Stanley, C., Aghi, K., Kim, Y. J., Cao, K., Kramer, R. H., Trauner, D., Flannery, J., & Isacoff, E. Y. (2017). Restoration of patterned vision with an engineered photoactivatable G protein-coupled receptor. *Nature Communications*, *8*(1), 1862. https://doi.org/10.1038/s41467-017-01990-7

Berry, M. H., Holt, A., Salari, A., Veit, J., Visel, M., Levitz, J., Aghi, K., Gaub, B. M., Sivyer, B., Flannery, J. G., & Isacoff, E. Y. (2019). Restoration of high-sensitivity and adapting vision with a cone opsin. *Nature Communications*, *10*(1), 1221. https://doi.org/10.1038/s41467-019-09124-x

Beyeler, M., Boynton, G. M., Fine, I., & Rokem, A. (2017a). *pulse2percept: A Python-based simulation framework for bionic vision*. https://doi.org/10.1101/148015

Beyeler, M., Boynton, G. M., Fine, I., & Rokem, A. (2017b). pulse2percept: A Python-based simulation framework for bionic vision. *Proceedings of the 16th Python in Science Conference*, 81–88. https://doi.org/10.25080/shinma-7f4c6e7-00c

Beyeler, M., Nanduri, D., Weiland, J. D., Rokem, A., Boynton, G. M., & Fine, I. (2019). A model of ganglion axon pathways accounts for percepts elicited by retinal implants. *Scientific Reports*, *9*(1), 9199. https://doi.org/10.1038/s41598-019-45416-4

Beyeler, M., Rokem, A., Boynton, G. M., & Fine, I. (2017). Learning to see again: Biological constraints on cortical plasticity and the implications for sight restoration technologies. *Journal of Neural Engineering*, *14*(5), 051003. https://doi.org/10.1088/1741-2552/aa795e

Bi, A., Cui, J., Ma, Y.-P., Olshevskaya, E., Pu, M., Dizhoor, A. M., & Pan, Z.-H. (2006). Ectopic Expression of a Microbial-Type Rhodopsin Restores Visual Responses in Mice with Photoreceptor Degeneration. *Neuron*, *50*(1), 23–33. https://doi.org/10.1016/j.neuron.2006.02.026

Bittner, A. K., Jeter, P., & Dagnelie, G. (2011). Grating Acuity and Contrast Tests for Clinical Trials of Severe Vision Loss. *Optometry and Vision Science*, *88*(10), 1153. https://doi.org/10.1097/OPX.0b013e3182271638

Bosking, W. H., Beauchamp, M. S., & Yoshor, D. (2017). Electrical Stimulation of Visual Cortex: Relevance for the Development of Visual Cortical Prosthetics. *Annual Review of Vision Science*, *3*(1), 141–166. https://doi.org/10.1146/annurev-vision-111815-114525

Bourne, R. R. A., Stevens, G. A., White, R. A., Smith, J. L., Flaxman, S. R., Price, H., Jonas, J. B., Keeffe, J., Leasher, J., Naidoo, K., Pesudovs, K., Resnikoff, S., & Taylor, H. R. (2013). Causes of vision loss worldwide, 1990–2010: A systematic analysis. *The Lancet Global Health*, *1*(6), e339–e349. https://doi.org/10.1016/S2214-109X(13)70113-X

Boyden, E. S., Zhang, F., Bamberg, E., Nagel, G., & Deisseroth, K. (2005). Millisecond-timescale, genetically targeted optical control of neural activity. *Nature Neuroscience*, *8*(9), 1263–1268. https://doi.org/10.1038/nn1525

Brindley, G. S., & Lewin, W. S. (1968). The sensations produced by electrical stimulation of the visual cortex. *The Journal of Physiology*, *196*(2), 479–493. https://doi.org/10.1113/jphysiol.1968.sp008519

Busskamp, V., Picaud, S., Sahel, J. A., & Roska, B. (2012). Optogenetic therapy for retinitis pigmentosa. *Gene Therapy*, *19*(2), 169–175. https://doi.org/10.1038/gt.2011.155

Caspi, A., Barry, M. P., Patel, U. K., Salas, M. A., Dorn, J. D., Roy, A., Niketeghad, S., Greenberg, R. J., & Pouratian, N. (2021). Eye movements and the perceived location of phosphenes generated by intracranial primary visual cortex stimulation in the blind. *Brain Stimulation*, *14*(4), 851–860. https://doi.org/10.1016/j.brs.2021.04.019

Caspi, A., Roy, A., Dorn, J. D., & Greenberg, R. J. (2017). Retinotopic to Spatiotopic Mapping in Blind Patients Implanted With the Argus II Retinal Prosthesis. *Investigative Opthalmology & Visual Science*, *58*(1), 119. https://doi.org/10.1167/iovs.16-20398

Caspi, A., & Zivotofsky, A. Z. (2015). Assessing the utility of visual acuity measures in visual prostheses. *Vision Research*, *108*, 77–84. https://doi.org/10.1016/j.visres.2015.01.006

Cehajic-Kapetanovic, J., Singh, M. S., Zrenner, E., & MacLaren, R. E. (2022). Bioengineering strategies for restoring vision. *Nature Biomedical Engineering*. https://doi.org/10.1038/s41551-021-00836-4

Cheng, D. L., Greenberg, P. B., & Borton, D. A. (2017). Advances in Retinal Prosthetic Research: A Systematic Review of Engineering and Clinical Characteristics of Current Prosthetic Initiatives. *Current Eye Research*, *42*(3), 334–347. https://doi.org/10.1080/02713683.2016.1270326

Curcio, C. A., Sloan, K. R., Kalina, R. E., & Hendrickson, A. E. (1990). Human photoreceptor topography. *Journal of Comparative Neurology*, *292*(4), 497–523. https://doi.org/10.1002/cne.902920402

da Cruz, L., Dorn, J. D., Humayun, M. S., Dagnelie, G., Handa, J., Barale, P.-O., Sahel, J.-A., Stanga, P. E., Hafezi, F., Safran, A. B., Salzmann, J., Santos, A., Birch, D., Spencer, R.,

Cideciyan, A. V., de Juan, E., Duncan, J. L., Eliott, D., Fawzi, A., … Greenberg, R. J. (2016). Five-Year Safety and Performance Results from the Argus II Retinal Prosthesis System Clinical Trial. *Ophthalmology*, *123*(10), 2248–2254. https://doi.org/10.1016/j.ophtha.2016.06.049

Dacey, D. (2004). *Origins of perception: Retinal ganglion cell diversity and the creation of parallel visual pathways*. 66.

Dacey, D. M. (1999). Primate retina: Cell types, circuits and color opponency. *Progress in Retinal and Eye Research*, *18*(6), 737–763. https://doi.org/10.1016/S1350-9462(98)00013-5

Dacey, D. M., & Petersen, M. R. (1992). Dendritic field size and morphology of midget and parasol ganglion cells of the human retina. *Proceedings of the National Academy of Sciences*, *89*(20), 9666–9670. https://doi.org/10.1073/pnas.89.20.9666

de Balthasar, C., Patel, S., Roy, A., Freda, R., Greenwald, S., Horsager, A., Mahadevappa, M., Yanai, D., McMahon, M. J., Humayun, M. S., Greenberg, R. J., Weiland, J. D., & Fine, I. (2008). Factors Affecting Perceptual Thresholds in Epiretinal Prostheses. *Investigative Opthalmology & Visual Science*, *49*(6), 2303. https://doi.org/10.1167/iovs.07-0696

Dias, M. F., Joo, K., Kemp, J. A., Fialho, S. L., da Silva Cunha, A., Woo, S. J., & Kwon, Y. J. (2018). Molecular genetics and emerging therapies for retinitis pigmentosa: Basic research and clinical perspectives. *Progress in Retinal and Eye Research*, *63*, 107–131. https://doi.org/10.1016/j.preteyeres.2017.10.004

Dobelle, W. H. (2000). Artificial Vision for the Blind by Connecting a Television Camera to the Visual Cortex. *ASAIO Journal*, *46*(1), 3.

Dobelle, W. H., Dobelle, W. H., Quest, D. O., Antunes, J. L., Roberts, T. S., & Girvin, J. P. (1979). Artificial Vision for the Blind by Electrical Stimulation of the Visual Cortex. *Neurosurgery*, *5*(4), 521–527. https://doi.org/10.1227/00006123-197910000-00022

Dowling, J. (1987). *The Retina*. Harvard University Press.

Drasdo, N., & Fowler, C. W. (1974). Non-linear projection of the retinal image in a wide-angle schematic eye. *British Journal of Ophthalmology*, *58*(8), 709–714. https://doi.org/10.1136/bjo.58.8.709

Editas Medicine, Inc. (2022). *Open-Label, Single Ascending Dose Study to Evaluate the Safety, Tolerability, and Efficacy of EDIT-101 in Adult and Pediatric Participants With Leber Congenital Amaurosis Type 10 (LCA10), With Centrosomal Protein 290 (CEP290)-Related Retinal Degeneration Caused by a Compound Heterozygous or Homozygous Mutation Involving c.2991+1655A>G in Intron 26 (IVS26) of the CEP290 Gene ("LCA10-IVS26")* (Clinical Trial Registration NCT03872479). clinicaltrials.gov. https://clinicaltrials.gov/ct2/show/NCT03872479

Erickson-Davis, C., & Korzybska, H. (2021). What do blind people "see" with retinal prostheses? Observations and qualitative reports of epiretinal implant users. *PLOS ONE*, *16*(2), e0229189. https://doi.org/10.1371/journal.pone.0229189

Esler, T. B., Kerr, R. R., Tahayori, B., Grayden, D. B., Meffin, H., & Burkitt, A. N. (2018). Minimizing activation of overlying axons with epiretinal stimulation: The role of fiber orientation and electrode configuration. *PLOS ONE*, *13*(3), e0193598. https://doi.org/10.1371/journal.pone.0193598

Esquenazi, R. B., Meier, K., Beyeler, M., Boynton, G. M., & Fine, I. (2021). Learning to see again: Perceptual learning of simulated abnormal on- off-cell population responses in sighted individuals. *Journal of Vision*, *21*(13), 10. https://doi.org/10.1167/jov.21.13.10

Euler, T., Haverkamp, S., Schubert, T., & Baden, T. (2014). Retinal bipolar cells: Elementary building blocks of vision. *Nature Reviews Neuroscience*, *15*(8), Article 8. https://doi.org/10.1038/nrn3783

Farnum, A., & Pelled, G. (2020). New Vision for Visual Prostheses. *Frontiers in Neuroscience*, *14*, 36. https://doi.org/10.3389/fnins.2020.00036

Fernández, E., Alfaro, A., Soto-Sánchez, C., Gonzalez-Lopez, P., Lozano, A. M., Peña, S., Grima, M. D., Rodil, A., Gómez, B., Chen, X., Roelfsema, P. R., Rolston, J. D., Davis, T. S., & Normann, R. A. (2021). Visual percepts evoked with an intracortical 96-channel microelectrode array inserted in human occipital cortex. *The Journal of Clinical Investigation*, *131*(23). https://doi.org/10.1172/JCI151331

Ferrari, U., Deny, S., Sengupta, A., Caplette, R., Trapani, F., Sahel, J.-A., Dalkara, D., Picaud, S., Duebel, J., & Marre, O. (2020). Towards optogenetic vision restoration with high resolution. *PLOS Computational Biology*, *16*(7), e1007857. https://doi.org/10.1371/journal.pcbi.1007857

Field, G. D., & Chichilnisky, E. J. (2007). Information Processing in the Primate Retina: Circuitry and Coding. *Annual Review of Neuroscience*, *30*(1), 1–30. https://doi.org/10.1146/annurev.neuro.30.051606.094252

Field, G. D., & Rieke, F. (2002). Nonlinear Signal Transfer from Mouse Rods to Bipolar Cells and Implications for Visual Sensitivity. *Neuron*, *34*(5), 773–785. https://doi.org/10.1016/S0896-6273(02)00700-6

Fine, I., & Boynton, G. M. (2015). Pulse trains to percepts: The challenge of creating a perceptually intelligible world with sight recovery technologies. *Philosophical Transactions of the Royal Society B: Biological Sciences*, *370*(1677), 20140208. https://doi.org/10.1098/rstb.2014.0208

Fishman, R. S. (1997). Gordon Holmes, the cortical retina, and the wounds of war: The seventh Charles B. Snyder lecture. *Documenta Ophthalmologica*, *93*(1–2), 9–28. https://doi.org/10.1007/BF02569044

Foerster, O. (1929). Beitrage zur pathophysiologie der sehbahn und der sehsphare. *J. Psychol. Neurol., Lpz.*, *39*, 463.

Fried, S. I., Lasker, A. C. W., Desai, N. J., Eddington, D. K., & Rizzo, J. F. (2009). Axonal Sodium-Channel Bands Shape the Response to Electric Stimulation in Retinal Ganglion Cells. *Journal of Neurophysiology*, *101*(4), 1972–1987. https://doi.org/10.1152/jn.91081.2008

Fujikado, T. (2017). Retinal Prosthesis by Suprachoroidal-Transretinal Stimulation (STS), Japanese Approach. In V. P. Gabel (Ed.), *Artificial Vision: A Clinical Guide* (pp. 139–150). Springer International Publishing. https://doi.org/10.1007/978-3-319-41876-6_11

Fujikado, T., Kamei, M., Sakaguchi, H., Kanda, H., Morimoto, T., Ikuno, Y., Nishida, K., Kishima, H., Maruo, T., Konoma, K., Ozawa, M., & Nishida, K. (2011a). Testing of Semichronically Implanted Retinal Prosthesis by Suprachoroidal-Transretinal Stimulation in Patients with Retinitis Pigmentosa. *Investigative Ophthalmology & Visual Science*, *52*(7), 4726–4733. https://doi.org/10.1167/iovs.10-6836

Fujikado, T., Kamei, M., Sakaguchi, H., Kanda, H., Morimoto, T., Ikuno, Y., Nishida, K., Kishima, H., Maruo, T., Konoma, K., Ozawa, M., & Nishida, K. (2011b). Testing of Semichronically Implanted Retinal Prosthesis by Suprachoroidal-Transretinal Stimulation in Patients with Retinitis Pigmentosa. *Investigative Opthalmology & Visual Science*, *52*(7), 4726. https://doi.org/10.1167/iovs.10-6836

Gauvain, G., Akolkar, H., Chaffiol, A., Arcizet, F., Khoei, M. A., Desrosiers, M., Jaillard, C., Caplette, R., Marre, O., Bertin, S., Fovet, C.-M., Demilly, J., Forster, V., Brazhnikova, E., Hantraye, P., Pouget, P., Douar, A., Pruneau, D., Chavas, J., … Picaud, S. (2021). Optogenetic therapy: High spatiotemporal resolution and pattern discrimination compatible with vision restoration in non-human primates. *Communications Biology*, *4*(1), 125. https://doi.org/10.1038/s42003-020-01594-w

Golden, J. R., Erickson-Davis, C., Cottaris, N. P., Parthasarathy, N., Rieke, F., Brainard, D. H., Wandell, B. A., & Chichilnisky, E. J. (2018). Simulation of visual perception and learning with a retinal prosthesis. *bioRxiv*, 206409. https://doi.org/10.1101/206409

Golden, J. R., Erickson-Davis, C., Cottaris, N. P., Parthasarathy, N., Rieke, F., Brainard, D. H., Wandell, B. A., & Chichilnisky, E. J. (2019). Simulation of visual perception and learning with a retinal prosthesis. *Journal of Neural Engineering*, *16*(2), 025003. https://doi.org/10.1088/1741-2552/aaf270

Granley, J., Fauvel, T., Chalk, M., & Beyeler, M. (2023). *Human-in-the-Loop Optimization for Deep Stimulus Encoding in Visual Prostheses* (arXiv:2306.13104). arXiv. http://arxiv.org/abs/2306.13104

Greenwald, S. H., Horsager, A., Humayun, M. S., Greenberg, R. J., McMahon, M. J., & Fine, I. (2009). Brightness as a Function of Current Amplitude in Human Retinal Electrical Stimulation. *Investigative Opthalmology & Visual Science*, *50*(11), 5017. https://doi.org/10.1167/iovs.08-2897

Gregori, N. Z., Callaway, N. F., Hoeppner, C., Yuan, A., Rachitskaya, A., Feuer, W., Ameri, H., Arevalo, J. F., Augustin, A. J., Birch, D. G., Dagnelie, G., Grisanti, S., Davis, J. L., Hahn, P., Handa, J. T., Ho, A. C., Huang, S. S., Humayun, M. S., Iezzi, R., … Zacks, D. N. (2018). Retinal Anatomy and Electrode Array Position in Retinitis Pigmentosa Patients After Argus II Implantation: An International Study. *American Journal of Ophthalmology*, *193*, 87–99. https://doi.org/10.1016/j.ajo.2018.06.012

Grimes, W. N., Songco-Aguas, A., & Rieke, F. (2018). Parallel Processing of Rod and Cone Signals: Retinal Function and Human Perception. *Annual Review of Vision Science*, *4*(1), 123–141. https://doi.org/10.1146/annurev-vision-091517-034055

Hecht, S., Shlaer, S., & Pirenne, M. H. (1942). ENERGY, QUANTA, AND VISION. *Journal of General Physiology*, *25*(6), 819–840. https://doi.org/10.1085/jgp.25.6.819

Ho, A. C., Humayun, M. S., Dorn, J. D., da Cruz, L., Dagnelie, G., Handa, J., Barale, P.-O., Sahel, J.-A., Stanga, P. E., Hafezi, F., Safran, A. B., Salzmann, J., Santos, A., Birch, D., Spencer, R., Cideciyan, A. V., de Juan, E., Duncan, J. L., Eliott, D., … Greenberg, R. J. (2015). Long-Term Results from an Epiretinal Prosthesis to Restore Sight to the Blind. *Ophthalmology*, *122*(8), 1547–1554. https://doi.org/10.1016/j.ophtha.2015.04.032

Holt, A., Berry, M. H., Lo, J., Donthamsetti, P., Visel, M., Broichhagen, J., Flannery, J. G., & Isacoff, E. Y. (2022). *Restoration of high-sensitivity patterned vision in motion with an engineered light-gated G protein-coupled receptor* [Preprint]. Neuroscience. https://doi.org/10.1101/2022.04.07.487476

Hornig, R., Dapper, M., Le Joliff, E., Hill, R., Ishaque, K., Posch, C., Benosman, R., LeMer, Y., Sahel, J.-A., & Picaud, S. (2017). Pixium Vision: First Clinical Results and Innovative Developments. In V. P. Gabel (Ed.), *Artificial Vision* (pp. 99–113). Springer International Publishing. https://doi.org/10.1007/978-3-319-41876-6_8

Horsager, A., Greenwald, S. H., Weiland, J. D., Humayun, M. S., Greenberg, R. J., McMahon, M. J., Boynton, G. M., & Fine, I. (2009). Predicting Visual Sensitivity in Retinal

Prosthesis Patients. *Investigative Opthalmology & Visual Science*, *50*(4), 1483. https://doi.org/10.1167/iovs.08-2595

Hubel, D. H., & Wiesel, T. N. (1962). Receptive fields, binocular interaction and functional architecture in the cat's visual cortex. *The Journal of Physiology*, *160*(1), 106–154. https://doi.org/10.1113/jphysiol.1962.sp006837

Humayun, M. S., de Juan Jr., E., Weiland, J. D., Dagnelie, G., Katona, S., Greenberg, R., & Suzuki, S. (1999). Pattern electrical stimulation of the human retina. *Vision Research*, *39*(15), 2569–2576. https://doi.org/10.1016/S0042-6989(99)00052-8

Humayun, M. S., Dorn, J. D., da Cruz, L., Dagnelie, G., Sahel, J.-A., Stanga, P. E., Cideciyan, A. V., Duncan, J. L., Eliott, D., Filley, E., Ho, A. C., Santos, A., Safran, A. B., Arditi, A., Del Priore, L. V., & Greenberg, R. J. (2012). Interim Results from the International Trial of Second Sight's Visual Prosthesis. *Ophthalmology*, *119*(4), 779–788. https://doi.org/10.1016/j.ophtha.2011.09.028

Humayun, M. S., & Olmos De Koo, L. C. (Eds.). (2018). *Retinal Prosthesis*. Springer International Publishing. https://doi.org/10.1007/978-3-319-67260-1

Humayun, M. S., Weiland, J. D., Fujii, G. Y., Greenberg, R., Williamson, R., Little, J., Mech, B., Cimmarusti, V., Van Boemel, G., Dagnelie, G., & de Juan, E. (2003). Visual perception in a blind subject with a chronic microelectronic retinal prosthesis. *Vision Research*, *43*(24), 2573–2581. https://doi.org/10.1016/S0042-6989(03)00457-7

Iezzi, R., & Finlayson, P. G. (2011). Neurotransmitter Stimulation for Retinal Prosthesis: The Artificial Synapse Chip. In G. Dagnelie (Ed.), *Visual Prosthetics: Physiology, Bioengineering, Rehabilitation* (pp. 173–191). Springer US. https://doi.org/10.1007/978-1-4419-0754-7_9

Jansonius, N. M., Nevalainen, J., Selig, B., Zangwill, L. M., Sample, P. A., Budde, W. M., Jonas, J. B., Lagrèze, W. A., Airaksinen, P. J., Vonthein, R., Levin, L. A., Paetzold, J., & Schiefer, U. (2009). A mathematical description of nerve fiber bundle trajectories and their variability in the human retina. *Vision Research*, *49*(17), 2157–2163. https://doi.org/10.1016/j.visres.2009.04.029

Jansonius, N. M., & Schiefer, U. (2020). Anatomical Location of the Raphe and Extended Raphe in the Human Retina: Implications for Assessment of the Optic Nerve with OCT. *Translational Vision Science & Technology*, *9*(11), 3. https://doi.org/10.1167/tvst.9.11.3

Jensen, R. J., Ziv, O. R., & Rizzo, J. F. (2005). Thresholds for Activation of Rabbit Retinal Ganglion Cells with Relatively Large, Extracellular Microelectrodes. *Investigative Opthalmology & Visual Science*, *46*(4), 1486. https://doi.org/10.1167/iovs.04-1018

Kaplan, E. (2008). *The P, M and K Streams of the Primate Visual System: What Do They Do for Vision?*

Kawamura, S., & Tachibanaki, S. (2022). Molecular bases of rod and cone differences. *Progress in Retinal and Eye Research*, *90*, 101040. https://doi.org/10.1016/j.preteyeres.2021.101040

Kelly, H. (1979a). *Motion and vision. 1. Stabilized images of stationary gratings*. 9.

Kelly, H. (1979b). *Motion and vision. 11.Stabilized spatio-temporal threshold surface*. 10.

Klauke, S., Goertz, M., Rein, S., Hoehl, D., Thomas, U., Eckhorn, R., Bremmer, F., & Wachtler, T. (2011). Stimulation with a Wireless Intraocular Epiretinal Implant Elicits Visual Percepts in Blind Humans. *Investigative Ophthalmology & Visual Science*, *52*(1), 449–455. https://doi.org/10.1167/iovs.09-4410

Kleiner, M., Brainard, D., & Pelli, D. (2007). What's new in Psychtoolbox-3? *Perception*, *36*(ECVP Abstract Supplement), 1–16.
Krause, F., & Schum, H. (1931). Die epileptischen Erkrankungen. *Neue Deutsche Chirurgie*, *49*, 482–486.
Kuang, X., Poletti, M., Victor, J. D., & Rucci, M. (2012). Temporal Encoding of Spatial Information during Active Visual Fixation. *Current Biology*, *22*(6), 510–514. https://doi.org/10.1016/j.cub.2012.01.050
Kulikowski, J. J. (1971). Effect of eye movements on the contrast sensitivity of spatio-temporal patterns. *Vision Research*, *11*(3), 261–273. https://doi.org/10.1016/0042-6989(71)90190-8
Kutner, M. H. (Ed.). (2005). *Applied linear statistical models* (5. ed). McGraw-Hill Irwin.
Lagnado, L. (2002). Signal Amplification: Let's Turn Down The Lights. *Current Biology*, *12*(6), R215–R217. https://doi.org/10.1016/S0960-9822(02)00754-6
Lauritzen, T. Z., Nanduri, D., Weiland, J., Dorn, J. D., McClure, K., Greenberg, R., & Group, A. I. S. (2011). Inter-electrode Discriminability Correlates With Spatial Visual Performance In ArgusTM II Subjects. *Investigative Ophthalmology & Visual Science*, *52*(14), 4927.
Lesmes, L. A., Lu, Z.-L., Baek, J., & Albright, T. D. (2010a). Bayesian adaptive estimation of the contrast sensitivity function: The quick CSF method. *Journal of Vision*, *10*(3), 17. https://doi.org/10.1167/10.3.17
Lesmes, L. A., Lu, Z.-L., Baek, J., & Albright, T. D. (2010b). Bayesian adaptive estimation of the contrast sensitivity function: The quick CSF method. *Journal of Vision*, *10*(3), 17. https://doi.org/10.1167/10.3.17
Levy, L., Ebadi, H., Peabody Smith, A., Taiclet, L., Pouratian, N., & Feinsinger, A. (2023). Disentangling Function from Benefit: Participant Perspectives from an Early Feasibility Trial for a Novel Visual Cortical Prosthesis. *AJOB Neuroscience*, *0*(0), 1–19. https://doi.org/10.1080/21507740.2023.2257152
Li, S., Chen, L., & Fu, Y. (2023). Nanotechnology-based ocular drug delivery systems: Recent advances and future prospects. *Journal of Nanobiotechnology*, *21*, 232. https://doi.org/10.1186/s12951-023-01992-2
Lin, T.-C., Wang, L.-C., Yue, L., Zhang, Y., Falabella, P., Zhu, D., Hinton, D. R., Rao, N. A., Birch, D. G., Spencer, R., Dorn, J. D., & Humayun, M. S. (2019). Histopathologic Assessment of Optic Nerves and Retina From a Patient With Chronically Implanted Argus II Retinal Prosthesis System. *Translational Vision Science & Technology*, *8*(3), 31. https://doi.org/10.1167/tvst.8.3.31
Lorach, H., Goetz, G., Smith, R., Lei, X., Mandel, Y., Kamins, T., Mathieson, K., Huie, P., Harris, J., Sher, A., & Palanker, D. (2015). Photovoltaic restoration of sight with high visual acuity. *Nature Medicine*, *21*(5), 476–482. https://doi.org/10.1038/nm.3851
Luo, Y. H.-L., & da Cruz, L. (2016). The Argus® II Retinal Prosthesis System. *Progress in Retinal and Eye Research*, *50*, 89–107. https://doi.org/10.1016/j.preteyeres.2015.09.003
Luo, Y. H.-L., Zhong, J. J., Clemo, M., & da Cruz, L. (2016). Long-term Repeatability and Reproducibility of Phosphene Characteristics in Chronically Implanted Argus II Retinal Prosthesis Subjects. *American Journal of Ophthalmology*, *170*, 100–109. https://doi.org/10.1016/j.ajo.2016.07.021
Mitchell, P., Liew, G., Gopinath, B., & Wong, T. Y. (2018). Age-related macular degeneration. *Lancet (London, England)*, *392*(10153), 1147–1159. https://doi.org/10.1016/S0140-6736(18)31550-2

Muqit, M. M. K., Velikay-Parel, M., Weber, M., Dupeyron, G., Audemard, D., Corcostegui, B., Sahel, J., & Le Mer, Y. (2019). Six-Month Safety and Efficacy of the Intelligent Retinal Implant System II Device in Retinitis Pigmentosa. *Ophthalmology*, *126*(4), 637–639. https://doi.org/10.1016/j.ophtha.2018.11.010

Nagel, G., Szellas, T., Huhn, W., Kateriya, S., Adeishvili, N., Berthold, P., Ollig, D., Hegemann, P., & Bamberg, E. (2003). Channelrhodopsin-2, a directly light-gated cation-selective membrane channel. *Proceedings of the National Academy of Sciences*, *100*(24), 13940–13945. https://doi.org/10.1073/pnas.1936192100

Naidu, A., Ghani, N., Yazdanie, M. S., & Chaudhary, K. (2020). Effect of the electrode array-retina gap distance on visual function in patients with the Argus II retinal prosthesis. *BMC Ophthalmology*, *20*(1), 366. https://doi.org/10.1186/s12886-020-01631-6

Nanduri, D., Fine, I., Horsager, A., Boynton, G. M., Humayun, M. S., Greenberg, R. J., & Weiland, J. D. (2012). Frequency and Amplitude Modulation Have Different Effects on the Percepts Elicited by Retinal Stimulation. *Investigative Opthalmology & Visual Science*, *53*(1), 205. https://doi.org/10.1167/iovs.11-8401

Nanduri, D., Humayun, M. S., Greenberg, R. J., McMahon, M. J., & Weiland, J. D. (2008). *Retinal prosthesis phosphene shape analysis*. 1785–1788. https://doi.org/10.1109/IEMBS.2008.4649524

Niketeghad, S., & Pouratian, N. (2019). Brain Machine Interfaces for Vision Restoration: The Current State of Cortical Visual Prosthetics. *Neurotherapeutics*, *16*(1), 134–143. https://doi.org/10.1007/s13311-018-0660-1

Nikonov, S. S., Kholodenko, R., Lem, J., & Pugh, E. N. (2006). Physiological Features of the S- and M-cone Photoreceptors of Wild-type Mice from Single-cell Recordings. *The Journal of General Physiology*, *127*(4), 359–374. https://doi.org/10.1085/jgp.200609490

Palanker, D., Le Mer, Y., Mohand-Said, S., & Sahel, J. A. (2022). Simultaneous perception of prosthetic and natural vision in AMD patients. *Nature Communications*, *13*(1), Article 1. https://doi.org/10.1038/s41467-022-28125-x

Palanker, D., Vankov, A., Huie, P., & Baccus, S. (2005). Design of a high-resolution optoelectronic retinal prosthesis. *Journal of Neural Engineering*, *2*(1), S105–S120. https://doi.org/10.1088/1741-2560/2/1/012

Patelli, F., Falleni, M., Colombo, L., Martinelli, C., Tosi, D., Bulfamante, G., & Rossetti, L. (2020). EPIRETINAL FIBROSIS REMOVAL IN AN ARGUS II–IMPLANTED EYE: Histological Characteristics and Functional Results. *Retina*, *40*(12), 2403–2409. https://doi.org/10.1097/IAE.0000000000002780

Peli, E. (2020). Testing Vision Is Not Testing For Vision. *Translational Vision Science & Technology*, *9*(13), 32. https://doi.org/10.1167/tvst.9.13.32

Pelli, D. G., & Bex, P. (2013). Measuring contrast sensitivity. *Vision Research*, *90*, 10–14. https://doi.org/10.1016/j.visres.2013.04.015

Penfield, W., & Rasmussen, T. (1950). *The cerebral cortex of man; a clinical study of localization of function* (pp. xv, 248). Macmillan.

Pérez Fornos, A., Sommerhalder, J., da Cruz, L., Sahel, J. A., Mohand-Said, S., Hafezi, F., & Pelizzone, M. (2012). Temporal properties of visual perception on electrical stimulation of the retina. *Investigative Ophthalmology & Visual Science*, *53*(6), 2720–2731. https://doi.org/10.1167/iovs.11-9344

Petoe, M. A., Titchener, S. A., Kolic, M., Kentler, W. G., Abbott, C. J., Nayagam, D. A. X., Baglin, E. K., Kvansakul, J., Barnes, N., Walker, J. G., Epp, S. B., Young, K. A., Ayton,

L. N., Luu, C. D., Allen, P. J., & for the Bionics Institute and Centre for Eye Research Australia Retinal Prosthesis Consortium. (2021). A Second-Generation (44-Channel) Suprachoroidal Retinal Prosthesis: Interim Clinical Trial Results. *Translational Vision Science & Technology*, *10*(10), 12. https://doi.org/10.1167/tvst.10.10.12

Petrs-Silva, H., & Linden, R. (2013). Advances in gene therapy technologies to treat retinitis pigmentosa. *Clinical Ophthalmology*, 127. https://doi.org/10.2147/OPTH.S38041

Pfeiffer, R. L., Marc, R. E., & Jones, B. W. (2020). Persistent remodeling and neurodegeneration in late-stage retinal degeneration. *Progress in Retinal and Eye Research*, *74*, 100771. https://doi.org/10.1016/j.preteyeres.2019.07.004

Pollock, S. C., & Miller, N. R. (1986). The retinal nerve fiber layer. *International Ophthalmology Clinics*, *26*(4), 201–221. https://doi.org/10.1097/00004397-198602640-00019

Prosseda, P. P., Tran, M., Kowal, T., Wang, B., & Sun, Y. (2022). Advances in Ophthalmic Optogenetics: Approaches and Applications. *Biomolecules*, *12*(2), Article 2. https://doi.org/10.3390/biom12020269

Rachitskaya, A. V., DeBenedictis, M., & Yuan, A. (2020). What Happened to Retinal Prostheses? *RETINA*, *40*(5), 803. https://doi.org/10.1097/IAE.0000000000002818

Ratnam, K., Domdei, N., Harmening, W. M., & Roorda, A. (2017). Benefits of retinal image motion at the limits of spatial vision. *Journal of Vision*, *17*(1), 30. https://doi.org/10.1167/17.1.30

Retina Implant—Your Expert for retinitis pigmentosa—Retina Implant. (2019, March 26). https://web.archive.org/web/20190326005315/https://www.retina-implant.de/en/

RetNet: Summaries. (n.d.). Retrieved December 12, 2022, from https://sph.uth.edu/retnet/sum-dis.htm

Rizzo, S., Belting, C., Cinelli, L., Allegrini, L., Genovesi-Ebert, F., Barca, F., & di Bartolo, E. (2014). The Argus II Retinal Prosthesis: 12-Month Outcomes from a Single-Study Center. *American Journal of Ophthalmology*, *157*(6), 1282–1290. https://doi.org/10.1016/j.ajo.2014.02.039

Rizzo, S., Cinelli, L., Finocchio, L., Tartaro, R., Santoro, F., & Gregori, N. Z. (2019). Assessment of Postoperative Morphologic Retinal Changes by Optical Coherence Tomography in Recipients of an Electronic Retinal Prosthesis Implant. *JAMA Ophthalmology*. https://doi.org/10.1001/jamaophthalmol.2018.6375

Rodieck, R. W. (1973). *The vertebrate retina: Principles of structure and function* (p. 1044). W. H. Freeman.

Rosenfeld, J. V., Wong, Y. T., Yan, E., Szlawski, J., Mohan, A., Clark, J. C., Rosa, M., & Lowery, A. (2020). Tissue response to a chronically implantable wireless intracortical visual prosthesis (Gennaris array). *Journal of Neural Engineering*, *17*(4), 046001. https://doi.org/10.1088/1741-2552/ab9e1c

Roska, B., & Sahel, J.-A. (2018). Restoring vision. *Nature*, *557*(7705), Article 7705. https://doi.org/10.1038/s41586-018-0076-4

Russell, S., Bennett, J., Wellman, J. A., Chung, D. C., Yu, Z.-F., Tillman, A., Wittes, J., Pappas, J., Elci, O., McCague, S., Cross, D., Marshall, K. A., Walshire, J., Kehoe, T. L., Reichert, H., Davis, M., Raffini, L., George, L. A., Hudson, F. P., … Maguire, A. M. (2017). Efficacy and safety of voretigene neparvovec (AAV2-hRPE65v2) in patients with RPE65-mediated inherited retinal dystrophy: A randomised, controlled, open-label, phase

3 trial. *The Lancet*, *390*(10097), 849–860. https://doi.org/10.1016/S0140-6736(17)31868-8

Sahel, J.-A., Boulanger-Scemama, E., Pagot, C., Arleo, A., Galluppi, F., Martel, J. N., Esposti, S. D., Delaux, A., de Saint Aubert, J.-B., de Montleau, C., Gutman, E., Audo, I., Duebel, J., Picaud, S., Dalkara, D., Blouin, L., Taiel, M., & Roska, B. (2021). Partial recovery of visual function in a blind patient after optogenetic therapy. *Nature Medicine*, *27*(7), 1223–1229. https://doi.org/10.1038/s41591-021-01351-4

Sandrian, M. G., Ng, E., Nguyen, T., & Eydelman, M. (2023). FDA's role in expediting innovation of bioelectronic implants for vision restoration. *J. Neural Eng.*

Schaffrath, K., Schellhase, H., Walter, P., Augustin, A., Chizzolini, M., Kirchhof, B., Grisanti, S., Wiedemann, P., Szurman, P., Richard, G., Greenberg, R. J., Dorn, J. D., Parmeggiani, F., & Rizzo, S. (2019). One-Year Safety and Performance Assessment of the Argus II Retinal Prosthesis: A Postapproval Study. *JAMA Ophthalmology*, *137*(8), 896. https://doi.org/10.1001/jamaophthalmol.2019.1476

Second Sight Medical Products Announces Successful Completion of its Merger with Nano Precision Medical and its Name Change to Vivani Medical, Inc. (2022, August 30). https://www.businesswire.com/news/home/20220830005423/en/Second-Sight-Medical-Products-Announces-Successful-Completion-of-its-Merger-with-Nano-Precision-Medical-and-its-Name-Change-to-Vivani-Medical-Inc.

Second Sight Medical Products Inc. (2013). *Argus® II Retinal Prosthesis System Surgeon Manual*. https://www.accessdata.fda.gov/cdrh_docs/pdf11/h110002c.pdf

Second Sight to Accelerate Development of Orion® Visual Cortical Prosthesis System. (2019, May 15). Vivani Medical, Inc. https://investors.vivani.com/investors/news-events/press-releases/detail/38/second-sight-to-accelerate-development-of-orion-visual

Shivdasani, M. N., Sinclair, N. C., Dimitrov, P. N., Varsamidis, M., Ayton, L. N., Luu, C. D., Perera, T., McDermott, H. J., & Blamey, P. J. (2014). Factors Affecting Perceptual Thresholds in a Suprachoroidal Retinal Prosthesis. *Investigative Ophthalmology & Visual Science*, *55*(10), 6467–6481. https://doi.org/10.1167/iovs.14-14396

Stingl, K., Bartz-Schmidt, K. U., Besch, D., Chee, C. K., Cottriall, C. L., Gekeler, F., Groppe, M., Jackson, T. L., MacLaren, R. E., Koitschev, A., Kusnyerik, A., Neffendorf, J., Nemeth, J., Naeem, M. A. N., Peters, T., Ramsden, J. D., Sachs, H., Simpson, A., Singh, M. S., … Zrenner, E. (2015). Subretinal Visual Implant Alpha IMS – Clinical trial interim report. *Vision Research*, *111*, 149–160. https://doi.org/10.1016/j.visres.2015.03.001

Stingl, K., Schippert, R., Bartz-Schmidt, K. U., Besch, D., Cottriall, C. L., Edwards, T. L., Gekeler, F., Greppmaier, U., Kiel, K., Koitschev, A., Kühlewein, L., MacLaren, R. E., Ramsden, J. D., Roider, J., Rothermel, A., Sachs, H., Schröder, G. S., Tode, J., Troelenberg, N., & Zrenner, E. (2017). Interim Results of a Multicenter Trial with the New Electronic Subretinal Implant Alpha AMS in 15 Patients Blind from Inherited Retinal Degenerations. *Frontiers in Neuroscience*, *11*. https://doi.org/10.3389/fnins.2017.00445

Stronks, H. C., & Dagnelie, G. (2014). The functional performance of the Argus II retinal prosthesis. *Expert Review of Medical Devices*, *11*(1), 23–30. https://doi.org/10.1586/17434440.2014.862494

Stryer, L. (1991). Visual excitation and recovery. *The Journal of Biological Chemistry*, *266*(17), 10711–10714.

Tong, W., Hejazi, M., Garrett, D. J., Esler, T., Prawer, S., Meffin, H., & Ibbotson, M. R. (2020). Minimizing axon bundle activation of retinal ganglion cells with oriented rectangular electrodes. *Journal of Neural Engineering*, *17*(3), 036016. https://doi.org/10.1088/1741-2552/ab909e

Towle, V. L., Pytel, P., Lane, F., Plass, J., Frim, D. M., & Troyk, P. R. (2020). Postmortem investigation of a human cortical visual prosthesis that was implanted for 36 years. *Journal of Neural Engineering*, *17*(4), 045010. https://doi.org/10.1088/1741-2552/ab9d11

Troyk, P. R. (2017). The Intracortical Visual Prosthesis Project. In V. P. Gabel (Ed.), *Artificial Vision: A Clinical Guide* (pp. 203–214). Springer International Publishing. https://doi.org/10.1007/978-3-319-41876-6_16

Umino, Y., Guo, Y., Chen, C.-K., Pasquale, R., & Solessio, E. (2019). Rod Photoresponse Kinetics Limit Temporal Contrast Sensitivity in Mesopic Vision. *Journal of Neuroscience*, *39*(16), 3041–3056. https://doi.org/10.1523/JNEUROSCI.1404-18.2019

U.S. Food and Drug Administration. (n.d.). *Humanitarian Device Exemption (HDE)*. Retrieved November 5, 2023, from https://www.accessdata.fda.gov/scripts/cdrh/cfdocs/cfhde/hde.cfm?id=H110002

Van Essen, D. C., Newsome, W. T., & Maunsell, J. H. R. (1984). The visual field representation in striate cortex of the macaque monkey: Asymmetries, anisotropies, and individual variability. *Vision Research*, *24*(5), 429–448. https://doi.org/10.1016/0042-6989(84)90041-5

Vilkhu, R. S., Madugula, S. S., Grosberg, L. E., Gogliettino, A. R., Hottowy, P., Dabrowski, W., Sher, A., Litke, A. M., Mitra, S., & Chichilnisky, E. J. (2021). Spatially patterned bi-electrode epiretinal stimulation for axon avoidance at cellular resolution. *Journal of Neural Engineering*, *18*(6), 066007. https://doi.org/10.1088/1741-2552/ac3450

Wandell, B. A. (1995). *Foundations of vision.* Sinauer Associates.

Waschkowski, F., Hesse, S., Rieck, A. C., Lohmann, T., Brockmann, C., Laube, T., Bornfeld, N., Thumann, G., Walter, P., Mokwa, W., Johnen, S., & Roessler, G. (2014). Development of very large electrode arrays for epiretinal stimulation (VLARS). *BioMedical Engineering OnLine*, *13*(1), 11. https://doi.org/10.1186/1475-925X-13-11

Wassle, H., & Boycott, B. B. (1991). Functional architecture of the mammalian retina. *Physiological Reviews*, *71*(2), 447–480. https://doi.org/10.1152/physrev.1991.71.2.447

Watson, A. B. (1979). Probability summation over time. *Vision Research*, *19*(5), 515–522. https://doi.org/10.1016/0042-6989(79)90136-6

Watson, A. B. (1986). *TEMPORAL SENSITIVITY*. 43.

Watson, A. B., & Ahumada, A. J., Jr. (2005). A standard model for foveal detection of spatial contrast. *Journal of Vision*, *5*(9), 6. https://doi.org/10.1167/5.9.6

Watson, A. B., & Pelli, D. G. (1983). Quest: A Bayesian adaptive psychometric method. *Perception & Psychophysics*, *33*(2), 113–120. https://doi.org/10.3758/BF03202828

Watson, A. B., & Robson, J. G. (1981). Discrimination at threshold: Labelled detectors in human vision. *Vision Research*, *21*(7), 1115–1122. https://doi.org/10.1016/0042-6989(81)90014-6

Watson, W. (1752). XXXI. An account of Mr. Benjamin Franklin's treatise, lately published, intituled, Experiments and observations on electricity, made at Philadelphia in America. *Philosophical Transactions of the Royal Society of London*, *47*, 202–211. https://doi.org/10.1098/rstl.1751.0032

Wichmann, F. A., & Hill, N. J. (2001). The psychometric function: I. Fitting, sampling, and goodness of fit. *Perception & Psychophysics*, *63*(8), 1293–1313. https://doi.org/10.3758/BF03194544

Wong, W. L., Su, X., Li, X., Cheung, C. M. G., Klein, R., Cheng, C.-Y., & Wong, T. Y. (2014). Global prevalence of age-related macular degeneration and disease burden projection for 2020 and 2040: A systematic review and meta-analysis. *The Lancet. Global Health*, *2*(2), e106-116. https://doi.org/10.1016/S2214-109X(13)70145-1

Xu, L. T., Rachitskaya, A. V., DeBenedictis, M. J., Bena, J., Morrison, S., & Yuan, A. (2021). Correlation between Argus II array–retina distance and electrical thresholds of stimulation is improved by measuring the entire array. *European Journal of Ophthalmology*, *31*(1), 194–203. https://doi.org/10.1177/1120672119885799

Yanai, D., Weiland, J. D., Mahadevappa, M., Greenberg, R. J., Fine, I., & Humayun, M. S. (2007). Visual Performance Using a Retinal Prosthesis in Three Subjects With Retinitis Pigmentosa. *American Journal of Ophthalmology*, *143*(5), 820-827.e2. https://doi.org/10.1016/j.ajo.2007.01.027

Yoon, Y. H., Yue, L., & Humayun, M. S. (2020). Argus II Prosthetic Vision. In A. Chang, W. F. Mieler, & M. Ohji (Eds.), *Macular Surgery* (pp. 463–486). Springer Singapore. https://doi.org/10.1007/978-981-15-7644-7_34

Yücel, E. I., Sadeghi, R., Kartha, A., Montezuma, S. R., Dagnelie, G., Rokem, A., Boynton, G. M., Fine, I., & Beyeler, M. (2022). Factors affecting two-point discrimination in Argus II patients. *Frontiers in Neuroscience*, *16*, 901337. https://doi.org/10.3389/fnins.2022.901337

Yue, L., Weiland, J. D., & Humayun, M. S. (2018). Retinal Prostheses: A Brief History. In M. S. Humayun & L. C. Olmos de Koo (Eds.), *Retinal Prosthesis: A Clinical Guide to Successful Implementation* (pp. 1–22). Springer International Publishing. https://doi.org/10.1007/978-3-319-67260-1_1

Yue, L., Wuyyuru, V., Gonzalez-Calle, A., Dorn, J. D., & Humayun, M. S. (2020). Retina–electrode interface properties and vision restoration by two generations of retinal prostheses in one patient—One in each eye. *Journal of Neural Engineering*, *17*(2), 026020. https://doi.org/10.1088/1741-2552/ab7c8f

SUPPLEMENTARY MATERIALS

Supplementary Table 1 Summary table of inherited retinal degenerative diseases and the number of identified and unidentified genes and loci, acquired from RetNet: Summaries, 2022.

Disease Category	Total No. of Genes and Loci	No. of Identified Genes
Bardet-Biedl syndrome, autosomal recessive	18	18
Chorioretinal atrophy or degeneration, autosomal dominant	1	1
Cone or cone-rod dystrophy, autosomal dominant	9	5
Cone or cone-rod dystrophy, autosomal recessive	19	18
Cone or cone-rod dystrophy, X-linked	1	0
Congenital stationary night blindness, autosomal dominant	1	1
Congenital stationary night blindness, autosomal recessive	10	10
Congenital stationary night blindness, X-linked	2	2
Leber congenital amaurosis, autosomal dominant	1	1
Leber congenital amaurosis, autosomal recessive	13	13
Macular degeneration, autosomal dominant	14	10
Macular degeneration, autosomal recessive	4	4
Ocular-retinal developmental disease, autosomal dominant	1	1
Optic atrophy, autosomal dominant	8	5
Optic atrophy, autosomal recessive	4	3
Optic atrophy, X-linked	1	0
Retinitis pigmentosa, autosomal dominant	24	23
Retinitis pigmentosa, autosomal recessive	46	44
Retinitis pigmentosa, X-linked	5	2
Syndromic/systemic diseases with retinopathy, autosomal dominant	9	8
Syndromic/systemic diseases with retinopathy, autosomal recessive	56	53
Syndromic/systemic diseases with retinopathy, X-linked	3	2
Usher syndrome, autosomal recessive	18	15
Other retinopathy, autosomal dominant	15	11
Other retinopathy, autosomal recessive	19	17
Other retinopathy, mitochondrial	7	7
Other retinopathy, X-linked	8	7

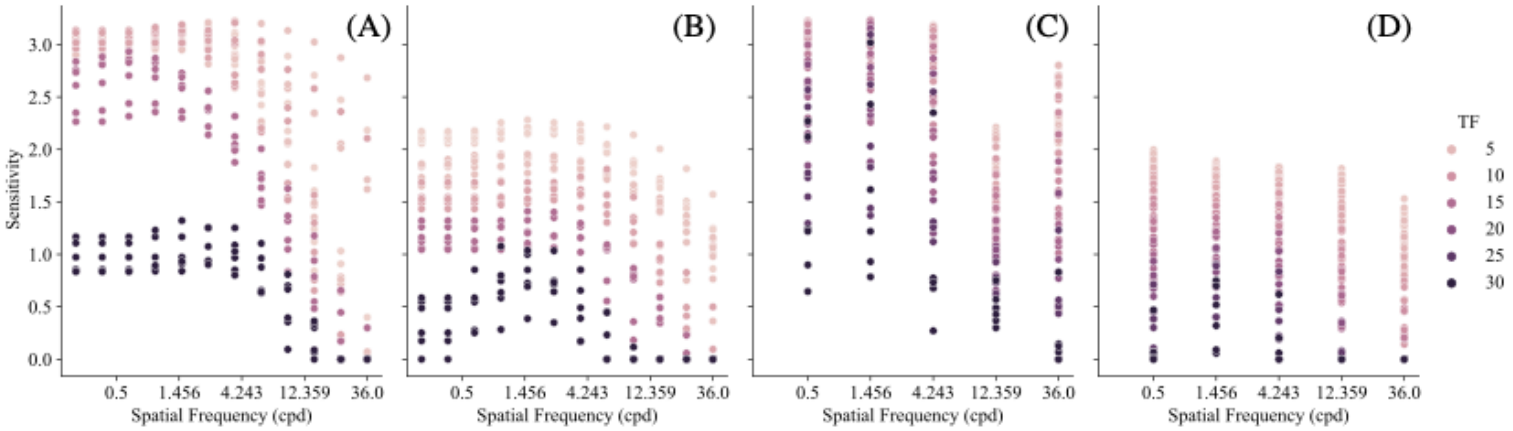

Supplementary Figure 1 Scatterplots of contrast sensitivity for all four conditions: (A) Baseline condition where the unfiltered stimulus is presented at five fixed temporal frequencies and spatial frequencies were fit using a staircase method (version 1). (B) Optogenetic condition where filtered stimulus is presented in the same way as (A). (C-D) In these conditions, temporal frequencies varied using a staircase method and spatial frequencies were fixed at five values.

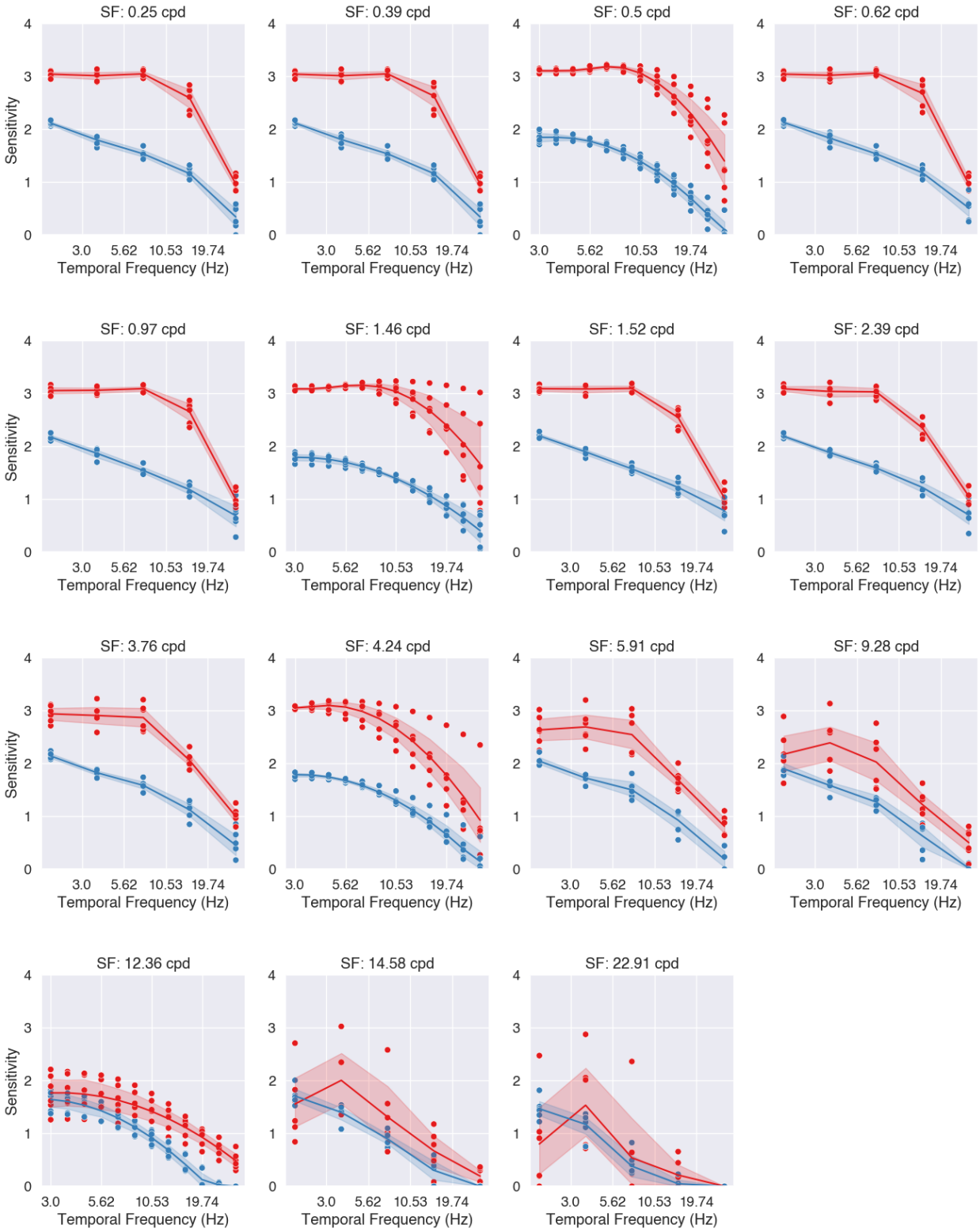

Supplementary Figure 2 Contrast sensitivity - temporal frequency relationship at every spatial frequency tested (except for 36 cpd). Both axes are on a log-scale.

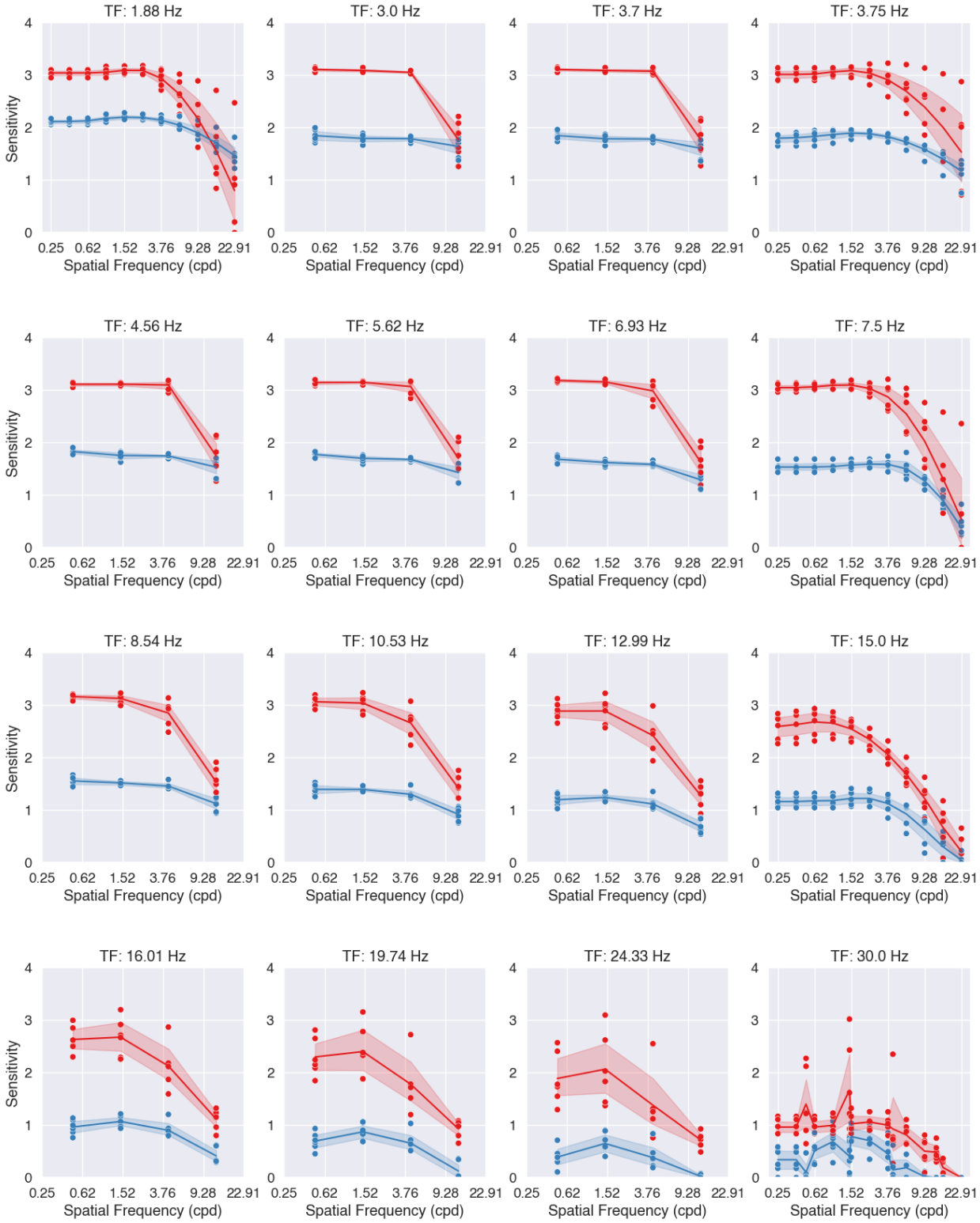

Supplementary Figure 3 Contrast sensitivity - spatial frequency relationship at every temporal frequency tested. Both axes are on a log-scale.